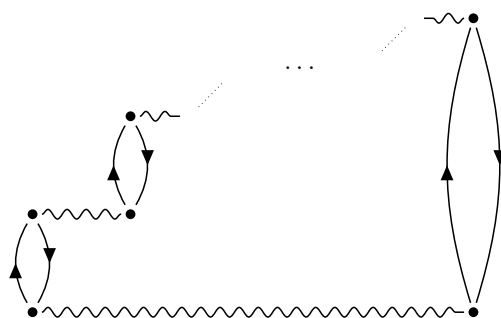


Dissertation zur Erlangung des Doktorgrades
der Fakultät für Chemie und Pharmazie
der Ludwig-Maximilians-Universität München

HIGHLY ACCURATE
RANDOM PHASE APPROXIMATION METHODS
WITH
LINEAR TIME COMPLEXITY



Henry Franz Schurkus

aus

Landshut
2017

Dissertation zur Erlangung des Doktorgrades
der Fakultät für Chemie und Pharmazie
der Ludwig-Maximilians-Universität München

HIGHLY ACCURATE
RANDOM PHASE APPROXIMATION METHODS
WITH
LINEAR TIME COMPLEXITY

Henry Franz Schurkus

aus

Landshut

2017

Erklärung

Diese Dissertation wurde im Sinne von §7 der Promotionsordnung vom 28. November 2011 von Herrn Prof. Dr. Christian Ochsenfeld betreut.

Eidesstattliche Versicherung

Diese Dissertation wurde eigenständig und ohne unerlaubte Hilfe erarbeitet.

München,

.....
(Henry Schurkus)

Dissertation eingereicht am07.07.2017.....
1. GutachterProf. Dr. Christian Ochsenfeld.....
2. GutachterProf. Dr. Hubert Ebert.....
Mündliche Prüfung am31.07.2017.....

Meinem Opa Franz-Josef Keite

Summary

One of the key challenges of electronic structure theory is to find formulations to compute electronic ground-state energies with high accuracy while being applicable to a wide range of chemical problems. For systems beyond the few atom scale often computations achieving higher accuracies than the so called double-hybrid density functional approximations become prohibitively expensive. Here, the random phase approximation, which is known to yield such higher accuracy results has been developed from a theory applicable only to molecules on the tens of atoms scale into a highly accurate and widely applicable theory. To this end, a mathematical understanding has been developed that, without changing the computational complexity, allows to eliminate the error introduced by the resolution-of-the-identity approximation which had been introduced in the previous formulation. Furthermore, in this work a new formulation of the random phase approximation for molecules has been presented which achieves linear-scaling of compute time with molecular size—thereby expanding the realm of molecules that can be treated on this level of theory to up to a thousand atoms on a simple desktop computer. Finally, the theory has been matured to allow for use of even extensive basis sets without drastically increasing runtimes. Overall, the presented theory is at least as accurate and even faster than the original formulation for all molecules for which compute time is significant and opens new possibilities for the highly accurate description of large quantum chemical systems.

List of publications

The present work is a cumulative dissertation, comprising three publications in peer-reviewed journals. The content of these is given completely in chapter 3 together with supporting information that was published conjointly.

- I “An effective linear-scaling atomic-orbital reformulation of the random-phase approximation using a contracted double-Laplace transformation”,
H. F. Schurkus and C. Ochsenfeld,
J. Chem. Phys. (Communication) **144**, 031101 (2016).
- II “Vanishing-Overhead Linear-Scaling Random Phase Approximation by Cholesky Decomposition and an Attenuated Coulomb-Metric”,
A. Luenser, H. F. Schurkus, and C. Ochsenfeld,
J. Chem. Theory Comput. **13**, 1647 (2017).
Contributions by H. F. Schurkus: *Conjoint development of the theory with A. Luenser. Contributions to implementation and major contributions to writing.*
- III “Almost error-free resolution-of-the-identity correlation methods by null space removal of the particle-hole interactions”,
H. F. Schurkus, A. Luenser, C. Ochsenfeld,
J. Chem. Phys. (Communication) **146**, 211106 (2017).
Contributions by H. F. Schurkus: *Conjoint development of the theory with A. Luenser. Development of the mathematical basis of the theory and derivation of the equations. Most of the calculations and writing. Contributions to implementation.*

Contents

1	Introduction	1
2	Theoretical Basics	5
2.1	Overview of Electronic Structure Theory	5
2.2	Computational Complexity	6
2.2.1	Asymptotic and Effective Time-Complexity	6
2.2.2	Measuring Time-Complexity	9
2.3	Resolution-Of-The-Identity	10
2.3.1	Overlap Metric Resolution-Of-The-Identity of Electron Repulsion Integrals	10
2.3.2	Density Fitting	13
2.4	Random Phase Approximation	14
2.4.1	Important Results from Green's Function Theory	14
2.4.2	Adiabatic Connection	18
2.4.3	Polarization Propagator and Random Phase Approximation	20
2.4.4	Evaluation of $i\Pi_0$ by Lehmann's Representation	23
2.4.5	Molecular Orbitals	26
3	Publications	29
3.1	AO-RI-RPA	29
3.2	ω -CDD-RPA	39
3.3	Kernel Projection	51
4	Conclusion	75

Chapter 1

Introduction

The field of theoretical chemistry is concerned with the theoretical description and prediction of atomic and molecular processes. To this end it is crucial to describe the electronic structure—including the quantum nature of electrons. It can be proven¹ that finding the exact solution for the Schrödinger equation for a general system of electrons is of the Quantum-Merlin-Arthur² complexity class, making it highly unlikely that it could be done without approximation. As the electronic Schrödinger equation³ already neglects all relativistic effects,⁴ even further approximations are necessary. Therefore a large part of electronic structure theory is concerned with the development of such approximations yielding numerically accurate results for a broad range of molecules.

One approximation to compute the electronic ground state in a fixed field of nuclei which has received a lot of attention in recent years is the random phase approximation⁵ (RPA). It can be shown to be far more accurate than the frequently employed density functional approximations (DFAs; e.g. the widely used B3LYP functional⁶), Hartree–Fock theory,^{7–10} and Møller–Plesset perturbation theory¹¹ (MP2). A more detailed discussion of where RPA fits into the bigger picture of electronic structure theory can be found in Sec. 2.1.

The RPA was originally conceived in work by Bohm and Pines⁵ in 1953, but has long been of little use to theoretical chemistry because its computational complexity limited its application to systems of a few atoms. For such systems, however, coupled cluster theories^{12,13} can also be applied, which would yield even better accuracies in comparison. This changed in 2010, when Furche and coworkers developed a theory combining the RPA with the resolution-of-the-identity^{14–18,33} (RI) to achieve an overall scaling with molecular size of $\mathcal{O}(M^4 \log(M))$.¹⁹ It allowed to apply their theory (RI-RPA) to systems of several tens of atoms—far beyond what is viable with accurate coupled cluster theories, yet still very limited. In Sec. 2.4 a more thorough elaboration on the RPA theory leading up to the present work can be found.

Although, the ideas of RI-RPA had shown that the RPA could be extended to small to medium sized molecules, for this it had been necessary to introduce the RI. The RI is formally exact but typically evaluated in auxiliary basis sets of limited size in practical calculations. This leads to significant errors in absolute energies. Also, many chemical questions exist, for which RPA quality results are desirable but which still could not be approached by RI-RPA due to their size. The publications of the present work have addressed both these issues, improving upon the achievable accuracy of RI-RPA and also making RPA quality results available for systems of up to a thousand atoms. This allows the RPA to become a viable level of theory for large scale applications in the

coming years.

In the first publication of this work a different formulation or more specifically metric of the RI than the Coulomb metric of RI-RPA is applied and a new integral transformation, called double-Laplace, related to the Laplace transform in linear scaling AO-MP2 theory²⁰ is derived. Combined, double-Laplace and the different RI metric allow to formulate a theory that achieves the same level of accuracy as RI-RPA but scales only linearly with molecular size. This theory can therefore be applied to molecules of up to a thousand atoms and ten thousand basis functions.²¹ To achieve linear-scaling behavior, the new theory exposes and exploits the physical locality of electron correlation within the random phase approximation. To this end it is based on (pseudo) density matrices in the atomic orbital (AO) basis and titled AO-RI-RPA. A more detailed discussion of RI and the related concept of density-fitting²² (DF) can be found in Sec. 2.3.

While the number of electrons scales only with system size, the number of atomic orbitals also scales with basis set size. Therefore, while AO-RI-RPA allows to compute systems untractable with RI-RPA due to their sheer size, for any fixed size molecule increasing the basis set size raises the computational cost of AO-RI-RPA faster than in the case of RI-RPA. This is remedied in the second publication of this work, where a Cholesky decomposition of the density matrices²³⁻²⁵ (CDD) is introduced. The technique had been explored in the context of AO-MP2 where the Laplace transform gives rise to one kind of pseudo density matrix. In this publication it was extended to also treat the second kind which stems from the new integral transform of AO-RI-RPA. With CDD the presented theory can then be denoted by CDD-RI-RPA and the scaling with basis set size is again the same as with RI-RPA, while at the same time CDD-RI-RPA still allows for linear scaling evaluation and therefore the computation of even larger systems than the previous AO-RI-RPA. With CDD-RI-RPA, converging results with basis sets of quadruple- ζ size becomes standard practice even for systems with several hundreds of atoms.²⁶

While the so called overlap metric RI was introduced in formulating AO-RI-RPA, the Coulomb metric is more commonly used in other theories as for example in DF-DFT and RI-MP2.²⁷ Accordingly, the auxiliary basis sets necessary for evaluation of the RI are mostly optimized and published for the Coulomb metric.²⁸⁻³² Also, it has been shown that the Coulomb metric is optimal for evaluation of the energy at least in the case of DF-DFT.³³ For this reason the second publication of this work furthermore develops the RI metric further. The core feature of the overlap metric that gives rise to the option of linear scaling in AO-RI-RPA is its locality. By introducing an attenuated Coulomb metric which has tunable locality, the best of both worlds can be combined:²⁶ The final ω -CDD-RPA theory allows for linear-scaling evaluation while at the same time results are identical to those obtained with Coulomb metric RI within numerical accuracy.

As indicated above, the RI is formally exact when the size of the auxiliary basis set tends to completeness. Preoptimized auxiliary basis sets²⁸⁻³² employed in practical calculations, however, are typically only about three times larger than the AO basis set. This is generally justified by the concept of DF and allows to reduce computational cost by a significant factor.^{14,22,33} However, this procedure also drastically deteriorates the accuracy of absolute energies of RI-employing theories. For relative energies a cancellation of this RI error has to be assumed. Therefore, the third publication of this work shows how results which are free of this RI error can be obtained by a small

modification of the RI scheme that still achieves evaluation times comparable to those of using standard preoptimized auxiliary basis sets.

To this end a new concept has been developed in the third publication, designated nullspace projection. Nullspace projection describes a procedure to project out the nullspace of an arbitrary operator chain and thereby reduce the matrix dimensions at the boundaries of the chain. It is shown that the physical-model operator of RPA in auxiliary basis representation is of limited rank and therefore nullspace projection allows to reduce the number of auxiliary basis functions without introduction of any error. By employing a converged auxiliary basis set and nullspace projecting the physical model, the error of the RI is *de-facto* eliminated for only slightly more compute time than with standard preoptimized auxiliary basis sets.⁷¹

In combination, the publications comprising this work supersede the original RI-RPA for any molecular application case. The present work extends the realm of systems for which RI-RPA quality results can be obtained from tens of atoms to several hundreds or even a thousand atoms, even when converging results with AO basis set size, drastically reduces the computational effort for moderately sized systems, and furthermore also allows for even more accurate results by eliminating the RI error. This allows to compute RPA quality results for almost any molecular system for which previously double-hybrid DFAs had been the highest quality results available and opens the door for highly accurate quantum chemistry of large molecular systems. Since the appearance of the first publication in 2016, the work has already proven relevant to the field with several other groups referring to it and building upon the presented publications.³⁴⁻³⁹

Chapter 2

Theoretical Basics

In this chapter the theoretical basis of the original research of chapter 3 is summarized. First, in Sec. 2.1, an overview of the field of electronic structure theory is given and the accuracy of the RPA contrasted with other approximation theories. In Sec. 2.2 important aspects of defining and measuring the computational cost of approximation theories are discussed. Computational costs limit the applicability of a theory and one of the key aspects of the research presented in chapter 3 is the dramatic reduction of cost for the RPA. In Sec. 2.3 the RI in overlap metric and Coulomb metric is introduced and the source of error of employing RI in approximation theories is discussed. The RI is a major theme of the publications of the following chapter, as the first two publications employ a change of metric to allow for a computationally efficient theory without deteriorating accuracy and the third publication develops a scheme to eliminate the error introduced by the RI completely for only slightly increased computational cost. Finally, in Sec. 2.4, a concise derivation of the RPA for molecular systems is presented. Although historically a more cumbersome derivation formed the basis of the first publication of chapter 3, it can be understood directly from this result obtained in a more physically motivated way.

2.1 Overview of Electronic Structure Theory

As stated in the introduction, the goal of electronic structure theory is the development of approximations that make evaluation possible and feasible for a wide range of molecules without diverging unnecessarily from the exact solution.

One approximation so common that it is often not even considered an approximation is the use of finite predefined basis sets^{28–32} to discretize the differential equations of quantum mechanics into a linear algebra of vectors, matrices, and higher order tensors. While for other applications different types of basis sets have proven useful—e.g. plane waves as the basis for calculations of periodic systems^{72,73}—for molecular systems atom-centered Gaussian type functions have been established as the predominant choice.

A theory containing only this one approximation is the full configuration interaction theory (FCI; cf. Ref. 40 and references therein). While it is highly accurate, it is computationally so expensive that it can only be applied to problems with very few electrons. Therefore it is necessary to develop further approximations aiming to make the application to systems of real relevance tractable while deteriorating the results only slightly.

Theories that do so purely from mathematical concepts are called *ab initio*. Within these there exists a strong order from highly accurate but computationally expensive to much less demanding but also less accurate theories. For the few atom regime coupled cluster theories^{12,13} (CC) are available, for larger molecules perturbation theories like second-order Møller–Plesset theory¹¹ (MP2) can be applied and for the largest molecules one is often restricted to Hartree–Fock theory^{7–10} (HF) in practice.

By introduction of empirical parameters often better quality results for the same expense as with *ab initio* theories can be achieved. This path is mainly explored with Kohn–Sham density functional theory⁴¹ (DFT) which is in contrast to *ab initio* theories sometimes also referred to as *first-principles*. DFT reformulates the problem by mapping the interacting system of electrons to a model system of non-interacting electrons. While this mapping can in principle be made exact, the necessary exact density functional is in general unknown and so it is necessary to introduce density functional approximations (DFAs). These often incorporate contributions from *ab initio* theories because those are already considered very accurate. The contributions from *ab initio* theories are then weighted by empirical factors together with other purely density based contributions. The DFAs can be grouped by the *ab initio* contributions they incorporate.⁴² DFAs that depend solely on the density can already describe the Coulomb interaction of electrons exactly and are known as (semi-)local DFAs. Hybrid DFAs additionally contain the so-called exact exchange contribution from HF theory. Lastly, double-hybrid DFAs additionally incorporate a contribution to the correlation energy as described by MP2 theory. While most DFAs aim to keep the number of weighting parameters low, also DFAs with hundreds of parameters exist.⁴³ The downside to these empirical parameters is that the order between the levels of theory becomes less rigorous as chances increase that the lower level of theory may be right for the wrong reason.⁴⁴

Most DFAs describe electron densities rather well and so the adiabatic connection⁴⁵ allows to formulate a perturbation theory on the electron density or equivalently the Kohn–Sham orbitals obtained from a DFA that in principle converges to the exact solution. Within this series again approximations can be introduced. The most prominent of these is the random phase approximation⁵ (RPA). The RPA neglects certain terms of the perturbation series but includes others exactly to infinite order. It is therefore rather robust against the choice of DFA with which the initial density is computed and also size-consistent. Energies are typically much better than those obtained with the different DFAs, HF or MP2, however not quite as good as those of coupled cluster theory with singles, doubles and perturbative triples contributions⁷⁴ (CCSD(T)) which remains the gold standard for highly accurate computations. A comparison of energies obtained with different DFAs and RPA calculations based on these DFAs referenced against this gold standard has previously been presented by the author.⁴⁶ It is reproduced below for illustration (Fig. 2.1).

2.2 Computational Complexity

2.2.1 Asymptotic and Effective Time-Complexity

In Sec. 2.1 the accuracy of different levels of theory has been discussed. Another important aspect is the applicability to different molecular systems. One specific question is the size of the system that can be treated in regular applications. This size is mainly

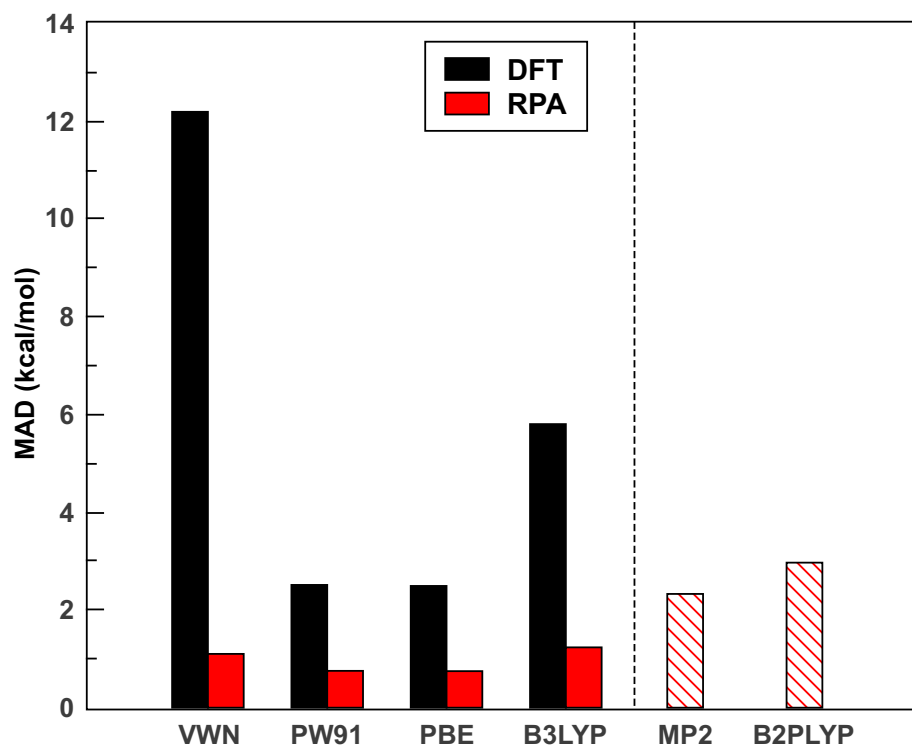


Figure 2.1: Comparison of energies obtained for the NBRC test set. CCSD(T) reference values are taken from [L. Goerigk and S. Grimme, *J. Chem. Theory Comput.* **6**, 107 (2010)]. Results with different DFAs and cc-pVQZ AO basis set are given in black and RPA calculations based on Kohn–Sham orbitals obtained with these DFAs are given in red. The DFAs are sorted by rung. VWN, PW91, and PBE are (semi-)local DFAs. B3LYP is a hybrid DFA and B2LYP is a double-hybrid DFA incorporating a correlation energy contribution of MP2. As MP2 is a perturbation theory, for the latter two, the energies are only given for comparison. Figure taken from [H. F. Schurkus, *Wissenschaftliche Arbeit im Rahmen der Promotionseignungsprüfung: “The Description of Electron Correlation with the Random Phase Approximation”* (LMU Munich, 2013)].

limited by the compute time necessary to evaluate the theory. When compute time requirements go beyond a few weeks for a single calculation they become practically unfeasible. On the one hand, because often the result of one calculation informs the configuration of the next and therefore research projects quickly require intolerable amounts of time. On the other hand, todays computers may malfunction or require intervention over a time scale of several weeks when put under heavy load and keeping calculations running much longer can therefore require significant effort.

Computational complexity denotes the time required for evaluation of an algorithm as a function of the problem size. As different problems of equal size may take differing time to compute by an algorithm one typically considers worst-case time complexity. The specific form of the time complexity function may be very involved. However, to estimate for which size of molecules runtime becomes limiting, it is often sufficient to approximate its limit by a polynomial. The Bachmann-Landau notation^{47,48} is used throughout computer science to formalize this process. According to this notation a function $t(M)$ is associated with a polynomial $\text{poly}(M)$ as

$$\begin{aligned}
 t(M) &\stackrel{M \rightarrow \infty}{\asymp} \mathcal{O}(\text{poly}(M)) \\
 &:\iff \\
 \exists \text{ const} \in \mathbb{R}, M_0 \in \mathbb{R} : \forall M \geq M_0 : |t(M)| &\leq \text{const} \cdot |\text{poly}(M)| \quad . \quad (2.1)
 \end{aligned}$$

In words, a time complexity is $\mathcal{O}(\text{poly}(M))$ exactly when for all systems of larger size than a certain size M_0 the evaluation time is smaller than a constant times this polynomial $\text{poly}(M)$.

It has been argued that electrons in many-atom systems express “nearsightedness”,⁴⁹ so that different potentials or densities beyond a certain distance have only limited effect on local electronic structure.⁵⁰ On this basis it seems plausible, that for any approximation theory that captures the physics of the electronic system correctly, there should exist a linear-scaling formulation.

How such a reformulation can be found is however in general not clear. To develop a linear-scaling theory without introducing additional approximations it is necessary to expose the physical locality that is hidden in the canonical formulation of the theory. It then has to be exploited by circumventing computational steps that due to this locality would yield only vanishing contributions to the final result.

Given the *de facto* time limit discussed above, the order of magnitude of molecular sizes treatable with a given theory is mainly dependent on the order of the asymptotic polynomial with molecular size M , because different prefactors are quickly overshadowed by any difference in polynomial order when molecular size increases. When comparing compute times of moderately sized molecules (where M is comparably small) or different algorithms of equal polynomial order, however, these prefactors can play a significant role in determining evaluation time.

One way in which prefactors may differ is due to differences specific to the underlying model of computation. These differences change prefactors by typically only a small multiple. Much more significant in contrast are contributions to the prefactor that are due to the algorithm scaling with another parameter of the system: The number of basis functions N . When molecular size is kept fixed, basis set size is proportional to the number of basis functions and increasing it does not allow for more exploitable locality. On the other hand, increasing the basis set size does not alter the number of electrons in the system, while increasing system size does. Therefore, computational

complexity with N is often of similar but not necessarily equal order as that with M . Even more subtle analyses can be made, when also auxiliary basis set size N_{aux} is taken into consideration (which is otherwise simply taken as proportional to N) and instead of molecular size M —which doesn’t discriminate between light and heavy atoms in the molecule—the number of electrons N_{el} is used.

Up to this point the asymptotic limit, Eq. 2.1, has been taken in discussing limiting compute time. One sometimes finds that certain steps of an algorithm may be asymptotically dominating but are not even detectable in actual runtime measurements, or timings for short. This may be caused by orders of magnitude lower prefactors of the corresponding steps in comparison to the other steps of the overall algorithm. In these cases it is more suitable to discuss effective scaling behavior than asymptotic scaling behavior, which means that the limit is taken not to theoretical infinity but to the largest molecules which can in fact be treated by the theory.

RI-RPA scales effectively $\mathcal{O}(M^4)$ with molecular size and $\mathcal{O}(N^3)$ with basis set size. The high order scaling with molecular size strongly constrains its applicability to molecules of limited size. AO-RI-RPA, which is presented in the first publication of this work, lowers the effective scaling with molecular size from $\mathcal{O}(M^4)$ to $\mathcal{O}(M)$ enabling its application to much larger systems. Because it also raises scaling with basis set size from $\mathcal{O}(N^3)$ to $\mathcal{O}(N^4)$, however, for small molecules or computations with large basis sets the RI-RPA evaluates faster. With CDD-RI-RPA, as presented in the second paper of this work, the effective scaling with molecular size is still $\mathcal{O}(M)$ but with basis set size it is again reduced to $\mathcal{O}(N^3)$ so that it evaluates faster than RI-RPA even for medium sized molecules. Only for the very smallest of molecules, where the description of the actual time complexity is not yet described by the polynomial, Eq. 2.1, CDD-RI-RPA is sometimes observed to take more time to evaluate than RI-RPA. This is of no concern however, because for these very small molecules absolute evaluation times are in the range of a few minutes or even less.

2.2.2 Measuring Time-Complexity

Different measures have been considered to analyze the time complexity of real implementations of quantum chemical theories. The most straightforward approach to approximate the order of the polynomial is by considering a systematically enlargable model system. Ideally this is a system of molecules, such that when a molecule with an x -fold number of atoms is chosen also every other extensive parameter is scaled x -fold: the number of basis functions, electrons, and physical interactions. This means, that the molecule should be of linear shape, because otherwise the number of physical interaction cannot be proportional to the number of electrons. Furthermore, the molecules should be built from repeating building blocks and either have no boundaries or boundaries with negligible effects. A good tradeoff between chemical realism and these requirements which can never be fulfilled by any truly realistic system to arbitrary size, is the system of linear alkanes. They are built up from repeating $-\text{CH}_2-$ units and due to the very local chemistry of alkanes only very few atoms along the chain will significantly interact directly with any given atom. This means that the boundaries affect only few atoms in very long alkane chains, as required. It is important to note, that while realistic alkanes are bend and rarely of the size considered in such a complexity analysis, they must be computed like this to use them for a sensible analysis of the underlying time complexity. Otherwise, the non-linearity of the physi-

cal interactions would get entangled with the time-complexity of the implementation under scrutiny.

A gross estimate of the time complexity can be made with such systematically enlargable molecules by considering two molecules, one of double the size of the other, and comparing their respective compute times. If they differ by a factor of two as well, the implementation is said to be linear, if the factor is four, the implementation is quadratic, and so on. This is equivalent to fitting $t(M)$ for the two molecules by a monomial with adjustable exponent and dropping the coefficient afterwards. The smallest system size for which a certain order is found in this way is then considered the onset of that asymptotic time complexity.

A more accurate representation of Eq. 2.1 is illustrated in Fig. 2.2 and can be given as follows: The largest molecules are fitted by

$$f(M) = \text{mono}(M) - \Delta \quad (2.2)$$

where $\text{mono}(M)$ is again a monomial and Δ is a variable positive M -independent offset. Then $\text{mono}(M)$ is always larger than the fit $f(M)$ and therefore larger than $t(M)$ for the fitted molecule sizes and Eq. 2.1 is fulfilled for all sizes in the fitting range. The coefficient can be dropped again or the whole monomial taken as the asymptotic time complexity. The smallest size for which a fit with this size as the lower end of the fitting range is well justified can be taken as the onset of the corresponding time complexity.

To fit Eq. 2.2 and also for better clearness of display it is sometimes useful to plot double logarithmically (Fig. 2.3). For monomials cM^x this leads to straight lines with slope x and offset $\log(c)/\log(M)$. In ranges where actual time complexity is very close to a monomial the order of the polynomial can therefore be read off a graphical display with ease and fitting is more robust in cases where the scaling is not linear.

2.3 Resolution-Of-The-Identity

As all electronic structure theories aim to solve the Schrödinger equation,³ which is a differential equation, a major ingredient that appears in almost all electronic structure theories are integrals containing basis functions and (differential) operators. The number of basis function indices, or centers, defines the order of the integral tensor. The higher this order, the higher the cost of computation and storage. Here, only real-valued basis functions will be considered. The resolution-of-the-identity^{14-18,33} is an idea to reduce the number of centers that occur in an integral by replacing a single integral with tensor products of multiple integrals of lower order.

2.3.1 Overlap Metric Resolution-Of-The-Identity of Electron Repulsion Integrals

The most prominent example of RI is its use in the context of electron repulsion integrals (ERIs), here in Mulliken notation

$$(\mu\nu|\hat{V}_{ee}|\lambda\sigma) = \iint d\mathbf{x} d\mathbf{x}' \chi_\mu(\mathbf{x})\chi_\nu(\mathbf{x})V_{ee}(\mathbf{x}, \mathbf{x}')\chi_\lambda(\mathbf{x}')\chi_\sigma(\mathbf{x}') . \quad (2.3)$$

If the operator in the integral is the electron interaction operator

$$V_{ee}(\mathbf{x}, \mathbf{x}') = \frac{1}{|\mathbf{x} - \mathbf{x}'|} \quad (2.4)$$

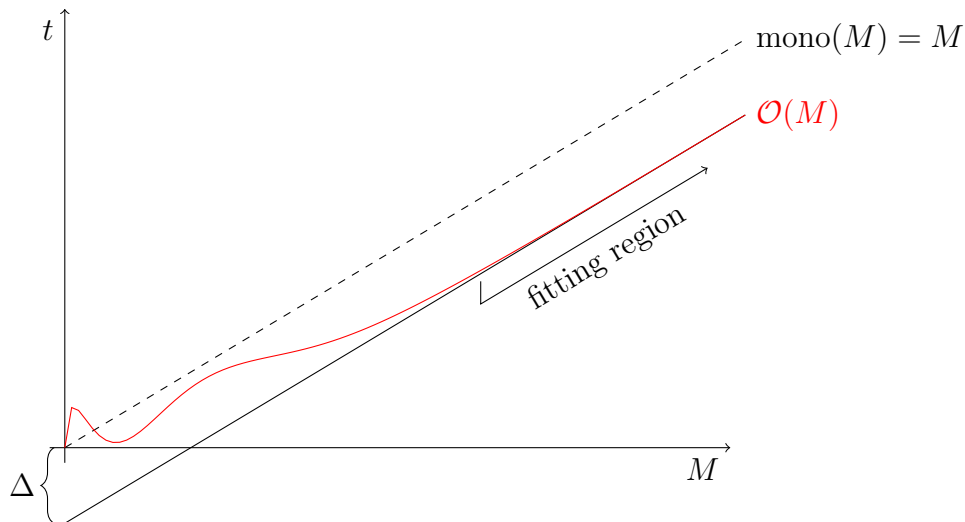


Figure 2.2: The effective scaling of an algorithm can be found by fitting the largest measured runtimes by Eq. 2.2. In this qualitative illustration the runtime behaves in a complex way up until a point when the behavior becomes essentially linear. A linear fit through all points from this point onwards predicts all points perfectly but does not pass the origin due to the complex behavior for small systems. For this reason the more simple approach fails. Shifting the fit line up by Δ however always overestimates the true runtime and is still linear. According to the Bachmann-Landau notation it is therefore $\mathcal{O}(M)$.

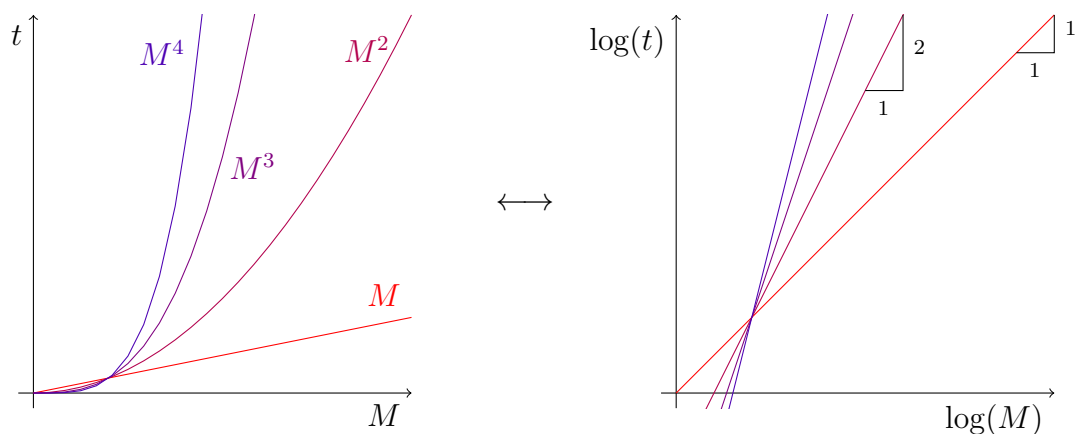


Figure 2.3: In a direct plot of runtime against system size different time-complexities can be difficult to distinguish. Double-logarithmic plots allow to read off the exponent of monomials from the slope of their plot lines.

the symbol can be dropped by convention

$$(\mu\nu|V_{ee}|\lambda\sigma) \equiv (\mu\nu|\lambda\sigma) . \quad (2.5)$$

In this section Einstein's sum convention is employed, which states that indices that appear twice in any term are implicitly summed over.⁵¹ This drastically simplifies notation of tensor contractions. As an example, for tensors of second order, i.e. matrices, the (μ, ν) -th element of the product of two matrices is simply given by

$$(\mathbf{AB})_{\mu\nu} = A_{\mu,\kappa}B_{\kappa,\nu} . \quad (2.6)$$

Matrix operations are to be taken before indexing in this work, e.g., the (μ, ν) -th element of the inverse of $(\mu\nu)$ is written as $(\mu\nu)^{-1}$.

A complete orthonormal set of states $|\Phi_n\rangle$ is defined as fulfilling

$$1 = |\Phi_n\rangle \langle \Phi_n| \quad (2.7)$$

Introduction of this resolved identity between the operator and the basis functions in Eq. 2.3 yields

$$(\mu\nu|\lambda\sigma) = (\mu\nu n)(n|m)(m\lambda\sigma) . \quad (2.8)$$

The two and three center integrals here are in consistence with Eq. 2.3 defined as

$$(\mu\nu m) = \int d\mathbf{x} \chi_\mu(\mathbf{x})\chi_\nu(\mathbf{x})\Phi_n(\mathbf{x}) \quad (2.9)$$

$$(n|m) = \int d\mathbf{x} d\mathbf{x}' \Phi_n(\mathbf{x})V_{ee}(\mathbf{x}, \mathbf{x}')\Phi_m(\mathbf{x}') . \quad (2.10)$$

Since the RI is introduced only in the vicinity of basis function products $|\mu\nu\rangle$, it is not necessary for Eq. 2.7 to represent a general identity over all space, but only over the subspace representable by such products. For Gaussian type basis sets

$$\chi_\mu(\mathbf{x}) = x^{m_\mu} y^{n_\mu} z^{l_\mu} e^{-\zeta_\mu|\mathbf{x}-\mathbf{R}_\mu|^2} \quad (2.11)$$

any such product is again a sum of Gaussian type functions because

$$e^{-\zeta_\mu|\mathbf{x}-\mathbf{R}_\mu|^2} e^{-\zeta_\nu|\mathbf{x}-\mathbf{R}_\nu|^2} = K e^{-\zeta|\mathbf{x}-\mathbf{R}|^2} \quad (2.12)$$

where

$$K = e^{\zeta|\mathbf{R}|^2 - \zeta_\mu|\mathbf{R}_\mu|^2 - \zeta_\nu|\mathbf{R}_\nu|^2} \quad (2.13)$$

$$\mathbf{R} = \frac{\zeta_\mu \mathbf{R}_\mu + \zeta_\nu \mathbf{R}_\nu}{\zeta} \quad (2.14)$$

$$\zeta = \zeta_\mu + \zeta_\nu \quad (2.15)$$

as can be seen by multiplication and comparison of the coefficients.

It would therefore be ideal if a set of Gaussian type functions could be found to be used as $|\Phi_n\rangle$ that is only complete in this restricted sense. From here on, complete will always refer to this case. As there are only a finite number of basis functions and therefore products of them for any given molecular system such a set could be finite without approximation.

Unfortunately, Gaussian type functions are not orthogonal to one another and so cannot fulfill Eq. 2.8. From a complete set of Gaussian type functions, or auxiliary (basis) functions χ_P as they will be called from here on, however, a complete orthonormal set can be constructed by Löwdin orthonormalization^{52–54}

$$|\Phi_P\rangle = |\chi_Q\rangle \langle \chi_Q | \chi_P \rangle^{-1/2} . \quad (2.16)$$

Insertion of Eq. 2.16 into Eq. 2.7 then yields for Eq. 2.8

$$(\mu\nu|\lambda\sigma) = (\mu\nu P)(PQ)^{-1}(Q|R)(RS)^{-1}(S\lambda\sigma) \quad (2.17)$$

For Eq. 2.17 to hold as an identity it is necessary for the auxiliary basis to be complete. To facilitate evaluation the auxiliary basis is typically taken to be atom-centered just as the regular basis set. It is then necessary to take very large auxiliary basis sets to still ensure completeness. Otherwise, Eq. 2.17 weakens to an approximation.

2.3.2 Density Fitting

An alternative derivation shows why such an approximation is viable. If two indices of the ERI are contracted with the density matrix, a matrix is obtained that represents the Coulomb interaction of a basis function pair with the charge density of all electrons

$$J_{\mu\nu} = (\mu\nu|\rho) = (\mu\nu|\lambda\sigma)P_{\lambda\sigma} \quad (2.18)$$

as it occurs in Hartree–Fock theory and Kohn–Sham DFT. The product pair can therefore be seen as a generalized density $\rho_{\lambda\sigma}$. Fitting this density with an incomplete set of auxiliary functions^{28–32} with coefficients $c_P^{\lambda\sigma}$

$$|\widetilde{\lambda\sigma}\rangle = c_P^{\lambda\sigma}|P\rangle \quad (2.19)$$

results in a deviation

$$\Delta\rho_{\lambda\sigma} = |\lambda\sigma\rangle - |\widetilde{\lambda\sigma}\rangle \quad (2.20)$$

which can be minimized by an appropriate choice of the coefficients.¹⁴

As the deviation is, however, still a function of space, a choice of metric has to be made to fold it into a single value which can then be minimized analytically. One approach is to take the overlap metric³³ and therefore deduce

$$0 \stackrel{!}{=} \frac{\partial}{\partial c_P^{\lambda\sigma}} (\Delta\rho_{\mu\nu} \Delta\rho_{\lambda\sigma}) \quad (2.21)$$

$$= \frac{\partial}{\partial c_P^{\lambda\sigma}} ((\Delta\rho_{\mu\nu} \rho_{\lambda\sigma}) - (\Delta\rho_{\mu\nu} P) c_P^{\lambda\sigma}) \quad (2.22)$$

$$= -(\Delta\rho_{\mu\nu} P) \quad (2.23)$$

$$= -((\mu\nu P) - c_Q^{\mu\nu}(QP)) \quad (2.24)$$

$$c_Q^{\mu\nu} = (\mu\nu P)(PQ)^{-1} \quad (2.25)$$

resulting in

$$(\mu\nu|\lambda\sigma) \approx (\widetilde{\mu\nu}|\widetilde{\lambda\sigma}) = (\mu\nu P)(PQ)^{-1}(Q|R)(RS)^{-1}(S\lambda\sigma) . \quad (2.26)$$

Because the deviation is in this case minimal in the overlap metric sense, Eq. 2.17 is titled overlap metric RI throughout this work.

Another metric which has been found to be optimal³³ for the evaluation of Eq. 2.18 is the choice of Coulomb metric

$$0 \stackrel{!}{=} \frac{\partial}{\partial c_P^{\lambda\sigma}} (\Delta\rho_{\mu\nu} | \Delta\rho_{\lambda\sigma}) \quad (2.27)$$

which accordingly leads to

$$(\mu\nu | \lambda\sigma) \approx (\widetilde{\mu\nu} | \widetilde{\lambda\sigma}) = (\mu\nu | P)(P|Q)^{-1}(Q | \lambda\sigma) . \quad (2.28)$$

The fitting approach applies in this form only to the special case of ERIs. It has been argued for the final equation to be identified as density fitting (DF) instead of RI.²² In the third publication of this work the derivation is carried out with the attenuated Coulomb metric in mind and it is shown in the accompanying supporting information that Eq. 2.28 can also be derived from the point of view of RI by expressing the complete orthonormal basis again in a complete non-orthogonal basis. The essential difference between RI and DF is then, that the RI can also be found in more general contexts and argues from the point of view of complete basis sets while the DF is mostly restricted to ERIs and argues from the point of incomplete basis sets.

2.4 Random Phase Approximation

The RPA⁵ can be derived within different contexts of electronic structure theory. Here, a derivation is given that employs Feynman–Dyson perturbation theory^{55–58} also known as Green’s function theory, for which Fetter and Walecka have written a very comprehensive account.⁵⁹ The essential results of Feynman–Dyson perturbation theory are restated in Sec. 2.4.1 and the RPA is rigorously derived from these in the succeeding sections.

2.4.1 Important Results from Green’s Function Theory

Second Quantization

Kohn–Sham DFT constructs a Fock operator \hat{F}_{KS} , so that the sum of squared eigenfunctions φ_p , fulfilling

$$\hat{F}_{KS}\varphi_p(x) = \varepsilon_p\varphi_p(x) \quad (2.29)$$

reproduces the exact density of the interacting system

$$n(x) = \sum_i |\varphi_i(x)|^2 \quad (2.30)$$

The orbital energies ε_p can generally be sorted in non-descending order and the indices $[1, \dots, N_{el}]$ are called occupied and all others unoccupied or virtual. Here and throughout this work sums over p, q, \dots run over all indices, i, j, \dots over the occupied indices, and a, b, \dots over the virtual indices. Also, Einstein’s sum convention⁵¹ is generalized from here on: Indices that appear twice within a term are implicitly summed over and coordinates that appear twice are implicitly integrated over.

The one particle Fock eigenfunctions φ_p can be combined into antisymmetrized products, called Slater determinants⁶⁰ that are then N_{el} -particle functions

$$\langle x_1 x_2 \cdots x_{N_{el}} | \varphi_p \varphi_q \cdots \varphi_r \rangle := \left(\frac{1}{N_{el}!} \right)^{1/2} \begin{vmatrix} \varphi_p(x_1) & \cdots & \varphi_p(x_1) \\ \vdots & \ddots & \vdots \\ \varphi_r(x_{N_{el}}) & \cdots & \varphi_r(x_{N_{el}}) \end{vmatrix} \quad (2.31)$$

To derive a correction to the Kohn–Sham DFT result it is useful to describe the theory in the basis of Slater determinants—which combined cover the space of all antisymmetrized wavefunctions. The non-relativistic second quantization formalism^{62–64} allows for a particularly straightforward derivation of the following results. In second quantization each Slater determinant is associated with a Fock state, which is an eigenstate of the number operator

$$\hat{n}_p = \hat{a}_p^\dagger \hat{a}_p \quad (2.32)$$

where \hat{a}_p^\dagger is the creation operator for the p -th one-particle function and \hat{a}_p the corresponding annihilation operator. The mode operators \hat{a}^\dagger and \hat{a} are defined by the canonical anticommutation relations

$$\{\hat{a}_p, \hat{a}_q^\dagger\} = \delta_{pq} \quad (2.33)$$

$$\{\hat{a}_p, \hat{a}_q\} = \{\hat{a}_p^\dagger, \hat{a}_q^\dagger\} = 0 \quad (2.34)$$

and can further be linearly combined into field operators

$$\hat{\psi}(x) = \varphi_p(x) \hat{a}_p \quad (2.35)$$

to allow for formulations in real space instead of mode space. This also allows for a very simple description of operators in second quantization, by integration of their matrix elements in space-representation with the corresponding field creation operators to the left and field annihilation operators to the right, e.g.

$$\hat{V}_{ee} = \hat{\psi}^\dagger(x) \hat{\psi}^\dagger(x') V_{ee}(x, x') \hat{\psi}(x') \hat{\psi}(x) . \quad (2.36)$$

Interaction Picture

The exact ground state of the full interacting Hamiltonian \hat{H} is defined by

$$\hat{H} |\Psi\rangle = E |\Psi\rangle . \quad (2.37)$$

In the Schrödinger picture the states $|\Psi(t)\rangle$ are time-dependent. Only in the Heisenberg picture, where all time-dependence is shifted to the operators can Eq. 2.37 truly be considered the time-independent Schrödinger equation. Because the time-dependence can be expressed by an operator that is due to the Hamiltonian and therefore trivially commutes with it, the time-dependence of \hat{H} vanishes. As Eq. 2.37 can in general not be solved exactly, one resorts to

$$\hat{H}_0 |\Phi\rangle = E_0 |\Phi\rangle \quad (2.38)$$

where \hat{H}_0 is given by

$$\hat{H}_0 = \sum \hat{F}_{KS} = \hat{h} + v \quad (2.39)$$

with the one-particle operator \hat{h} and the Kohn–Sham potential v , so that $|\Phi\rangle$ is the ground state Slater determinant. $|\Phi\rangle$ is only time-independent in a universe that is completely described by \hat{H}_0 —a universe in which all particles are non-interacting. In a universe that is described by \hat{H} , however, $|\Phi\rangle$ develops with time.

The interaction picture shifts only the time-dependence due to \hat{H}_0 into the operators and keeps the other time-dependence due to the then time-dependent interaction

$$\hat{H}_1(t) := \hat{H}(t) - \hat{H}_0 \quad (2.40)$$

with the state. The state then propagates due to the time propagation operator⁶¹ $\hat{U}(t, t_0)$

$$|\Phi(t)\rangle =: \hat{U}(t, t_0) |\Phi(t_0)\rangle . \quad (2.41)$$

Gell-Mann–Low Theorem

The key idea to the Gell-Mann–Low theorem⁶⁵ is to consider an adiabatic process of switching on the interaction \hat{H}_1 in the universe adiabatically slowly

$$\hat{H} = \hat{H}_0 + e^{-\epsilon|t|} \hat{H}_1 , \quad (2.42)$$

where ϵ is send to zero later. This means, that at finite times (around $t = 0$) the universe behaves due to the physical, i.e. interacting, Hamiltonian \hat{H} . On the other hand, at infinitely early and late times the universe behaves according to the non-interacting Hamiltonian \hat{H}_0 and the exact ground state is therefore known for these points in time. In this picture, the time propagation operator is explicitly obtained as

$$\hat{U}(t, t_0) = \sum_{n=0}^{\infty} \frac{(-i)^n}{n!} \int_{t_0}^t dt_1 \cdots \int_{t_0}^t dt_n \mathbb{T} [\hat{H}_1(t_1) \cdots \hat{H}_1(t_n)] \quad (2.43)$$

$$\equiv \mathbb{T} \left[e^{-i \int_{t_0}^t dt' \hat{H}_1(t')} \right] \quad (2.44)$$

with the time-ordering operation $\mathbb{T}[\cdots]$. A product of operators $\hat{O}_1(t)\hat{O}_2(t')$ is said to be time ordered if $t > t'$ and the time-ordering operation permutes its argument into time order. Depending on the number of permutations the global sign changes under this operation.

With the time propagation operator defined by Eq. 2.44, the Gell-Mann–Low theorem⁶⁵ states that if

$$\lim_{\epsilon \rightarrow 0} \frac{\hat{U}_\epsilon(0, \pm\infty) |\Phi\rangle}{\langle \Phi | \hat{U}_\epsilon(0, \pm\infty) | \Phi \rangle} \equiv \frac{|\Psi\rangle}{\langle \Phi | \Psi \rangle} \quad (2.45)$$

exists to all orders of perturbation theory, it is an eigenstate (usually the ground state) of the exact Hamiltonian.

$$\hat{H} \frac{|\Psi\rangle}{\langle \Phi | \Psi \rangle} = E \frac{|\Psi\rangle}{\langle \Phi | \Psi \rangle} \quad (2.46)$$

Wick Theorem

To evaluate expectation values due to this interacting ground state it is useful to observe that for a Heisenberg operator $\hat{O}_H(t)$

$$\frac{\langle \Psi | \hat{O}_H(t) | \Psi \rangle}{\langle \Psi | \Psi \rangle} = \frac{1}{\langle \Phi | \hat{S} | \Phi \rangle} \sum_n \frac{(-i)^n}{n!} \int_{-\infty}^{\infty} \cdots \int_{-\infty}^{\infty} \langle \Phi | \mathbb{T} [\hat{H}_1(t_1) \cdots \hat{H}_1(t_n) \hat{O}_I(t)] | \Phi \rangle \quad (2.47)$$

where

$$\hat{S} = \hat{U}(\infty, -\infty) \quad (2.48)$$

and \hat{O}_I is the same operator chain in the interaction picture. This result extends naturally when a time-ordered chain of operators is used instead of $\hat{O}_H(t)$.

Besides time-order introduced above, another useful order of operators is normal order, and $N[\dots]$ is the corresponding normal-ordering operation. A chain of operators is said to be normal ordered if the $|\Phi\rangle$ expectation value of it vanishes, so

$$\langle \Phi | N [\hat{O}_1 \hat{O}_2 \dots] | \Phi \rangle = 0. \quad (2.49)$$

Combined the two ordering operations allow to define the contraction of two operators

$$\overline{\hat{O}_1 \hat{O}_2} := T [\hat{O}_1 \hat{O}_2] - N [\hat{O}_1 \hat{O}_2] \quad (2.50)$$

While time ordering and normal ordering affect whole operator chains, each contraction affects only two operators. Wick's Theorem⁶⁶ thus allows to evaluate the time-ordered chain in Eq. 2.47 by stating that a time-ordered chain of operators is equal to the sum of normal-ordering of all possible contractions over the chain

$$\begin{aligned} T [\hat{O}_1 \hat{O}_2 \hat{O}_3 \dots] &= N \left[\overline{\hat{O}_1 \hat{O}_2} \hat{O}_3 \dots \right] + N \left[\overline{\hat{O}_1 \hat{O}_2 \hat{O}_3} \dots \right] + \dots \\ &+ N \left[\overline{\hat{O}_1 \hat{O}_2} \overline{\hat{O}_3 \dots} \right] + \dots \\ &+ \dots \end{aligned} \quad (2.51)$$

Because the time-ordered product in Eq. 2.47 occurs between $|\Phi\rangle$, all incomplete contractions vanish trivially (cmp. Eq. 2.49). Wick's theorem reduces the problem of evaluating an expectation value of the interacting ground state to summing up a series of terms consisting only of products of contractions.

Green's Function

The most important contraction in second quantization is the non-interacting Green's function, also called propagator,⁶⁷⁻⁶⁹ which is the contraction of a field destruction and field creation operator.

$$iG_0(x, x') := \langle \Phi | T [\hat{\psi}(x) \hat{\psi}^\dagger(x')] | \Phi \rangle \quad (2.52)$$

$$= \langle \Phi | T [\hat{\psi}(x) \hat{\psi}^\dagger(x')] - N [\hat{\psi}(x) \hat{\psi}^\dagger(x')] | \Phi \rangle \quad (2.53)$$

$$= \langle \Phi | \overline{\hat{\psi}(x) \hat{\psi}^\dagger(x')} | \Phi \rangle \quad (2.54)$$

$$= \hat{\psi}(x) \hat{\psi}^\dagger(x') \quad (2.55)$$

The index zero denotes that the expectation value is to be taken with respect to $|\Phi\rangle$ which is the non-interacting ground state of \hat{H}_0 . The interacting Green's function is accordingly defined as

$$iG(x, x') := \frac{\langle \Psi | T [\hat{\psi}(x) \hat{\psi}^\dagger(x')] | \Psi \rangle}{\langle \Psi | \Psi \rangle} \quad (2.56)$$

and can be evaluated according to Eq. 2.47.

Feynman Diagrams

Eqs. 2.47 and 2.51 are still unwieldy to work with. To allow for a more accessible notation, Feynman put forward the idea of writing diagrams to represent the respective terms.^{55,56} Each diagram consists of nodes and lines between them. The nodes correspond to points in space-time. A non-interacting Green's function $iG_0(x, x')$ is represented by a curved or straight line with an arrow pointing from the x' to the x position.

$$iG_0(x, x') = \begin{array}{c} x \qquad \qquad x' \\ \bullet \text{---} \longleftarrow \bullet \end{array} \quad (2.57)$$

The matrix element of the bare Coulomb interaction $V_{ee}(x, x')$ is represented by a wiggly line connecting x and x'

$$V_{ee}(x, x') = \begin{array}{c} x \qquad \qquad x' \\ \bullet \text{---} \text{~~~~~} \text{---} \bullet \end{array} \quad (2.58)$$

and the one-particle potential $v(x)$ can be represented by a cross.

$$v(x) = \begin{array}{c} x \\ \times \end{array} \quad (2.59)$$

By convention, all positions corresponding to inner nodes are integrated over all space-time. As stated above, all operators have to be contracted for the complete term not to vanish so all non-vanishing terms can be described by such diagrams. The denominator of Eq. 2.47, $\langle \Phi | \hat{S} | \Phi \rangle$ exactly cancels all parts of diagrams that are not connected to \hat{O}_I , so the expectation value can be evaluated from just considering all ‘‘connected’’ diagrams

$$\langle \Psi | \hat{O}_I | \Psi \rangle_C \quad (2.60)$$

2.4.2 Adiabatic Connection

The most straightforward way to evaluate the exact energy within Green's function theory follows from the Gell-Mann–Low theorem as

$$E = \frac{\langle \Psi | \hat{H} | \Psi \rangle}{\langle \Psi | \Psi \rangle} = \frac{\langle \Psi | \hat{H} | \Psi \rangle}{\langle \Phi | \hat{S} | \Phi \rangle} = \langle \Psi | \hat{H} | \Psi \rangle_C \quad (2.61)$$

The exact Hamiltonian \hat{H} , however, is the sum of two different operators, \hat{h} and \hat{V}_{ee} , which leads to two types of diagrams. A much simpler formulation can be derived by the adiabatic connection (AC). The AC continuates the transition from the non-interacting to the interacting system to cancel the \hat{h} -containing diagrams. It does so by introduction of an intermediary integration that will be carried out explicitly later.

Because \hat{H}_0 also contains \hat{h} one may be inclined to compute

$$E - E_0 = \langle \Psi | \hat{H} | \Psi \rangle_C - \langle \Phi | \hat{H}_0 | \Phi \rangle \quad (2.62)$$

$$= \langle \Psi | \hat{h} + \hat{V}_{ee} | \Psi \rangle_C - \langle \Phi | \hat{h} + v | \Phi \rangle \quad (2.63)$$

because E_0 is simply computed from the preceding DFT calculation as

$$E_0 := \langle \Phi | \hat{H}_0 | \Phi \rangle = \sum_i \varepsilon_i . \quad (2.64)$$

However, the one particle operator can not be cancelled in this approach, because its expectation value is to be taken with respect to different states.

The AC solves this by introducing a continuous transition from the non-interacting \hat{H}_0 to the interacting \hat{H} via intermediary \hat{H}_λ defined as

$$\hat{H}_\lambda = \hat{h} + \lambda \hat{V}_{ee} + v_\lambda \quad (2.65)$$

where v_λ is a one particle potential that is constructed such that the same density is obtained with any value for λ . Specifically, this means that v_1 has to vanish and $v_0 = v$ is the Kohn-Sham potential. $\hat{H}_{\lambda=0}$ then reproduces the non-interacting Kohn-Sham Hamiltonian \hat{H}_0 and $\hat{H}_{\lambda=1}$ the full interacting Hamiltonian \hat{H} . This process is orthogonal to the adiabatic switching-on that builds the basis of Green's function theory (cmp. Fig. 2.4).

AC allows to eliminate the λ independent part \hat{h} as

$$E - E_0 = \int_0^1 d\lambda \frac{\partial}{\partial \lambda} \langle \Psi^\lambda | \hat{H}_\lambda | \Psi^\lambda \rangle_C \quad (2.66)$$

$$= \int_0^1 d\lambda \langle \Psi^\lambda | \frac{\partial \hat{H}_\lambda}{\partial \lambda} | \Psi^\lambda \rangle_C \quad (2.67)$$

$$= \int_0^1 d\lambda \langle \Psi^\lambda | \hat{V}_{ee} + \frac{\partial v_\lambda}{\partial \lambda} | \Psi^\lambda \rangle_C \quad (2.68)$$

where

$$\hat{H}_\lambda | \Psi^\lambda \rangle = E_\lambda | \Psi^\lambda \rangle \quad (2.69)$$

has been used with the Hellmann-Feynman theorem

$$\frac{\partial}{\partial \lambda} \langle \Psi^\lambda | \hat{H}_\lambda | \Psi^\lambda \rangle = (\partial_\lambda \langle \Psi^\lambda |) \underbrace{\hat{H}_\lambda | \Psi^\lambda \rangle}_{=| \Psi^\lambda \rangle E_\lambda} + \underbrace{\langle \Psi^\lambda | \hat{H}_\lambda (\partial_\lambda | \Psi^\lambda \rangle)}_{=E_\lambda \langle \Psi^\lambda |} + \langle \Psi^\lambda | \frac{\partial \hat{H}_\lambda}{\partial \lambda} | \Psi^\lambda \rangle \quad (2.70)$$

$$= E_\lambda \underbrace{(\partial_\lambda \langle \Psi^\lambda | \Psi^\lambda \rangle)}_{=0} + \langle \Psi^\lambda | \frac{\partial \hat{H}_\lambda}{\partial \lambda} | \Psi^\lambda \rangle \quad (2.71)$$

$$= \langle \Psi^\lambda | \frac{\partial \hat{H}_\lambda}{\partial \lambda} | \Psi^\lambda \rangle \quad (2.72)$$

with $|\Psi^\lambda\rangle$ as a shorthand for $\frac{|\Psi^\lambda\rangle}{\langle \Psi^\lambda | \Psi^\lambda \rangle^{1/2}}$ to simplify notation.

Because v_λ is a one-particle potential term and therefore multiplicative and the density is kept fixed along the λ integration by construction (Eq. 2.65), the second summand in Eq. 2.68 can be simplified

$$\int_0^1 d\lambda \langle \Psi^\lambda | \frac{\partial v_\lambda}{\partial \lambda} | \Psi^\lambda \rangle_C = \int_0^1 d\lambda \int dx n(x) \frac{\partial v_\lambda}{\partial \lambda}(x) \quad (2.73)$$

$$= \int dx n(x) (v_1(x) - v_0(x)) \quad (2.74)$$

$$= -\langle \Phi | v | \Phi \rangle \quad (2.75)$$

because as stated above v_1 has to vanish by construction and $v_0 = v$.

While this approach has eliminated the \hat{h} -dependence it has introduced a dependence on v . This can however simply be remedied by changing the reference point from E_0 in Eq. 2.68 to

$$E_\Phi = \langle \Phi | \hat{H} | \Phi \rangle \quad (2.76)$$

which is almost as simple to compute from the preceding DFT calculation by using the Kohn–Sham Slater determinant to evaluate the energy by a Hartree-Fock step. This energy difference is commonly known as the correlation energy E^C within the AC

$$E^C := E - E_\Phi = E - \langle \Phi | \hat{H}_0 + \hat{H}_1 | \Phi \rangle \quad (2.77)$$

$$= E - E_0 - \langle \Phi | \hat{V}_{ee} - v | \Phi \rangle \quad (2.78)$$

$$= \int_0^1 d\lambda \langle \Psi^\lambda | \hat{V}_{ee} | \Psi^\lambda \rangle_C - \langle \Phi | v | \Phi \rangle - \langle \Phi | \hat{V}_{ee} - v | \Phi \rangle \quad (2.79)$$

$$= \int_0^1 d\lambda \langle \Psi^\lambda | \hat{V}_{ee} | \Psi^\lambda \rangle_C - \langle \Phi | \hat{V}_{ee} | \Phi \rangle \quad (2.80)$$

This result is often considered synonymic to the concept with which it was derived as the AC.

Eq. 2.80 requires the evaluation of the expectation value of \hat{V}_{ee} with respect to the interacting groundstate with interaction strength λ ,

$$\langle \hat{V}_{ee} \rangle_\lambda = \frac{\langle \Psi^\lambda | \hat{V}_{ee} | \Psi^\lambda \rangle}{\langle \Psi^\lambda | \Psi^\lambda \rangle} = \frac{1}{2} V_{ee}(x, x') \langle \hat{\psi}^\dagger(x) \hat{\psi}^\dagger(x') \hat{\psi}(x') \hat{\psi}(x) \rangle_\lambda \quad (2.81)$$

which can be transformed into time-ordered terms by the canonical commutation relations

$$\langle V_{ee} \rangle_\lambda = \frac{1}{2} V_{ee}(x, x') (\langle \hat{n}(x) \hat{n}(x') \rangle_\lambda - \delta(x - x') n(x)) \quad (2.82)$$

$$= \frac{1}{2} V_{ee}(x, x') (\langle \tilde{n}(x) \tilde{n}(x') \rangle_\lambda + n(x) n(x') - \delta(x - x') n(x)) \quad (2.83)$$

where the terms that only depend on the λ -independent density have been separated off by introducing the density fluctuation operator

$$\tilde{n}(x) = \hat{n}(x) - n(x) . \quad (2.84)$$

This reduces Eq. 2.80 to

$$E^C = \int_0^1 d\lambda \frac{1}{2} V_{ee}(x, x') (\langle \tilde{n}(x) \tilde{n}(x') \rangle_\lambda - \langle \tilde{n}(x) \tilde{n}(x') \rangle_0) . \quad (2.85)$$

2.4.3 Polarization Propagator and Random Phase Approximation

Polarization Propagator

The correlation energy within the AC (Eq. 2.85) depends on the expectation value of the time-ordered product of density fluctuation operators.

$$\langle \tilde{n}(x) \tilde{n}(x') \rangle_\lambda = \frac{\langle \Psi^\lambda | \text{T} [\tilde{n}(x) \tilde{n}(x')] | \Psi^\lambda \rangle}{\langle \Psi^\lambda | \Psi^\lambda \rangle} =: i\Pi_\lambda(x, x') \quad (2.86)$$

This bears great resemblance with the Green's function⁵⁵⁻⁵⁸ or propagator (Eq. 2.56) which is the expectation value of time-ordered field operators. $\Pi(x, x')$ is therefore known as the polarization propagator⁵⁹ and the constant prefactor i chosen for convenience. Eq. 2.85 can now be written as

$$E^C = \frac{1}{2} \int_0^1 d\lambda (i\Pi_\lambda(x', x) - i\Pi_0(x', x)) V_{ee}(x, x') \quad (2.87)$$

because $i\Pi$ (the matrix of which $i\Pi(x, x')$ is the (x, x') -th matrix element) is symmetric.

Dyson's Equation

When evaluating $i\Pi$ (Eq. 2.86) with the Feynman rules it is important to note that

$$\text{T} \left[\hat{H}_1 \hat{H}_1 \cdots \hat{H}_1 \tilde{n}(x) \tilde{n}(x') \right] = \text{T} \left[\hat{H}_1 \hat{H}_1 \cdots \hat{H}_1 \left(\underbrace{\hat{\psi}^\dagger(x) \hat{\psi}(x)}_{=n(x)} - n(x) \right) \tilde{n}(x') \right] = 0 \quad (2.88)$$

so that diagrams with internal contractions at x and x' exactly cancel the terms containing the corresponding density $n(x)$ or $n(x')$ respectively.

$$\begin{array}{c} \circlearrowleft \\ \bullet \\ x \end{array} = n(x) \quad (2.89)$$

$i\Pi_0$ is therefore obtained as

$$i\Pi_0(x, x') = \begin{array}{c} \bullet \\ x' \\ \curvearrowright \\ \bullet \\ x \end{array} = -iG_0(x, x')G_0(x', x) \quad (2.90)$$

and the interacting polarization propagator is given by

$$i\Pi_\lambda(x, x') = \begin{array}{c} \bullet \\ x' \\ \curvearrowright \\ \bullet \\ x \end{array} + \lambda \left[\begin{array}{c} \bullet \\ x' \\ \curvearrowright \\ \bullet \\ \text{---} \\ \bullet \\ \text{---} \\ \bullet \\ x \end{array} + \underbrace{\begin{array}{c} \bullet \\ x' \\ \curvearrowright \\ \bullet \\ \text{---} \\ \bullet \\ \text{---} \\ \bullet \\ x \end{array}}_J + \underbrace{\begin{array}{c} \bullet \\ x' \\ \curvearrowright \\ \bullet \\ \text{---} \\ \bullet \\ \text{---} \\ \bullet \\ x \end{array}}_X + \underbrace{\begin{array}{c} \bullet \\ x' \\ \curvearrowright \\ \bullet \\ \text{---} \\ \bullet \\ \text{---} \\ \bullet \\ \text{---} \\ \bullet \\ \text{---} \\ \bullet \\ x \end{array}}_C + \begin{array}{c} \bullet \\ x' \\ \curvearrowright \\ \bullet \\ \text{---} \\ \bullet \\ \text{---} \\ \times \\ \bullet \\ x \end{array} \right] + \mathcal{O}(\hat{H}_1^2) \quad (2.91)$$

Random Phase Approximation

The RPA is defined by neglecting all terms with exact exchange (X) or Kohn–Sham correlation (C) type interaction in the polarization propagator. However all Coulomb (J) type integrals are kept to infinite order.

The λ -integration introduced with the AC can now be carried out term by term and the scaled terms collected into a closed expression afterwards. Yet, an even more elegant derivation can be given by using Dyson's scheme^{57,58} to collect the terms first.

$$i\Pi_\lambda = \text{blob} = \text{loop} + \text{loop} \text{ with } \lambda \text{ wavy line} + \text{loop with } 2 \text{ } \lambda \text{ wavy lines} + \dots \quad (2.92)$$

$$= \text{loop} + \text{loop with } \lambda \text{ wavy line} \text{ connected to blob} \quad (2.93)$$

$$i\Pi_\lambda = i\Pi_0 + (i\Pi_0)\lambda\mathbf{V}_{ee}(i\Pi_\lambda) \quad (2.94)$$

$$(1 - i\Pi_0\lambda\mathbf{V}_{ee})i\Pi_\lambda = i\Pi_0 \quad (2.95)$$

$$i\Pi_\lambda = (1 - i\Pi_0\lambda\mathbf{V}_{ee})^{-1}i\Pi_0 \quad (2.96)$$

Eq. 2.96, or Dyson's equation for short, allows for a very simple evaluation of the λ -integral as

$$\int_0^1 d\lambda (1 - \lambda i\Pi_0\mathbf{V}_{ee})^{-1}i\Pi_0 = -\log(1 - i\Pi_0\mathbf{V}_{ee})(i\Pi_0\mathbf{V}_{ee})^{-1}i\Pi_0 \quad (2.97)$$

and the first term in the correlation energy (Eq. 2.87) thus simplifies to

$$\int_0^1 d\lambda \text{Tr} \{i\Pi_\lambda\mathbf{V}_{ee}\} = -\text{Tr} \{\log(1 - i\Pi_0\mathbf{V}_{ee})\} . \quad (2.98)$$

The second term in Eq. 2.87 is independent of λ and the integral therefore trivially evaluated. This renders the correlation energy as

$$E^C = -\frac{1}{2}\text{Tr} \{\log(1 - i\Pi_0\mathbf{V}_{ee}) + i\Pi_0\mathbf{V}_{ee}\} . \quad (2.99)$$

2.4.4 Evaluation of $i\Pi_0$ by Lehmann's Representation

Up until this point all (Heisenberg) operators have depended on both space and time $x = (\mathbf{x}, t)$. This makes evaluation of $i\Pi_0$ in Eq. 2.99 difficult as it necessarily is inherently time-dependent. As the (interacting) Hamiltonian is not explicitly time-dependent, however, the final result can not be time-dependent and all operators can at most depend on time-differences. This can be exposed by Fourier transformation which is sometimes referred to as Lehmann's representation.⁷⁰

Extraction of the time-dependence

To derive the Fourier transform of $i\Pi_0$ it is necessary to express the time-ordering operation by the Heaviside θ -function

$$\theta(t - t') = \begin{cases} 1 & | \quad t > t' \\ 0 & | \quad t' > t \end{cases} \quad (2.100)$$

Eq. 2.90 then becomes

$$i\Pi_0(x, x') = \theta(t - t') \langle \Phi | \tilde{n}(x) \tilde{n}(x') | \Phi \rangle + \theta(t' - t) \langle \Phi | \tilde{n}(x') \tilde{n}(x) | \Phi \rangle \quad (2.101)$$

As the density fluctuation operators are Heisenberg operators, their time-dependence is given by

$$\tilde{n}(x) = e^{i\hat{H}t} \tilde{n}(\mathbf{x}) e^{-i\hat{H}t} \quad (2.102)$$

and by a resolution-of-the-identity

$$1 = |\Phi_n\rangle \langle \Phi_n| \quad (2.103)$$

the following expression is obtained

$$\begin{aligned} i\Pi_0(x, x') &= \theta(t - t') \langle \Phi | e^{iEt} \tilde{n}(\mathbf{x}) e^{-iE_n t} | \Phi_n \rangle \langle \Phi_n | e^{iE_n t'} \tilde{n}(\mathbf{x}') e^{-iE t'} | \Phi \rangle \\ &\quad + \theta(t' - t) \langle \Phi | e^{iE t'} \tilde{n}(\mathbf{x}') e^{-iE_n t'} | \Phi_n \rangle \langle \Phi_n | e^{iE_n t} \tilde{n}(\mathbf{x}) e^{-iE t} | \Phi \rangle \end{aligned} \quad (2.104)$$

$$\begin{aligned} &= \theta(t - t') e^{-i(E_n - E)(t - t')} \langle \Phi | \tilde{n}(\mathbf{x}) | \Phi_n \rangle \langle \Phi_n | \tilde{n}(\mathbf{x}') | \Phi \rangle \\ &\quad + \theta(t' - t) e^{i(E_n - E)(t - t')} \langle \Phi | \tilde{n}(\mathbf{x}') | \Phi_n \rangle \langle \Phi_n | \tilde{n}(\mathbf{x}) | \Phi \rangle \end{aligned} \quad (2.105)$$

The sum in Eq. 2.103 runs over a complete set of states in principle. But as the density fluctuation operator is number conserving (it commutes with the number operator) the sum can be restricted to states containing the same number of particles as $|\Phi\rangle$ in Eq. 2.105, and so the set consisting of $|\Phi\rangle$ and all its excitations is a viable choice.

Lehmann's Representation

Having extracted the time-dependence as a multiplicative function, Fourier transformation can be carried out to obtain Lehmann's representation of $i\Pi^0$. To this end it is helpful to convince oneself that the Heaviside function has the following integral representation

$$\theta(t - t') = - \int_{-\infty}^{\infty} \frac{d\kappa}{2\pi i} \frac{e^{-i\kappa(t-t')}}{\kappa + i\eta} \quad (2.106)$$

where η tends to zero, as can be seen from the residue theorem

$$\int_{\Gamma} f = 2\pi i \sum_{a \in A(\Gamma)} Res_a f \quad (2.107)$$

where Γ is a closed counter-clockwise path in the complex plane that does not cross itself and $A(\Gamma)$ is the area enclosed by this path (cmp. Fig. 2.5). Similarly it is straightforward to show that

$$\int_{-\infty}^{\infty} \frac{1}{2\pi} e^{i\kappa t} dt = \delta(\kappa) . \quad (2.108)$$

With Eqs. 2.105, 2.106, and 2.108 the Fourier transform of the polarization propagator is given by

$$\Pi_0(\mathbf{x}, \mathbf{x}', \omega) := \int d(t-t') e^{i\omega(t-t')} \Pi_0(\mathbf{x}, \mathbf{x}', t-t') \quad (2.109)$$

$$= i \int d(t-t') e^{i\omega(t-t')} \left(\int_{-\infty}^{\infty} \frac{d\kappa}{2\pi i} \frac{e^{-i\kappa(t-t')}}{\kappa + i\eta} e^{-i(E_n - E)(t-t')} \langle \Phi | \tilde{n}(\mathbf{x}) | \Phi_n \rangle \langle \Phi_n | \tilde{n}(\mathbf{x}') | \Phi \rangle \right. \\ \left. + \int_{-\infty}^{\infty} \frac{d\kappa}{2\pi i} \frac{e^{i\kappa(t-t')}}{\kappa + i\eta} e^{i(E_n - E)(t-t')} \langle \Phi | \tilde{n}(\mathbf{x}') | \Phi_n \rangle \langle \Phi_n | \tilde{n}(\mathbf{x}) | \Phi \rangle \right) \quad (2.110)$$

$$= \int d\kappa \left(\delta(\omega - (E_n - E) - \kappa) \frac{\langle \Phi | \tilde{n}(\mathbf{x}) | \Phi_n \rangle \langle \Phi_n | \tilde{n}(\mathbf{x}') | \Phi \rangle}{\kappa + i\eta} \right. \\ \left. + \delta(\omega + (E_n - E) + \kappa) \frac{\langle \Phi | \tilde{n}(\mathbf{x}') | \Phi_n \rangle \langle \Phi_n | \tilde{n}(\mathbf{x}) | \Phi \rangle}{\kappa + i\eta} \right) \quad (2.111)$$

$$= \frac{\langle \Phi | \tilde{n}(\mathbf{x}) | \Phi_n \rangle \langle \Phi_n | \tilde{n}(\mathbf{x}') | \Phi \rangle}{\omega - (E_n - E) + i\eta} - \frac{\langle \Phi | \tilde{n}(\mathbf{x}') | \Phi_n \rangle \langle \Phi_n | \tilde{n}(\mathbf{x}) | \Phi \rangle}{\omega + (E_n - E) - i\eta} \quad (2.112)$$

Replacing $\mathbf{\Pi}_0$ in Eq. 2.99 by reverse Fourier transformation

$$\Pi_0(\mathbf{x}, \mathbf{x}', t-t') = \frac{1}{2\pi} \int d\omega \Pi^0(\mathbf{x}, \mathbf{x}', \omega) e^{-i\omega(t-t')} \quad (2.113)$$

the Fourier factors cancel

$$e^{-i\omega(t-t')} e^{-i\omega(t'-t'')} \dots e^{-i\omega(t^{(n)}-t)} = 1 . \quad (2.114)$$

Therefore the time-dependence of $i\mathbf{\Pi}_0$ in the correlation energy (Eq. 2.99) can be accounted for with a simple frequency integration.

$$E^C = -\frac{1}{2} \frac{1}{2\pi} \int d\omega \text{Tr} \{ \log(1 - i\mathbf{\Pi}_0(\omega) \mathbf{V}_{ee}) + i\mathbf{\Pi}_0(\omega) \mathbf{V}_{ee} \} \quad (2.115)$$

where $i\mathbf{\Pi}_0(\omega)$ can be evaluated according to Eq. 2.112.

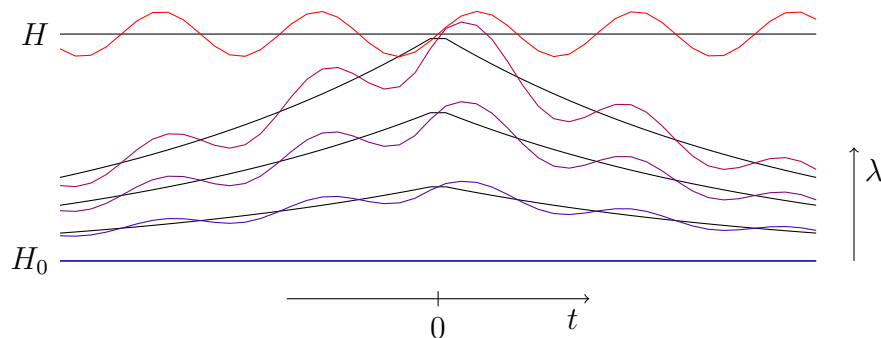


Figure 2.4: The adiabatic connection is orthogonal to the adiabatic interaction of the Gell-Mann–Low theorem. The time-dependence of Hamiltonians in the interaction picture is depicted here by fluctuations around the respective baselines. The non-interacting Hamiltonian is constant in time by construction and the full-interacting Hamiltonian is time-dependent throughout time, rendering solvation for its eigenstates difficult. Within the Gell-Mann–Low description the eigenstates are found for the non-interacting Hamiltonian and propagated due to a Hamiltonian that interpolates from the non-interacting to the interacting Hamiltonian infinitely slowly, so that the fully interacting solution is found for $t = 0$. The adiabatic connection considers this process infinitely many times, following this process to various continuous degrees of physical interaction.

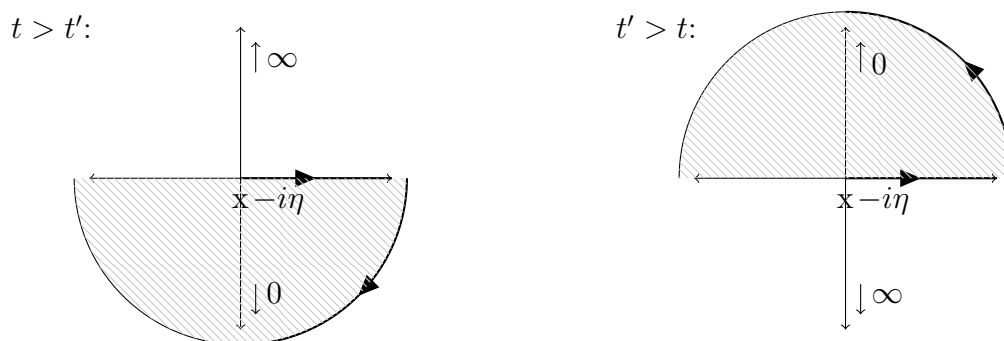


Figure 2.5: The Heaviside θ -function can be expressed according to Eq. 2.106. The denominator gives rise to a first-order pole at $-i\eta$ in the lower complex half-plane. When $t > t'$ the numerator tends to zero when the argument tends to $-i\infty$ and the integration contour can be closed over the lower half-plane to yield 1 by the residue theorem. Correspondingly, when $t' > t$ the integral has to be closed over the upper half-plane and no pole lies inside the enclosed area.

2.4.5 Molecular Orbitals

Lehmann's Representation in Molecular Orbitals

It yet remains to be shown how the transition values of the density fluctuation operator appearing in Eq. 2.112 can be evaluated in a molecular orbital basis. The sum over states $|\Phi_n\rangle$ can be restricted to excited states by noting

$$\langle \Phi | \tilde{n}(x) | \Phi_n \rangle = \langle \Phi | \hat{n}(x) - n(x) | \Phi \rangle = \begin{cases} 0 & | \quad n = 0 \\ \langle \Phi | \hat{n}(x) | \Phi_n \rangle & | \quad n \neq 0 \end{cases} \quad (2.116)$$

For excited states the transition density can be rewritten with the definition of the field operators (Eq. 2.35) as

$$\langle \Phi | \hat{n}(x) | \Phi_n \rangle = \varphi_p^*(x) \varphi_q(x) \langle \Phi | \hat{a}_p^\dagger \hat{a}_q | \Phi_n \rangle . \quad (2.117)$$

Unless $|\Phi_n\rangle$ is a singles excitation on $|\Phi\rangle$ (e.g. $|\Phi_i^a\rangle$), in which case Eq. 2.117 evaluates to 1, it vanishes exactly. For singles excitations the energy difference to the ground state is particularly simple to evaluate and Eq. 2.112 becomes

$$\Pi_0(\mathbf{x}, \mathbf{x}', \omega) = \frac{\varphi_i^*(\mathbf{x}) \varphi_a(\mathbf{x}) \varphi_a^*(\mathbf{x}') \varphi_i(\mathbf{x}')}{\omega - (\varepsilon_a - \varepsilon_i) + i\eta} - \frac{\varphi_i^*(\mathbf{x}') \varphi_a(\mathbf{x}') \varphi_a^*(\mathbf{x}) \varphi_i(\mathbf{x})}{\omega + (\varepsilon_a - \varepsilon_i) - i\eta} . \quad (2.118)$$

Real Molecular Orbitals

When all orbitals are real-valued ($\varphi_p = \varphi_p^*$), this allows for further simplification by a change of integration variable. As the numerators of both terms of $\Pi_0(\omega)$ are equal in this case, they can be factored out

$$i\Pi_0(\mathbf{x}, \mathbf{x}', \omega) = \varphi_i(\mathbf{x}') \varphi_a(\mathbf{x}') \varphi_a(\mathbf{x}) \varphi_i(\mathbf{x}) iP_{ia}(\omega) \quad (2.119)$$

with

$$P_{ia}(\omega) = \frac{1}{\omega - (\varepsilon_a - \varepsilon_i) + i\eta} - \frac{1}{\omega + (\varepsilon_a - \varepsilon_i) - i\eta} . \quad (2.120)$$

$P_{ia}(\omega)$ vanishes for all of complex infinity, because

$$\omega \pm (\varepsilon_a - \varepsilon_i) \pm i\eta \xrightarrow{|\omega| \rightarrow \infty} \omega = |\omega| e^{i\phi_\omega} . \quad (2.121)$$

Therefore the integral over ω along the real axis in Eq. 2.115 can be closed over the upper half-plane. By comparison of the enclosed residues it becomes obvious that the integral from $-i\infty$ to $i\infty$ closed over the left half-plane yields the identical result (cmp. Fig. 2.6).

Exchanging the integration variable for “imaginary frequency” $u = i\omega$ therefore results in

$$\int_{-\infty}^{\infty} iP_{ia}(\omega) d\omega = i \int_{-\infty}^{\infty} \frac{1}{\omega - (\varepsilon_a - \varepsilon_i) + i\eta} - \frac{1}{\omega + (\varepsilon_a - \varepsilon_i) - i\eta} d\omega \quad (2.122)$$

$$= \int_{-\infty}^{\infty} \frac{1}{-iu - (\varepsilon_a - \varepsilon_i)} - \frac{1}{-iu + (\varepsilon_a - \varepsilon_i)} du \quad (2.123)$$

$$= -2 \int_{-\infty}^{\infty} \frac{\varepsilon_a - \varepsilon_i}{(\varepsilon_a - \varepsilon_i)^2 + u^2} du \quad (2.124)$$

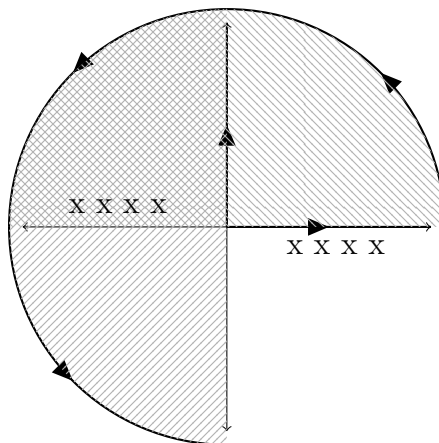


Figure 2.6: The frequency integral over the polarization propagator in real Kohn–Sham orbitals can be carried out equivalently along the real axis or the imaginary axis. The contour can in both cases be closed in counter-clockwise direction and the only residues contained are those in the upper-left quadrant of the complex plane.

where η has been set identically to zero after the change of contour because it was only necessary to move the residues away from the integration (real) axis.

A regrouping of the terms, e.g.

$$\text{Tr} \{i\Pi_0(\omega)\mathbf{V}_{ee}\} = \varphi_i(\mathbf{x})\varphi_a(\mathbf{x})iP_{ia}(\omega)\varphi_i(\mathbf{x}')\varphi_a(\mathbf{x}')V_{ee}(\mathbf{x}', \mathbf{x}) \quad (2.125)$$

$$= iP_{ia}(\omega)(ia|ia) \quad (2.126)$$

and similarly

$$\text{Tr} \{i\Pi_0(\omega)\mathbf{V}_{ee}i\Pi_0(\omega)\mathbf{V}_{ee}\} = iP_{ia}(\omega)(ia|jb)iP_{jb}(\omega)(jb|ia) \quad (2.127)$$

delivers the final formulation of the correlation energy in real molecular orbitals

$$E^C = - \int \frac{du}{4\pi} \text{Tr} \{ \log(1 + \mathbf{Q}(u)\mathbf{V}) - \mathbf{Q}(u)\mathbf{V} \} \quad (2.128)$$

with

$$Q_{ia,jb}(\omega) = 2 \frac{\varepsilon_a - \varepsilon_i}{(\varepsilon_a - \varepsilon_i)^2 + \omega^2} \delta_{ia,jb} \quad (2.129)$$

$$V_{ia,jb} = (ia|jb) . \quad (2.130)$$

Chapter 3

Publications

In this chapter, the original research of the present work will be presented. It was first published in peer-reviewed journals and is reprinted on the following pages in the original format. The supporting materials that have been published together with the manuscripts are also reproduced for completeness.

3.1 AO-RI-RPA

H. F. Schurkus and C. Ochsenfeld,
J. Chem. Phys. (Communication) **144**, 031101 (2016)

An effective linear-scaling atomic-orbital reformulation of the random-phase approximation using a contracted double-Laplace transformation

Abstract from the publication: An atomic orbital (AO) reformulation of the random-phase approximation (RPA) correlation energy is presented allowing to reduce the steep computational scaling to linear, so that large systems can be studied on simple desktop computers with fully numerically controlled accuracy. Our AO-RPA formulation introduces a contracted double-Laplace transform and employs the overlap-metric resolution-of-the-identity. First timings of our pilot code illustrate the reduced scaling with systems comprising up to 1262 atoms and 10 090 basis functions.

The following article is reproduced in agreement with its publisher (AIP Publishing LLC) and can be found online at

<http://aip.scitation.org/doi/pdf/10.1063/1.4939841>.



Communication: An effective linear-scaling atomic-orbital reformulation of the random-phase approximation using a contracted double-Laplace transformation

Henry F. Schurkus and Christian Ochsenfeld

*Chair of Theoretical Chemistry and Center for Integrated Protein Science Munich (CIPSM),
Department of Chemistry, University of Munich (LMU), D-81377 Munich, Germany*

(Received 2 December 2015; accepted 30 December 2015; published online 20 January 2016)

An atomic-orbital (AO) reformulation of the random-phase approximation (RPA) correlation energy is presented allowing to reduce the steep computational scaling to linear, so that large systems can be studied on simple desktop computers with fully numerically controlled accuracy. Our AO-RPA formulation introduces a contracted double-Laplace transform and employs the overlap-metric resolution-of-the-identity. First timings of our pilot code illustrate the reduced scaling with systems comprising up to 1262 atoms and 10 090 basis functions. © 2016 AIP Publishing LLC. [<http://dx.doi.org/10.1063/1.4939841>]

I. INTRODUCTION

The random phase approximation (RPA) originally introduced by Bohm and Pines¹ has become of wide interest for describing electron-correlation both in solid-state and molecular systems offering important advantages also for vanishing electronic gap systems. However, the applicability of RPA to larger systems has always suffered from its huge computational cost. For molecular systems the currently most widespread RPA formulation employing the resolution-of-the-identity (RI) approximation was proposed by Furche *et al.*,²⁻⁴ on the basis of formulations by Langreth and Perdew,^{5,6} and reduces the effective scaling from $O(M^6)$ to $O(M^4)$ with system size M . This opened the way for more extensive benchmarking beyond the few atoms scale. Many authors have consequently shown the usefulness and applicability of RPA.⁷⁻¹² Developments include analytical forces and first-order properties by Rekkedal *et al.*¹³ and Burow *et al.*,¹⁴ the stochastic reformulation by Gao *et al.*,¹⁵ and a complete basis set extrapolation by Mezei *et al.*¹⁶ Recently, Kállay¹⁷ presented an effective linear-scaling approximation using a local correlation domain-based approach. While not all of the employed approximations for preselecting domains are rigorous, Kállay presented for the tightest selection criteria deviations in relative energies on the order of 1 kcal/mol for a range of selected molecular systems. However, further increasing the accuracy, full rigorosity, and, e.g., avoiding domain changes on a potential energy surface remain difficult.

In our work, we present an effective linear-scaling RPA atomic orbital (AO) reformulation entirely avoiding ad-hoc approximations in order to recover the exact RPA results and allows for full numerical control of the accuracy by simple thresholding in the spirit of direct SCF or other rigorous AO-based methods. This opens up the possibility to study molecules of several hundreds to thousands of atoms at the RPA level on a simple desktop computer, while the accuracy remains fully numerically controlled.

Our formulation employs a contracted double-Laplace transformation and a RI-expansion in the overlap-metric

formulation. While the Coulomb-metric formulation is far more common than the overlap-metric nowadays, the three-center overlap allows us directly to reformulate all time-limiting steps in sparse quantities allowing for linear scaling sparse matrix algebra. In contrast to the widespread expectation that the overlap-metric would entail the need for very large auxiliary basis sets, we do find errors much smaller than the intrinsic error of RPA already for standard auxiliary basis sets (e.g., cc-pVQZ-RI for the cc-pVQZ basis¹⁸⁻²²).

Yang and co-workers²³ have previously suggested to use tensor hypercontraction (THC) methods instead of the RI-expansion for rank reduction within RPA. THC allows to express the electron repulsion integrals solely by rank-2 tensors, while the overlap metric RI also includes rank-3 tensors. The highest rank tensors in RI are, on the other hand, limited to linear increase of significant elements with molecular size, which is a necessity of our linear scaling reformulation. In the context of periodic systems computed with plane wave basis sets, Kresse and co-workers²⁴ have recently used the simple Laplace integration together with a Fourier transformation scheme to reduce the scaling to cubic, finding that the grids originally developed for second-order Møller-Plesset (MP2) theory are also suited for use with RPA. This goes well with our finding that also for our new contracted double-Laplace scheme the original MP2 grids already perform sufficiently well.

In the following, first the derivation of our RPA reformulation is given, including a discussion on numerical stability. Then the efficiency and scaling behavior of our pilot implementation are described. Finally, a brief outlook on possible further improvements is presented.

II. THEORY

RPA has been found to be a highly useful correlation method for going beyond approximative forms of Kohn-Sham density-functional theory (KS-DFT).^{2,7-12} Here, RPA is generally derived from the adiabatic connection²⁵ as presented

by Langreth and Perdew^{5,6} and the total energy can thus be expressed as

$$E = E_T[\{\phi^{KS}\}] + E_J[\{\phi^{KS}\}] + E_X[\{\phi^{KS}\}] + E_C, \quad (1)$$

where the kinetic E_T , Coulomb E_J , and exact exchange E_X energies are evaluated using the Kohn-Sham orbitals from a preceding DFT calculation. Since a multitude of methods have been developed for evaluating HF and DFT in a linear-scaling fashion (see, e.g., Ref. 26 for a recent review), the first three terms are of no concern for developing a linear-scaling RPA method. Therefore, we will focus on the last term known as RPA correlation energy.

In the following, the Einstein sum convention²⁷ is used for simplicity. All slashed symbols denote matrices that are sparse for sufficiently large system sizes with non-vanishing electronic gap. Indices i, j, \dots denote occupied orbitals from the underlying DFT calculation, a, b, \dots virtual orbitals, μ, ν, \dots basis functions, and P, Q, \dots auxiliary basis functions arising from the RI-expansion.

We start our reformulation from Furche's original $O(M^6)$ formulation of the RPA correlation energy (E_C)^{8,28}

$$E_C = \frac{1}{2} \text{Tr} \left\{ M^{\frac{1}{2}} - A \right\}, \quad (2)$$

with

$$M = (A - B)^{\frac{1}{2}} (A + B) (A - B)^{\frac{1}{2}} \quad (3)$$

and

$$A_{ia,jb} = d_{ia,jb} + (ia|jb), \quad (4)$$

$$B_{ia,jb} = (ia|jb), \quad (5)$$

where $d_{ia,jb} = (\varepsilon_a - \varepsilon_i) \delta_{ia,jb}$ denotes a diagonal matrix with diagonal elements given by the difference of the Kohn-Sham orbital energies and $(ia|jb)$ denote the electron repulsion integrals in Mulliken notation.

For evaluating the energy given by Eq. (2), we follow the basic idea of Eshuis, Bates, and Furche²⁹ to employ the RI approximation.³⁰ However, we do not employ the Coulomb-metric RI, but use the overlap-metric RI instead (see also Ref. 31 on the discussion of various RI approximations), given by

$$\begin{aligned} (ia|jb) &\approx (iaP)(S^{-1})_{P,Q} C_{Q,R} (S^{-1})_{R,L} (Ljb) \\ &=: \mathcal{B}_{ia,P} C_{P,Q} \mathcal{B}_{Q,jb}^T, \end{aligned} \quad (6)$$

where the electron repulsion integral $(ia|jb)$ is expressed via 3-center overlaps (iaP) , 2-center overlaps $S_{P,Q} = (PQ)$, and 2-center 2-electron integrals $C_{P,Q} = (P|Q)$ over auxiliary functions.

Along the lines of Ref. 3, Eqs. (15)–(28), using the matrix square root formula by Hale *et al.*³² and the Woodbury matrix identity,³³ one arrives at

$$E_C = 2 \int_0^\infty \frac{dw}{4\pi} \text{Tr} [\ln(1 + \mathcal{Q}(w)C) - \mathcal{Q}(w)C], \quad (7)$$

where we have defined

$$D = (w^2 + d^2), \quad (8)$$

$$\mathcal{Q}(w) = 2\mathcal{B}^T dD(w)^{-1} \mathcal{B}. \quad (9)$$

For its computation in an atomic-orbital basis, one first needs to decouple the Kohn-Sham energy based $dD(w)^{-1}$. While the quadratic denominator prohibits direct use of the Laplace transformation as in AO-based second-order Møller-Plesset (AO-MP2) theory^{34–37} that allows for linear scaling by distance-including integral screening methods,^{38,39} we are able to achieve decoupling in RPA by the following contracted double-Laplace expansion:

$$\begin{aligned} (dD(w)^{-1})_{ia,jb} &= \frac{d_{ia,jb}}{d_{ia,jb}^2 + w^2} \\ &= d_{ia,jb} \int_0^\infty \frac{\sin(wp)}{w} e^{-d_{ia,jb}p} dp. \end{aligned} \quad (10)$$

Inserting this transformation into Eq. (9) yields

$$\mathcal{Q}(w) = 2 \int_0^\infty \frac{\sin(wp)}{w} \mathcal{F}^{(p)} dp, \quad (11)$$

with

$$\mathcal{F}_{PQ}^{(p)} = e^{-\varepsilon_a p} e^{\varepsilon_i p} (\varepsilon_a - \varepsilon_i) \mathcal{B}_{ia,P} \mathcal{B}_{ia,Q} \quad (12)$$

$$= e^{-\varepsilon_a p} e^{\varepsilon_i p} (\varepsilon_a - \varepsilon_i) C_{\mu i} C_{\nu a} C_{\lambda i} C_{\sigma a} \mathcal{B}_{\mu\nu,P} \mathcal{B}_{\lambda\sigma,Q} \quad (13)$$

$$= \mathcal{B}_{\mu\nu,P} \left\{ \begin{array}{l} P_{\nu\sigma}^{(p)} \overline{P}_{\nu\sigma}^{(p)} \\ - \overline{P}_{\mu\lambda}^{(p)} P_{\nu\sigma}^{(p)} \end{array} \right\} \mathcal{B}_{\lambda\sigma,Q}, \quad (14)$$

where $\mathcal{F}^{(p)}$ is written in the AO basis (LCAO ansatz: $|i\rangle = C_{\mu i} |\mu\rangle$). In addition to the commonly defined pseudo-densities in AO-formulation^{37,40,41}

$$\underline{P}_{\mu\nu}^{(p)} = C_{\mu i} e^{\varepsilon_i p} C_{\nu i} = (e^{pPF} P)_{\mu\nu}, \quad (15)$$

$$\overline{P}_{\mu\nu}^{(p)} = C_{\mu a} e^{-\varepsilon_a p} C_{\nu a} = (e^{-pQF} Q)_{\mu\nu}, \quad (16)$$

we have further introduced energy-weighted pseudo-densities which can also be seen as derivatives of the pseudo-densities (a fact that we will make use of below (Eq. (19)))

$$\underline{P}_{\mu\nu}^{(p)} = \partial_p \underline{P}_{\mu\nu}^{(p)} = C_{\mu i} e^{\varepsilon_i p} \varepsilon_i C_{\nu i} = (PF e^{pPF} P)_{\mu\nu}, \quad (17)$$

$$\overline{P}_{\mu\nu}^{(p)} = -\partial_p \overline{P}_{\mu\nu}^{(p)} = C_{\mu a} e^{-\varepsilon_a p} \varepsilon_a C_{\nu a} = (QF e^{-pQF} Q)_{\mu\nu}, \quad (18)$$

with the Fock matrix F and the occupied and virtual one-particle density matrices P and Q , respectively. As F, P, Q in Eqs. (15)–(18) are known to become sparse for large molecular systems,^{37,40,41} the pseudo-densities and derivative-densities are themselves sparse for such systems and can be computed by sparse-matrix algebra.

Eq. (11) can be simplified by partial integration

$$\left(\mathcal{F}_{\text{INT}}^{(p)} \right)_{PQ} := - \int_0^p \mathcal{F}_{PQ}^{(q)} dq = \mathcal{B}_{\mu\nu,P} \underline{P}_{\mu\lambda}^{(p)} \overline{P}_{\nu\sigma}^{(p)} \mathcal{B}_{\lambda\sigma,Q} \quad (19)$$

resulting in

$$\mathcal{Q}(w) = 2 \int_0^\infty \cos(wp) \mathcal{F}_{\text{INT}}^{(p)} dp. \quad (20)$$

However, since the cosine function does not decay at large argument values this formulation causes strong oscillations and therefore numerical instabilities occur when w approaches infinity. Here, the opposite partial integration is more easily applicable

$$\mathcal{Q}(w) = 2\frac{\mathbb{F}^{(0)}}{w^2} + 2\int_0^\infty \frac{\cos(wP)}{w^2} \mathbb{F}_D^{(p)} dp, \quad (21)$$

where

$$\mathbb{F}_D^{(p)} = \mathbb{B}_{\mu\nu,P} \left\{ 2\overline{\overline{P}}_{\nu\sigma}^{(p)} - \overline{\overline{P}}_{\nu\sigma}^{(p)} - \overline{\overline{P}}_{\nu\sigma}^{(p)} \right\} \mathbb{B}_{\lambda\sigma,Q}, \quad (22)$$

$$\mathbb{F}_{PQ}^{(0)} = \mathbb{B}_{\mu\nu,P} \{ (PFP)_{\mu\lambda} Q_{\nu\sigma} - P_{\mu\lambda} (QFQ)_{\nu\sigma} \} \mathbb{B}_{\lambda\sigma,Q} \quad (23)$$

The double weighted pseudo-densities have been defined in analogy to Eq. (18) as

$$\overline{\overline{P}} = \partial_p \overline{P}; \quad \overline{\overline{P}} = -\partial_p \overline{P}. \quad (24)$$

This formulation, however, suffers from numerical instability where w tends to zero as there divisions by very small numbers occur. We thus conclude that the energy is to be computed by Eq. (7) with the matrix \mathcal{Q} evaluated by Eq. (20) (denoted as ‘‘INT-formulation’’) for small values of w and by Eq. (21) (denoted as ‘‘D-formulation’’) for large values of w . In Fig. 1, we show the energy integrand values computed by each of the two formulations for the example case of the methane molecule. While both coincide over a large range of values, thus making the system dependent choice of the w -separation value a robust one, it is apparent that only by computing the small- w -part of the integrand in INT-formulation and the large- w -part in D-formulation the exact integrand can be recovered. Another choice besides the w -separation value is the upper limit of the quadrature in Eq. (7) which we term Λ -cutoff in analogy to the custom in the quantum-field theories. This quadrature can then be carried out by the Clenshaw-Curtis scheme which allows to adaptively augment and distribute the nodes to the desired accuracy. Even when requiring mHartree accuracy as few as 60 node points have proven to be sufficient for most molecules. Because of this small number of evaluations the matrix valued logarithm in

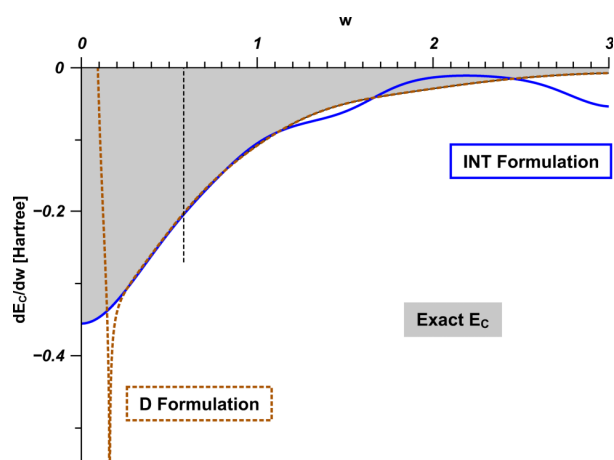


FIG. 1. The correlation energy can be computed via the integral Eq. (7) where the integrand is dependent on $\mathcal{Q}(w)$, which can be given in either the INT-formulation (Eq. (20)) or the D-formulation (Eq. (21)). Here, we show the integrand in both formulations for methane evaluated with the pc-2 basis set.⁴² Although the INT-formulation deviates at $w < 0.3$ and the D-formulation at $w > 1$, splitting the integral at any value of w in between allows to obtain the correct correlation energy as the combined area-under-the-curve.

Eq. (7) is best computed by direct diagonalization. Although, in principle, also this step could be reduced in computational effort by a series expansion, the presently chosen cubic-scaling diagonalization step will in practice hardly ever become significant due to the very small prefactor (see Fig. S1 in the supplementary material).⁴³ With the boundaries of w now being effectively finite, one can make use of the results by Takatsuka, Ten-No, and Hackbusch⁴⁴ who gave optimal p -integration-points and weights in a minimax sense for the original Laplace transformation. Although our transformation is very different from that, we still find that mHartree accuracy can be achieved when, for example, the range up to $\Lambda = 50$ is described by 15 of their nodes. We expect however, that even less points will suffice when optimized specifically for our transformation (Eq. (10)). We finally note that one could, without a change to the derivation, redefine the Coulomb matrix C to contain the inverse overlap matrices instead of the \mathbb{B} matrices. In this way, the Laplace summation could be carried out over slightly more sparse matrices which could accelerate the computation of Eqs. (11), (20), and (21).

All tuning parameters of our reformulation are monotonically convergent in the sense, that larger Λ -cutoff values, number of Laplace points, and number of integration nodes, and smaller sparsity threshold always improve the result quality. In the limiting case the result equals the exact RI-RPA result. We therefore term our reformulation fully numerically controlled in its accuracy.

III. RESULTS

Our pilot code of AO-RPA has been realized in the FermiONS++ program^{45,46} with thresholds chosen such that all energies are precise to below 1 mHartree.

To estimate the number of Laplace points and Λ -cutoff needed, we have conducted preliminary investigations on several molecules with medium sized to large basis sets. We have found for all tested cases that the results were essentially converged with the number of Laplace points at about 12 p -sampling points for a Λ -cutoff at 50. To ascertain that using the thus very conservative choice of 15 p -integration-points and 0.5 as the w -separator are sufficient choices for the desired accuracy, we first tested these settings for the computation of Grimme’s NBRC test set⁴⁷ with cc-pVQZ/cc-pVQZ-RI as the basis, finding a mean absolute deviation of only 0.86 kcal/mol which is below the so called chemical accuracy of 1 kcal/mol. For the sake of comparison, the canonical RI-RPA implementation in TURBOMOLE results in a deviation of 0.75 kcal/mol for the same test set. Since our theory does not make use of any screening, the only source for further errors arising for larger systems would stem from the sparse-algebra thresholds from our sparse-algebra implementation, based on the block compressed sparse row format.^{48,49} To make sure no such errors arise we choose block dimensions of 50 elements and set the threshold to the tight value of 1×10^{-8} .

The formal scaling behavior is defined as the increase in computational time with the cardinality of the physical interactions of a system, the observed behavior with respect

to the number of atoms. While the first gives the true physical boundary, the second can be easily measured by timing the method on a systematically enlarged test molecule. Only in the asymptotic limit, where the molecule is grown in one direction until the extents in the other directions are comparably negligible, the two definitions coincide. Therefore, for studying the formal scaling behavior with molecules of limited size, quasi-one-dimensional systems are ideally suited.

In Fig. 2 evaluation times for the first pilot implementation of our new RPA method are shown for linear alkanes of increasing size. While our code is not yet fully optimized, run times are already short (single core) and effective linear-scaling behavior is observed. The timings were evaluated with the def2-svp basis set. Since the currently available RI auxiliary basis sets are optimized for the Coulomb-metric RI, we employ the same basis set for both the AO and the auxiliary indices as AO-RPA-optimized basis sets have not yet been developed.

Furthermore, we tested the scaling behavior by studying polypeptide chains as models for biochemical systems. The timings show the same linear scaling behavior as the alkane chains (Fig. 2 inset).

To test the limits for the regular user without access to high performance computers, we calculated our largest system ($C_{420}H_{842}$) comprising 1262 atoms and 10 090 basis functions on a normal desktop computer (Intel Core i7-3770

CPU 3.40 GHz). With the same thresholds as in the other computations the evaluation time is 79 h.

IV. CONCLUSION AND OUTLOOK

We have presented an AO-based reformulation of RPA that allows evaluating the correlation energy in linear time. Here, we have introduced a contracted double-Laplace transformation to allow for a purely AO-based formulation and employ the overlap-metric RI scheme to separate the long-ranged Coulomb interaction.

For a proof-of-concept we have further presented results obtained with a pilot implementation of our theory. With sufficiently large auxiliary basis sets, mHartree accuracy can be readily achieved. Preliminary timings on more modest basis sets illustrate the linear-scaling time-complexity and low computational effort of our pilot implementation with the largest system comprising 1262 atoms and 10 090 basis functions.

While there are many ways for improving our AO-RPA method in the future, we will focus first on aspects such as the (1) optimization of our preliminary pilot code and parallelization, (2) use of screening procedures, (3) introduction of a Cholesky decomposition for the pseudo-density matrices in order to reduce dimensions (along the lines of, e.g., Refs. 50–52), and (4) development of efficient basis sets for overlap-metric RI expansions.

Nevertheless, already our preliminary pilot AO-RPA implementation shows fairly early crossovers and effective linear time-complexity and in this way opens new possibilities to account for electron-correlation effects in large complex systems.

ACKNOWLEDGMENTS

The authors thank Dr. Jörg Kussmann (LMU Munich) for help in implementing AO-RPA within the framework of the FermiONs++ quantum chemistry package. Financial support by the DFG funding initiatives SFB749 (C7) and the Excellence Cluster EXC114 (CIPSM) is acknowledged.

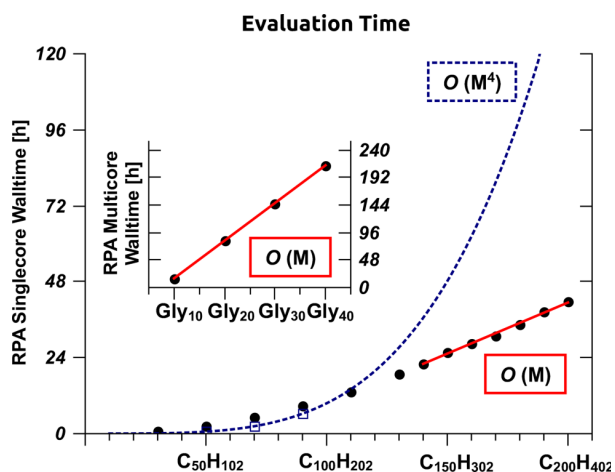


FIG. 2. Wall times for the single threaded execution of our AO-RPA pilot implementation illustrating linear time complexity with molecular size ($O(M)$) for linear alkane test systems (def2-svp basis, $\Lambda = 50$, 15 p -integration-points, integrand separation about $w = 0.5$ and 65 node points of Clenshaw-Curtis quadrature in every case for consistency. Computer: Intel Xeon E5-2620 CPU 2.0 GHz). Although comparing different program packages has to be taken with great care due to the many subtle differences, we compare also evaluation times for the $O(M^4)$ -scaling RI-RPA formulation implemented in the program package TURBOMOLE, which is the *de facto* standard of molecular RPA theory to date. Although we use equivalent settings, the data can only indicate that we are in a reasonable ballpark and that early crossovers can be expected. TURBOMOLE times for systems larger than 90 carbon atoms are extrapolated using scaling from earlier points as these could not be computed with the program version available to us. Inset: Wall times for glycine chains of increasing length. The computations were carried out on the same architecture and with the same parameters. 12 threads were used for the matrix multiplications.

- ¹D. Bohm and D. Pines, *Phys. Rev.* **92**, 609 (1953).
- ²F. Furche, *J. Chem. Phys.* **129**, 114105 (2008).
- ³H. Eshuis, J. Yarkony, and F. Furche, *J. Chem. Phys.* **132**, 234114 (2010).
- ⁴H. Eshuis and F. Furche, *J. Chem. Phys.* **136**, 084105 (2012).
- ⁵D. C. Langreth and J. P. Perdew, *Solid State Commun.* **17**, 1425 (1975).
- ⁶D. C. Langreth and J. P. Perdew, *Phys. Rev. B* **15**, 2884 (1977).
- ⁷H. Eshuis and F. Furche, *J. Phys. Chem. Lett.* **2**, 983 (2011).
- ⁸F. Furche, *Phys. Rev. B* **64**, 195120 (2001).
- ⁹H. Jiang and E. Engel, *J. Chem. Phys.* **127**, 184108 (2007).
- ¹⁰B. Mussard, P. Reinhardt, J. G. Ángyán, and J. Toulouse, *J. Chem. Phys.* **142**, 154123 (2015).
- ¹¹J. Paier, X. Ren, P. Rinke, G. E. Scuseria, A. Grüneis, G. Kresse, and M. Scheffler, *New J. Phys.* **14**, 043002 (2012).
- ¹²X. Ren, P. Rinke, C. Joas, and M. Scheffler, *J. Mater. Sci.* **47**, 7447 (2012).
- ¹³J. Rekkedal, S. Coriani, M. F. Izzi, A. M. Teale, T. Helgaker, and T. B. Pedersen, *J. Chem. Phys.* **139**, 081101 (2013).
- ¹⁴A. M. Burow, E. Bates, F. Furche, and H. Eshuis, *J. Chem. Theory Comput.* **10**, 180 (2014).
- ¹⁵Y. Gao, D. Neuhauser, R. Baer, and E. Rabani, *J. Chem. Phys.* **142**, 034106 (2015).
- ¹⁶P. D. Mezei, G. I. Csonka, and A. Ruzsinszky, *J. Chem. Theory Comput.* **11**, 3961 (2015).

031101-5 H. F. Schurkus and C. Ochsenfeld

J. Chem. Phys. **144**, 031101 (2016)

- ¹⁷M. Kállay, *J. Chem. Phys.* **142**, 204105 (2015).
- ¹⁸T. H. Dunning, Jr., *J. Chem. Phys.* **90**, 1007 (1989).
- ¹⁹R. A. Kendall, T. H. Dunning, Jr., and R. J. Harrison, *J. Chem. Phys.* **96**, 6796 (1992).
- ²⁰D. E. Woon and T. H. Dunning, Jr., *J. Chem. Phys.* **98**, 1358 (1993).
- ²¹K. A. Peterson, D. E. Woon, and T. H. Dunning, Jr., *J. Chem. Phys.* **100**, 7410 (1994).
- ²²A. K. Wilson, T. van Mourik, and T. H. Dunning, Jr., *J. Mol. Struct.* **388**, 339 (1996).
- ²³N. Shenvi, H. van Aggelen, Y. Yang, and W. Yang, *J. Chem. Phys.* **141**, 024119 (2014).
- ²⁴M. Kaltak, J. Klimes, and G. Kresse, *J. Chem. Theory Comput.* **10**, 2498 (2014).
- ²⁵O. Gunnarson and B. I. Lundqvist, *Phys. Rev. B* **13**, 4274 (1976).
- ²⁶J. Kussmann, M. Beer, and C. Ochsenfeld, *Wiley Interdiscip. Rev.: Comput. Mol. Sci.* **3**, 614 (2013).
- ²⁷A. Einstein, *Ann. Phys.* **49**, 769 (1916).
- ²⁸F. Furche and T. Van Voorhis, *J. Chem. Phys.* **122**, 164106 (2005).
- ²⁹H. Eshuis, J. E. Bates, and F. Furche, *Theor. Chem. Acc.* **131**, 1084 (2012).
- ³⁰B. I. Dunlap and N. Rösch, *J. Chim. Phys. Phys.-Chim. Biol.* **86**, 671 (1989).
- ³¹O. Vahtras, J. Almlöf, and M. W. Feyereisen, *Chem. Phys. Lett.* **213**, 514 (1993).
- ³²N. Hale, N. J. Higham, and L. N. Trefethen, *SIAM J. Numer. Anal.* **46**, 2505 (2008).
- ³³W. W. Hager, *SIAM Rev.* **31**, 221 (1989).
- ³⁴J. Almlöf, *Chem. Phys. Lett.* **181**, 319 (1991).
- ³⁵M. Häser and J. Almlöf, *J. Chem. Phys.* **96**, 489 (1992).
- ³⁶M. Häser, *Theor. Chim. Acta* **87**, 147 (1993).
- ³⁷P. Y. Ayala and G. E. Scuseria, *J. Chem. Phys.* **110**, 3660 (1999).
- ³⁸B. Doser, D. S. Lambrecht, J. Kussmann, and C. Ochsenfeld, *J. Chem. Phys.* **130**, 064107 (2009).
- ³⁹S. A. Maurer, D. S. Lambrecht, J. Kussmann, and C. Ochsenfeld, *J. Chem. Phys.* **138**, 014101 (2013).
- ⁴⁰P. R. Surján, *Chem. Phys. Lett.* **406**, 318 (2005).
- ⁴¹S. Schweizer, B. Doser, and C. Ochsenfeld, *J. Chem. Phys.* **128**, 154101 (2008).
- ⁴²F. Jensen, *J. Chem. Phys.* **115**, 9113 (2001).
- ⁴³See supplementary material at <http://dx.doi.org/10.1063/1.4939841> for a comparison to the cubic step.
- ⁴⁴A. Takatsuka, S. Ten-No, and W. Hackbusch, *J. Chem. Phys.* **129**, 044112 (2008).
- ⁴⁵J. Kussmann and C. Ochsenfeld, *J. Chem. Phys.* **138**, 134114 (2013).
- ⁴⁶J. Kussmann and C. Ochsenfeld, *J. Chem. Theory Comput.* **11**, 918 (2015).
- ⁴⁷L. Goerigk and S. Grimme, *J. Chem. Theory Comput.* **6**, 107 (2010).
- ⁴⁸F. G. Gustavson, *ACM Trans. Math. Software* **4**, 250 (1978).
- ⁴⁹J. Kussmann and C. Ochsenfeld, *J. Chem. Phys.* **127**, 054103 (2007).
- ⁵⁰J. Zienau, L. Clin, B. Doser, and C. Ochsenfeld, *J. Chem. Phys.* **130**, 204112 (2009).
- ⁵¹S. A. Maurer, L. Clin, and C. Ochsenfeld, *J. Chem. Phys.* **140**, 224112 (2014).
- ⁵²S. A. Maurer, J. Kussmann, and C. Ochsenfeld, *J. Chem. Phys.* **141**, 051106 (2014).

Supplementary Material

An Effective Linear-Scaling Atomic-Orbital Reformulation of the Random-Phase Approximation Using a Contracted Double-Laplace Transformation

Henry F. Schurkus and Christian Ochsenfeld

*Chair of Theoretical Chemistry, Department of Chemistry,
University of Munich (LMU), Butenandtstr. 7, D-81377 Munich, Germany
and*

*Center for Integrated Protein Science Munich (CIPSM) at the
Department of Chemistry, University of Munich (LMU), Butenandtstr. 5-13,
D-81377 Munich, Germany*

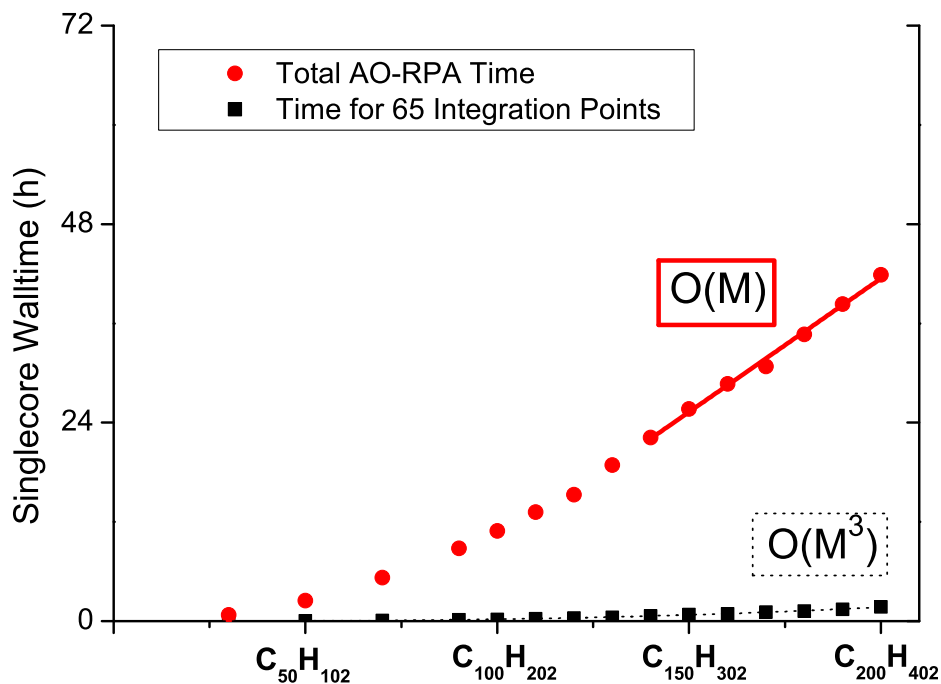


FIG. 1. Comparison of the total singlecore walltime for the AO-RPA evaluation on linear alkane chains of increasing length to the fraction that is due to the evaluation of the integration points. For each integration point a matrix logarithm is needed, which we evaluate in our implementation by explicit diagonalization. Although this causes this step to formally scale as $O(M^3)$, the very low prefactor causes it to hardly ever become significant. All other steps scale linearly with molecular size.

3.2 ω -CDD-RPA

A. Luenser, H. F. Schurkus, and C. Ochsenfeld,
J. Chem. Theory Comput. **13**, 1647 (2017)

Vanishing-Overhead Linear-Scaling Random Phase Approximation by Cholesky Decomposition and an Attenuated Coulomb-Metric

Abstract from the publication: A reformulation of the random phase approximation within the resolution-of-the-identity (RI) scheme is presented, that is competitive to canonical molecular orbital RI-RPA already for small- to medium-sized molecules. For electronically sparse systems drastic speedups due to the reduced scaling behavior compared to the molecular orbital formulation are demonstrated. Our reformulation is based on two ideas, which are independently useful: First, a Cholesky decomposition of density matrices that reduces the scaling with basis set size for a fixed-size molecule by one order, leading to massive performance improvements. Second, replacement of the overlap RI metric used in the original AO-RPA by an attenuated Coulomb metric. Accuracy is significantly improved compared to the overlap metric, while locality and sparsity of the integrals are retained, as is the effective linear scaling behavior.

The following article is reproduced in accordance with the American Chemical Society Journal Publishing Agreement and can be found online at

<http://pubs.acs.org/articlesonrequest/AOR-qyPdNCJAmamIX97YvS3J>.

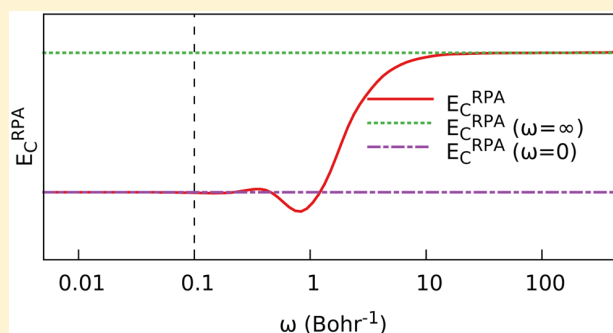
Vanishing-Overhead Linear-Scaling Random Phase Approximation by Cholesky Decomposition and an Attenuated Coulomb-Metric

Arne Luenser, Henry F. Schurkus, and Christian Ochsenfeld*[✉]

Chair of Theoretical Chemistry, Department of Chemistry, University of Munich (LMU), Butenandtstrasse 5-13, D-81377 Munich, Germany

Center for Integrated Protein Science Munich (CIPSM), Butenandtstrasse 5-13, D-81377 Munich, Germany

ABSTRACT: A reformulation of the random phase approximation within the resolution-of-the-identity (RI) scheme is presented, that is competitive to canonical molecular orbital RI-RPA already for small- to medium-sized molecules. For electronically sparse systems drastic speedups due to the reduced scaling behavior compared to the molecular orbital formulation are demonstrated. Our reformulation is based on two ideas, which are independently useful: First, a Cholesky decomposition of density matrices that reduces the scaling with basis set size for a fixed-size molecule by one order, leading to massive performance improvements. Second, replacement of the overlap RI metric used in the original AO-RPA by an attenuated Coulomb metric. Accuracy is significantly improved compared to the overlap metric, while locality and sparsity of the integrals are retained, as is the effective linear scaling behavior.



1. INTRODUCTION

The random phase approximation (RPA) correlation method has for its excellent description of long-ranged correlation effects piqued the interest of many researchers in the field of quantum chemistry, especially since its advancement from a computationally prohibitively expensive method in the original $O(M^6)$ formulation^{1,2} to a method computationally tractable enough for use within rung five³ DFT schemes.⁴ Many authors have contributed to this algorithmic improvement: Furche and co-workers^{5–8} put forward an effective $O(M^4)$ scaling formulation. While their approach employs the resolution-of-the-identity (RI) approximation,⁹ Yang and co-workers¹⁰ suggested to employ the tensor hypercontraction (THC) developed by Martinez and co-workers^{11–13} instead. Kresse and co-workers¹⁴ were able to reduce the scaling to $O(M^3)$ for periodic systems. Kallay¹⁵ and also ourselves¹⁶ have shown how to further reduce the effective computational complexity to linear for molecules with nonvanishing band gaps. Most recently, Hutter and co-workers¹⁷ have made significant steps toward highly parallelized evaluation of these formulations. Extensive analysis of the results obtainable within these new formulations has since shown the many strengths of the RPA.^{5,18–22} Analytical gradients for the RPA energy are given in refs 23 and 24. Benchmark studies have shown the importance of evaluating the RPA with large basis sets of up to quadruple- ζ size.

Our previously presented atomic orbital (AO) formulation shows linear scaling with the molecule size M and thus extends the applicability of the RPA to molecules comprising thousands of atoms. To do so, we moved from the Coulomb RI metric,

which gives the most accurate results for the commonly employed auxiliary basis sets, to the potentially less accurate short-range overlap metric. Also, the scaling with basis set size N_{basis} and auxiliary basis set size N_{aux} for any fixed molecular size ($N_{\text{occ}} = \text{const}$), which is important for the prefactor of the evaluation time, increases from $O(N_{\text{aux}}^2 N_{\text{basis}} N_{\text{occ}})$ to $O(N_{\text{aux}}^2 N_{\text{basis}}^2)$, thereby limiting the applicability to basis sets much smaller than quadruple- ζ sizes.

The present work supplies remedies for these drawbacks by introducing two concepts from related fields to the context of RPA. First, by pivoted Cholesky decomposition^{25–27} of the density and pseudodensity matrices (CDD^{28,29}) within the AO formulation the scaling with basis set size is brought back down to $O(N_{\text{aux}}^2 N_{\text{basis}} N_{\text{occ}})$ (section 3.1). We attain a prefactor which allows—even in the case of small molecules—for evaluation times competitive with the canonical MO-based formulation as will be shown in section 4.1. Second, by exchanging the overlap metric RI for a formulation using the Coulomb metric attenuated by the complementary error function^{30–32} in section 3.2 we arrive at a formulation that can smoothly interpolate between the overlap metric and exact Coulomb metric result. We show in section 4.2 that choices for the attenuation parameter ω are available which combine the best of both worlds—rendering results numerically equivalent to the Coulomb metric results, but local enough to be evaluated in linear time.

Neither of these concepts change the complexity with molecular size, thus either one or both can be applied while still allowing

Received: December 21, 2016

Published: March 6, 2017

for linear scaling evaluation as will be verified in section 4.3. By combining the two, we finally arrive at a formulation we term ω -CDD-RPA, which is competitive with the canonical $O(M^4)$ formulation regardless of molecule and basis set size but has the additional advantage of $O(M)$ scaling, allowing for the application to extended systems.

2. REVIEW

2.1. RI-RPA in Molecular and Atomic Orbital Bases. In the following, we will use μ, ν for atomic orbitals (AOs), i, j for occupied molecular orbitals (MOs), a, b for virtual molecular orbitals, and M, N for auxiliary RI functions. The RI-RPA correlation energy in its standard Coulomb metric form is⁶

$$E_C^{\text{RPA}} = \frac{1}{2\pi} \int_0^\infty \text{Tr}(\ln[\mathbf{1} + \mathbf{Q}(u)] - \mathbf{Q}(u)) du \quad (1)$$

where

$$\mathbf{Q}_{MN}(u) = 2\mathbf{S}_M^T \mathbf{G}(u) \mathbf{S}_N \quad (2)$$

$$G_{ai,bj}(u) = \frac{(\epsilon_a - \epsilon_i)\delta_{ai,bj}}{(\epsilon_a - \epsilon_i)^2 + u^2} \quad (3)$$

$$S_{ai}^M = \sum_N (ai|N)L_{NM} \quad (4)$$

$$\mathbf{L}\mathbf{L}^T = \mathbf{C}^{-1} \quad (5)$$

$$C_{MN} = \left(M \left| \frac{1}{r_{12}} \right| N \right) \quad (6)$$

using the Mulliken notation for two- and three-center integrals. The frequency integration in eq 1 is performed by Clenshaw-Curtis quadrature.⁶ Computational complexity is $O(N_{\text{aux}}^2 N_{\text{occ}} N_{\text{virt}})$ per frequency point u , where N_{aux} is the number of auxiliary functions, and N_{occ} and N_{virt} are the numbers of occupied and virtual MOs, respectively.

The reformulation in the atomic orbital basis presented by two of us, Schurkus and Ochsenfeld,¹⁶ used the integral transform

$$\frac{1}{(\epsilon_a - \epsilon_i)^2 + u^2} = \int_0^\infty \frac{\sin(ut)}{u} e^{-(\epsilon_a - \epsilon_i)t} dt \quad (7)$$

which together with the overlap RI metric

$$(ailbj) \approx \sum_{MN} B_{ai}^M \tilde{C}_{MN} B_{bj}^N \quad (8)$$

$$\tilde{\mathbf{C}} = \mathbf{S}^{-1} \mathbf{C} \mathbf{S}^{-1} \quad (9)$$

$$B_{\mu\nu}^M = (\mu\nu|M) = \int \chi_\mu(\mathbf{r}) \chi_\nu(\mathbf{r}) \chi_M(\mathbf{r}) d\mathbf{r} \quad (10)$$

and

$$\mathbf{Q}(u) = \begin{cases} u < u^*: 2 \sum_{\alpha=1}^{\tau} w_\alpha \cos(ut_\alpha) \mathbf{F}_{\text{INT}}^{(t_\alpha)} \\ u > u^*: \frac{2}{u^2} \mathbf{F}_0 + 2 \sum_{\alpha=1}^{\tau} w_\alpha \frac{\cos(ut_\alpha)}{u^2} \mathbf{F}_D^{(t_\alpha)} \end{cases} \quad (11)$$

enabled effective linear scaling. u^* specifies the frequency where we switch from one formula to the other, which was chosen as

0.5 au. w_α and t_α are the weights and roots for the quadrature of the integral in eq 7. Equation 1 is modified to

$$E_C^{\text{AO-RPA}} = \frac{1}{2\pi} \int_0^\infty \text{Tr}(\ln[\mathbf{1} + \mathbf{Q}(u)\tilde{\mathbf{C}}] - \mathbf{Q}(u)\tilde{\mathbf{C}}) du \quad (12)$$

that is, multiplication with the long-range $\frac{1}{r_{12}}$ -operator matrix $\tilde{\mathbf{C}}$ is deferred until the last step of the algorithm. All other matrices are local and sparse for large molecules. The three types of \mathbf{F} matrices are given by

$$(\mathbf{F}_0)_{MN} = \text{Tr}(\mathbf{P}\mathbf{F}\mathbf{P}\mathbf{B}_M \bar{\mathbf{P}}\mathbf{B}_N) - \text{Tr}(\mathbf{P}\mathbf{B}_M \bar{\mathbf{P}}\mathbf{F}\mathbf{P}\mathbf{B}_N) \quad (13)$$

$$(\mathbf{F}_{\text{INT}}^{(t_\alpha)})_{MN} = \text{Tr}(\underline{\mathbf{P}}^{(\alpha)} \mathbf{B}_M \bar{\mathbf{P}}^{(\alpha)} \mathbf{B}_N) \quad (14)$$

$$(\mathbf{F}_D^{(t_\alpha)})_{MN} = 2\text{Tr}(\underline{\underline{\mathbf{P}}}^{(\alpha)} \mathbf{B}_M \bar{\bar{\mathbf{P}}}^{(\alpha)} \mathbf{B}_N) - \text{Tr}(\underline{\underline{\mathbf{P}}}^{(\alpha)} \mathbf{B}_M \bar{\mathbf{P}}^{(\alpha)} \mathbf{B}_N) - \text{Tr}(\underline{\mathbf{P}}^{(\alpha)} \mathbf{B}_M \bar{\bar{\bar{\mathbf{P}}}}^{(\alpha)} \mathbf{B}_N) \quad (15)$$

$\mathbf{P}, \bar{\mathbf{P}}$, and \mathbf{F} are occupied and virtual one-particle density matrices, and the Kohn–Sham matrix, respectively. $\underline{\mathbf{P}}^{(\alpha)}$ and $\bar{\mathbf{P}}^{(\alpha)}$, as well as their first ($\underline{\underline{\mathbf{P}}}^{(\alpha)}$, $\bar{\bar{\mathbf{P}}}^{(\alpha)}$) and second ($\underline{\underline{\underline{\mathbf{P}}}}^{(\alpha)}$, $\bar{\bar{\bar{\mathbf{P}}}}^{(\alpha)}$) derivatives with respect to t_α are the usual Laplace pseudodensity matrices defined in ref 16.

2.2. Notes on the Frequency Quadrature. The trace of the matrix logarithm in eq 12 can be more efficiently evaluated by Cholesky-factorizing $\tilde{\mathbf{C}} = \mathbf{L}\mathbf{L}^T$, and using the Mercator series for $\ln(1+x)$ to rewrite

$$\text{Tr} \ln(\mathbf{1} + \mathbf{Q}(u)\tilde{\mathbf{C}}) = \text{Tr} \ln(\mathbf{1} + \mathbf{L}^T \mathbf{Q}(u) \mathbf{L}) \quad (16)$$

$$= \ln(\det \mathbf{L}' \det \mathbf{L}'^T) \quad (17)$$

$$= 2 \ln \prod_i L'_{ii} \quad (18)$$

where $\mathbf{1} + \mathbf{L}^T \mathbf{Q}(u) \mathbf{L}$ itself was Cholesky-factorized as $\mathbf{L}'/\mathbf{L}'^T$.¹⁴ This strategy is about $10 \times$ faster than diagonalization of $\mathbf{1} + \mathbf{Q}(u)\tilde{\mathbf{C}}$ (which is not symmetric). The point at which the $O(N_{\text{aux}}^3)$ evaluation of eq 16 becomes the time-determining step is thus pushed further outward.

An important and possibly under-appreciated advantage of computing $\mathbf{Q}(u)$ by eq 11 (AO¹⁶) versus eq 2 (MO⁶) lies in the decoupling of the u -integration from the time-determining step. In eq 2, $\mathbf{G}(u)$ must be recalculated from scratch for each u -frequency point and contracted with three-center integrals S_{ai}^M from left and right, which is the dominant step at $O(N_u N_{\text{aux}}^2 N_{\text{occ}} N_{\text{virt}})$, where N_u is the number of u -quadrature nodes. In other words, the computational time required for conventional RI-RPA is directly proportional to the number of u -quadrature nodes. In contrast, the integral transform in eq 7 enables us to precompute the matrices \mathbf{F}_0 , $\mathbf{F}_{\text{INT}}^{(t_\alpha)}$, and $\mathbf{F}_D^{(t_\alpha)}$ at a formal cost of $O(\tau N_{\text{aux}}^2 N_{\text{basis}}^2)$, where τ is the number of Laplace quadrature nodes, because they do not depend on u . $\mathbf{Q}(u)$ is then constructed via eq 11 at a negligible cost of $O(\tau N_{\text{aux}}^2)$ per u -quadrature node, making it possible to employ hundreds of quadrature nodes essentially for free. When the electronic structure is sparse and a local RI metric is used, eq 11 (AO) asymptotically scales linearly, whereas eq 2 (MO) always scales quartically.

3. THEORY AND RESULTS

3.1. Complexity Reduction through Cholesky Factorization. In this work, we report dramatic performance improvements to the RI-RPA energy evaluation by pivoted Cholesky factorization. Formal complexity is reduced from $O(N_{\text{aux}}^2 N_{\text{basis}}^2)$ to $O(N_{\text{aux}}^2 N_{\text{basis}} N_{\text{occ}})$, resulting in drastic runtime reductions especially for the large basis sets typically used in RPA calculations.

We emphasize that we use the term “pivoted Cholesky factorization”²⁶ in the following sense: a positive semidefinite matrix \mathbf{A} may be decomposed as $\mathbf{P}^{-1}\mathbf{A}\mathbf{P} = \mathbf{L}\mathbf{L}^T$, where \mathbf{L} is lower triangular, and \mathbf{P} is a permutation matrix, or equivalently $\mathbf{A} = \mathbf{P}\mathbf{L}\mathbf{L}^T\mathbf{P}^{-1}$. A permutation matrix \mathbf{P} is a unitary matrix which permutes the rows of a matrix \mathbf{A} when premultiplied ($\mathbf{P}\mathbf{A}$), or the columns when postmultiplied ($\mathbf{A}\mathbf{P}$). $\mathbf{P}\mathbf{L}$ has dimension $\dim \mathbf{A} \times \text{rank } \mathbf{A}$ and is *not* lower triangular. After resorting the columns of $\mathbf{P}\mathbf{L}$ by another permutation matrix \mathbf{U} to enhance useable sparsity (see ref 33 for details on this reordering procedure), the complete factorization is $\mathbf{A} = \mathbf{P}\mathbf{L}\mathbf{U}\mathbf{U}^{-1}\mathbf{L}^T\mathbf{P}^{-1}$, which we abbreviate as “ $\mathbf{A} = \mathbf{L}\mathbf{L}^T$ ”.

We proceed by performing pivoted Cholesky decompositions of all occupied-type density matrices (\mathbf{P} , $\mathbf{P}\mathbf{F}\mathbf{P}$, $\underline{\mathbf{P}}^{(\alpha)}$, $\underline{\mathbf{P}}^{(\alpha)}$, and $\underline{\mathbf{P}}^{(\alpha)}$) in eqs 13–15. This reveals the matrices’ ranks, which is N_{occ} or smaller. We then reorder the columns of each left Cholesky factor for sparsity, as described in ref 33. The resulting Cholesky factor is a transformation matrix to a local pseudo-MO basis.^{28,29} We transform one AO index of the three-center integrals \mathbf{B}_M to this local basis, which reduces the dimension of each \mathbf{B}_M from $N_{\text{basis}} \times N_{\text{basis}}$ to $N_{\text{basis}} \times N_{\text{occ}}$ while at the same time preserving any sparsity of the original matrix (see remarks below). The resulting expressions for \mathbf{F}_0 , $\mathbf{F}_{\text{INT}}^{(t_a)}$, and $\mathbf{F}_D^{(t_a)}$ are

$$(\mathbf{F}_0)_{MN} = -\text{Tr}(\mathbf{V}_M^T \mathbf{P} \mathbf{V}_N) - \text{Tr}(\mathbf{W}_M^T \mathbf{P} \mathbf{F} \mathbf{P} \mathbf{W}_N) \quad (19)$$

$$(\mathbf{F}_{\text{INT}}^{(t_a)})_{MN} = \text{Tr}(\mathbf{Z}_M^{(\alpha)T} \underline{\mathbf{P}}^{(\alpha)} \mathbf{Z}_N^{(\alpha)}) \quad (20)$$

$$(\mathbf{F}_D^{(t_a)})_{MN} = -2\text{Tr}(\mathbf{X}_M^{(\alpha)T} \underline{\mathbf{P}}^{(\alpha)} \mathbf{X}_N^{(\alpha)}) - \text{Tr}(\mathbf{Y}_M^{(\alpha)T} \underline{\mathbf{P}}^{(\alpha)} \mathbf{Y}_N^{(\alpha)}) - \text{Tr}(\mathbf{Z}_M^{(\alpha)T} \underline{\mathbf{P}}^{(\alpha)} \mathbf{Z}_N^{(\alpha)}) \quad (21)$$

where the occupied density matrices have been absorbed:

$$\mathbf{V}_M = \mathbf{B}_M \mathbf{L}' \text{ with } -\mathbf{P}\mathbf{F}\mathbf{P} = \mathbf{L}'\mathbf{L}'^T \quad (22)$$

$$\mathbf{W}_M = \mathbf{B}_M \mathbf{L} \text{ with } \mathbf{P} = \mathbf{L}\mathbf{L}^T \quad (23)$$

$$\mathbf{X}_M^{(\alpha)} = \mathbf{B}_M \underline{\mathbf{L}}^{(\alpha)} \text{ with } -\underline{\mathbf{P}}^{(\alpha)} = \underline{\mathbf{L}}^{(\alpha)} \underline{\mathbf{L}}^{(\alpha)T} \quad (24)$$

$$\mathbf{Y}_M^{(\alpha)} = \mathbf{B}_M \underline{\mathbf{L}}^{(\alpha)} \text{ with } \underline{\mathbf{P}}^{(\alpha)} = \underline{\mathbf{L}}^{(\alpha)} \underline{\mathbf{L}}^{(\alpha)T} \quad (25)$$

$$\mathbf{Z}_M^{(\alpha)} = \mathbf{B}_M \underline{\mathbf{L}}^{(\alpha)} \text{ with } \underline{\mathbf{P}}^{(\alpha)} = \underline{\mathbf{L}}^{(\alpha)} \underline{\mathbf{L}}^{(\alpha)T} \quad (26)$$

Note that $\mathbf{P}\mathbf{F}\mathbf{P}$ and $\underline{\mathbf{P}}^{(\alpha)}$ are negative semidefinite and are therefore multiplied by -1 before factorization, which leads to sign changes in eqs 19 and 21 compared to eqs 13 and 15. Shifting the MO energies downward uniformly by $\frac{1}{2}(\epsilon_{\text{HOMO}} + \epsilon_{\text{LUMO}})$ (as described in ref 34; HOMO is highest occupied MO and LUMO is the lowest unoccupied MO) before constructing the pseudodensity matrices gives the numerically most stable results.

The question of whether to also factorize the virtual pseudodensities arises naturally. In the context of coupled-perturbed self-consistent field calculations, factorization of the virtual

subspace has performance benefits,³⁵ mostly due to numerical rank deficiency of some pseudodensities far beyond their analytical rank of N_{virt} . In AO-RPA, doing the same results in simpler and more symmetric equations, which are given in Appendix A. When it comes to performance, however, we have found this approach disappointing. The reason is twofold. First, correlation methods such as RPA require large bases for good results, in which case $N_{\text{basis}} \approx N_{\text{virt}}$ and the rank reduction from factorization is negligible. Second, the Cholesky factorization of the virtual subspace preserves sparsity less well than in the occupied subspace. Consequently, the rank reduction is often counteracted by loss of sparsity, and performance degrades. For small systems, when no sparse algebra is used, however, we do use the equations given in Appendix A.

Finally, we point out another surprising pitfall. The pivoted Cholesky decomposition will sometimes yield pseudo-MOs of which a small number are not local, but extend over the whole AO space, which thwarts attempts to benefit from blocked sparse algebra. We have found this problem can be solved by orthogonalizing the density matrices in the contravariant AO basis before Cholesky factorization, and reverting the orthogonalization afterward. However, the orthogonalization cannot be Löwdin’s symmetric orthogonalization, but must be some sparsity-preserving but nonsymmetric orthogonalization. We use the Cholesky factors of the AO overlap matrix.

3.2. RI-RPA Using the erfc-Attenuated Coulomb Metric. Key to reduce the computational effort and scaling in extended molecules is the choice of the RI metric. As mentioned above, ref 16 uses the overlap metric³⁶ (eq 10), which is local in the sense that auxiliary functions M do not overlap with AO basis function pairs $\mu\nu$ if there is enough distance between their centers, which leads to sparsity in the matrix representations. In contrast, the Coulomb metric (eq 4) couples auxiliary functions and AO basis function pairs over effectively infinite distances ($\frac{1}{r_{12}}$ decay), and no sparsity can be gained.

The Coulomb metric has been shown to be optimal in fitting density-like repulsions,³⁷ and has subsequently been the ubiquitous choice. This metric has no disadvantage when transforming to the canonical MO basis where all sparsity is lost anyway. In local bases, such as the atomic orbitals and Cholesky pseudo-MOs (see section 3.1), local RI metrics have important advantages.

The overlap metric is very local, because it decays as $\exp(-r_{12}^2)$ in Gaussian basis sets. The downside is decreased accuracy.³⁷ Other metrics have been described in the literature, especially Coulomb metrics attenuated by a complementary error function (erfc)^{30,31} or by a Gaussian function.³² For correlation energy calculations, the erfc-attenuated Coulomb metric was first used by Jung et al.³¹ for scaled-opposite-spin MP2 calculations.

Here, we employ the erfc-attenuated Coulomb metric within RI-RPA for the first time, and show that it combines the advantages of the Coulomb and overlap metrics.

The two- and three-center integrals necessary are given by

$$(M|\mu\nu)_\omega = \left(M \left| \frac{\text{erfc}(\omega r_{12})}{r_{12}} \right| \mu\nu \right) \quad (27)$$

$$(\mathbf{S}_\omega)_{MN} = \left(M \left| \frac{\text{erfc}(\omega r_{12})}{r_{12}} \right| N \right) \quad (28)$$

$$\tilde{\mathbf{C}}_\omega = \mathbf{S}_\omega^{-1} \mathbf{C} \mathbf{S}_\omega^{-1} \quad (29)$$

such that the resolution-of-the-identity is formally

$$(ailbj) = \sum_{MN} (ailM)_\omega (\tilde{C}_\omega)_{MN} (N|bj)_\omega \quad (30)$$

Adamson et al.³⁸ have described how to efficiently calculate these integrals. \tilde{C}_ω is most reliably computed as $(S_\omega C^{-1} S_\omega)^{-1}$. As with the overlap metric, deferring the multiplication with the two-center integrals to the last step of the algorithm (eq 12) is necessary to retain locality through the time-determining steps. The attenuation strength is controlled by the parameter ω . erfc-attenuation has the pleasant property of allowing continuous variation between the $\frac{1}{r_{12}}$ and overlap operators

$$\lim_{\omega \rightarrow 0} \frac{\text{erfc}(\omega r_{12})}{r_{12}} = \frac{1}{r_{12}} \quad (31)$$

$$\lim_{\omega \rightarrow \infty} \frac{\text{erfc}(\omega r_{12})}{r_{12}} = \delta(r_{12}) \quad (32)$$

where δ is Dirac's function.

Figure 1 shows the effect of different values for ω over several orders of magnitude. Plotted are the RPA correlation energy

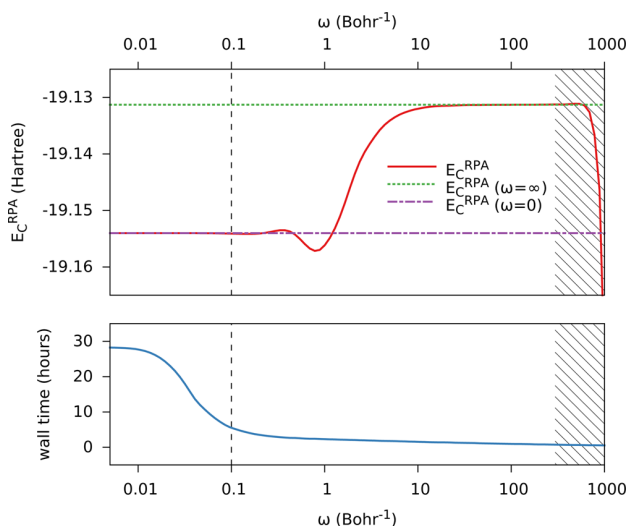


Figure 1. Effect of the attenuation parameter ω on the accuracy and performance of ω -CDD-RPA in the erfc-Coulomb metric for linear n -C₈₀H₁₆₂ (def2-SVP). The dashed horizontal lines are reference energy values calculated with the Coulomb ($\omega = 0$) and overlap ($\omega = \infty$) RI metrics. For a wide range $\omega \in [0, 0.1]$, the erfc-Coulomb metric reproduces the (optimal) Coulomb metric results to sub-mHartree accuracy in absolute energies at a fraction of the cost. Our recommended value of $\omega = 0.1$ is indicated by the dashed vertical line. Divergence (presumably because of limited floating point precision) is observed after $\omega \gtrsim 500$ (shaded graph area).

(top) and the wall time required (bottom, 12 threads on an Intel Xeon E5-2620 machine) as a function of ω (logarithmic scale). The limits of $\omega \rightarrow 0$ and $\omega \rightarrow \infty$ are correctly recovered. The overlap metric as well as high- ω attenuation violate the variational upper bound property⁶ of the Coulomb metric. For relative energies, this bound does not hold for the Coulomb metric either, though. For $\omega \gtrsim 500$, our implementation begins to diverge, presumably due to the limits of double precision floating point arithmetic. For ω -values between approximately 0.5 and 1.1, the erfc-attenuated absolute energies are lower than for the Coulomb metric. The computational effort

rises dramatically as the attenuation approaches zero, exceeding 28 h, and bottoms out at around 30 min for maximum attenuation. The most interesting region is between $\omega \simeq 0.1$ (where the Coulomb metric result is recovered to within 100 μ Hartree in the absolute energy) and $\omega \simeq 1$ (where the correlation energy starts to move toward the overlap metric result). The wall times required for calculations in this ω -interval are around 2 h, but yield *absolute* energies within mHartree of the Coulomb metric result, which takes over 10 \times as long to compute. We will present more data in sections 4.1 and 4.2, including from calculations with larger basis sets, which corroborate these findings. From the combined results, we recommend $\omega = 0.1$ as a starting point when using the erfc-attenuated Coulomb metric in RI-RPA.

4. CALCULATIONS

We used the Perdew–Burke–Ernzerhof (PBE) functional^{39,40} to obtain Kohn–Sham orbitals, using def2-SVP, def2-TZVP, and def2-QZVP basis sets.^{41,42} The RI approximation uses the corresponding RI counterparts.^{43,44} We use RI only for $(ailbj)$ -type integrals in the correlation part of the RPA energy, not for the Hamiltonian expectation value with the Kohn–Sham orbitals or during the preceding SCF calculation. All calculations use 100 quadrature nodes for the frequency integration, and a fixed integration interval of $u \in [0; 400]$ a.u., using the coordinate mapping described in ref 6. We emphasize that 100 quadrature nodes is more than typically used in RI-RPA calculations. We chose a generous number of nodes and a large integration interval to eliminate any errors from the quadrature, and used that same number of quadrature nodes for all calculations in this work in order to facilitate easy comparisons. We stress that fewer quadrature nodes may be sufficient (depending on the system under study), which would improve the efficiency of the MO-based formulation.

Where applicable, 15 Laplace quadrature points using the weights and nodes of ref 45. were employed. Core orbitals were frozen in all calculations. None of the results presented include corrections for possible basis set superposition errors. While this may render the statistical results slightly worse, the error is expected to be systematic across all methods presented. Some caution is advised when comparing the results below to counterpoise-corrected results.

Our ω -CDD-RPA method as well as the MO (ref 6) and AO (ref 16) formulations of RI-RPA, as well as RI-free RPA were implemented in the FermiONs++ program.^{46,47} We checked our MO-RI implementation against the canonical implementation in Turbomole7.0⁴⁸ to verify correctness and comparable performance. All runtimes given are wall times, not CPU times.

4.1. Performance: S66 Set. The full S66 set⁴⁹ of small-molecule interaction energies (mean reference interaction energy -5.5 kcal mol⁻¹, maximum reference interaction energy -19.8 kcal mol⁻¹) in double-, triple-, and quadruple- ζ bases serves as a performance and accuracy benchmark for small molecules. All calculations were performed using 12 threads on a dual-processor Intel Xeon E5–2620 machine. The small size of the molecules in the test set means no sparsity in the RI integrals or density matrices can be expected and no computational efficiency can be gained from a local metric, that is, all metrics yield identical performance.

The following results, therefore, measure (1) the RI-independent performance of the AO, ω -CDD, and MO formulations of RI-RPA for small systems without electronic sparsity and (2) their accuracy using different RI metrics, also including RI-free RPA results (computed via eq 9 in ref 6). The accuracy of all methods and

Table 1. S66: Root Mean Square (RMSD), Mean Absolute (MAD), and Maximum Absolute (MAX) Deviations from the Updated CCSD(T)/CBS Reference Interaction Energies⁵⁰ in kcal mol⁻¹ for Coulomb-, erfc-Attenuated Coulomb- ($\omega = 0.1$, $\omega = 0.5$), and Overlap-RI Metric RPA in the AO, ω -CDD, and MO Formulations, as well as for RI-Free RPA

basis	RI metric	RMSD/kcal mol ⁻¹			MAD/kcal mol ⁻¹			MAX/kcal mol ⁻¹		
		AO	ω -CDD	MO	AO	ω -CDD	MO	AO	ω -CDD	MO
def2-SVP	no RI			0.95			0.75			3.43
	Coulomb	0.98	0.98	0.97	0.77	0.77	0.77	3.45	3.45	3.46
	$\omega = 0.1$	0.98	0.98	0.97	0.77	0.77	0.77	3.44	3.44	3.46
	$\omega = 0.5$	1.00	1.00	1.00	0.81	0.81	0.81	3.44	3.44	3.45
	overlap	1.04	1.04	1.04	0.87	0.87	0.87	3.57	3.57	3.58
def2-TZVP	no RI			0.88			0.56			3.83
	Coulomb	0.86	0.86	0.88	0.56	0.56	0.56	3.81	3.81	3.83
	$\omega = 0.1$	0.87	0.87	0.88	0.56	0.56	0.56	3.81	3.81	3.83
	$\omega = 0.5$	0.90	0.90	0.91	0.59	0.59	0.59	3.88	3.88	3.89
	overlap	0.95	0.95	0.96	0.64	0.64	0.65	3.99	3.99	4.01
def2-QZVP	no RI			0.62			0.47			3.11
	Coulomb	0.62	0.62	0.62	0.47	0.47	0.46	3.11	3.11	3.11
	$\omega = 0.1$	0.62	0.62	0.62	0.47	0.47	0.46	3.11	3.11	3.11
	$\omega = 0.5$	0.63	0.63	0.63	0.48	0.48	0.47	3.11	3.11	3.11
	overlap	0.64	0.64	0.64	0.51	0.51	0.50	3.11	3.11	3.11

RI metrics for the S66 set can be summarized briefly as being very similar. Detailed values for the root mean square (RMSD), mean absolute (MAD), and maximum absolute (MAX) deviations from the updated⁵⁰ CCSD(T)/CBS reference interaction energies can be found in Table 1. We note the Laplace transform of eq 7 and its quadrature introduces no significant error in the S66 set. Likewise, the Cholesky decompositions of section 3.1 do not introduce any error over the AO formulation.

Regarding the RI metric, the Coulomb metric is generally best. However, the moderately erfc-attenuated ($\omega = 0.1$) Coulomb metric gives practically identical results. Increasing the attenuation to $\omega = 0.5$ leads to slightly inferior results, which are, however, magnitudes below the error inherent to RPA. Overlap metric results are slightly worse, but still an order of magnitude below the RPA error itself. Increasing the attenuation systematically increases the error for a given RI basis set, but only very slightly. Generally, the differences between RI metrics decrease for larger AO bases (and correspondingly larger RI bases). For quadruple- ζ bases, the differences between different RI metrics almost vanish for the S66 test set.

We now move to performance characteristics. Cumulative wall times for the complete S66 set ($3 \times 66 = 198$ calculations) are given in Table 2 for AO-RPA and ω -CDD-RPA. Exploiting the

Table 2. S66: Accumulated Wall Times and Speedups for AO- and ω -CDD-RPA Correlation Energy Calculations ($\omega = 0.1$)

basis	time (s)		speedup
	AO	ω -CDD	ω -CDD v AO
def2-SVP	2453	373	7×
def2-TZVP	16408	1476	11×
def2-QZVP	432405	15879	27×

rank deficiency of occupied (pseudo-) density matrices leads to large performance improvements of ω -CDD. The speedups are larger for larger bases, reaching 27× for a quadruple- ζ basis. As was discussed in section 3.1, ω -CDD reduces the computational complexity with respect to basis set size for a fixed-size molecule from N^4 to N^3 , the same as MO-RI-RPA, while the linear scaling of AO-RPA with molecular size remains unchanged.

ω -CDD-RPA is also competitive with MO-RI-RPA, slightly outperforming it for double- and triple- ζ bases, and showing equal performance for a quadruple- ζ basis. ω -CDD-RPA has extremely low overhead and the same scaling behavior as MO-RI-RPA in the limit of dense matrices (i.e., no usable matrix sparsity, such as in the S66 set). We emphasize that runtimes of ω -CDD-RPA are proportional to the number τ of Laplace quadrature points, while runtimes of MO-RI-RPA are proportional to the number N_u of u -frequency quadrature points. Theoretical parity is reached when $4\tau + 2 = N_u$. Which of the two formulations will outperform the other depends on which quadrature can be carried out with fewer points.

4.2. Accuracy: L7 Set. The L7 benchmark set⁵¹ comprises dispersion-dominated molecular systems of much larger size (up to 112 atoms, mean reference interaction energy -18.2 kcal mol⁻¹, maximum reference interaction energy -31.3 kcal mol⁻¹) than those in the S66 set. Using the def2-TZVP basis, we calculated RMSD, MAD, and MAX deviations from the QCISD(T)/CBS reference interaction energies⁵¹ for different attenuation parameters ω for both the MO and ω -CDD formulations of RI-RPA. The results are shown in Figure 2.

ω -CDD-RPA yields lower errors throughout, which is clearly fortuitous. The more significant result is between the different attenuation parameters ω . Unlike the smaller molecules of the S66 test set, the larger molecules of the L7 set are sensitive to the choice of the RI metric. For all three measures (RMSD, MAD, MAX), the unattenuated Coulomb metric consistently yields the best results. Similarly to the results of section 4.1, lower attenuation yields superior results. However, a moderate attenuation of $\omega = 0.1$ degrades the accuracy by only 0.02 kcal mol⁻¹ in RMSD and MAD, and 0.05 kcal mol⁻¹ in MAX, which we consider numerical noise. Increasing the attenuation to $\omega = 0.2$ or $\omega = 0.5$ increases the error measures very slightly. The overlap metric ($\omega = \infty$), however, yields an RMSD almost one kcal mol⁻¹ higher than the Coulomb metric, an MAD which is 0.6 kcal mol⁻¹ higher, and a maximum absolute error 2.5 kcal mol⁻¹ higher. Combined with the results presented in sections 3.2 and 4.1, this strongly supports the erfc-attenuated Coulomb metric in place of the overlap metric in RI-RPA calculations.

Finally, we note that while the systems comprising this benchmark set are considerably larger than those of the S66 set

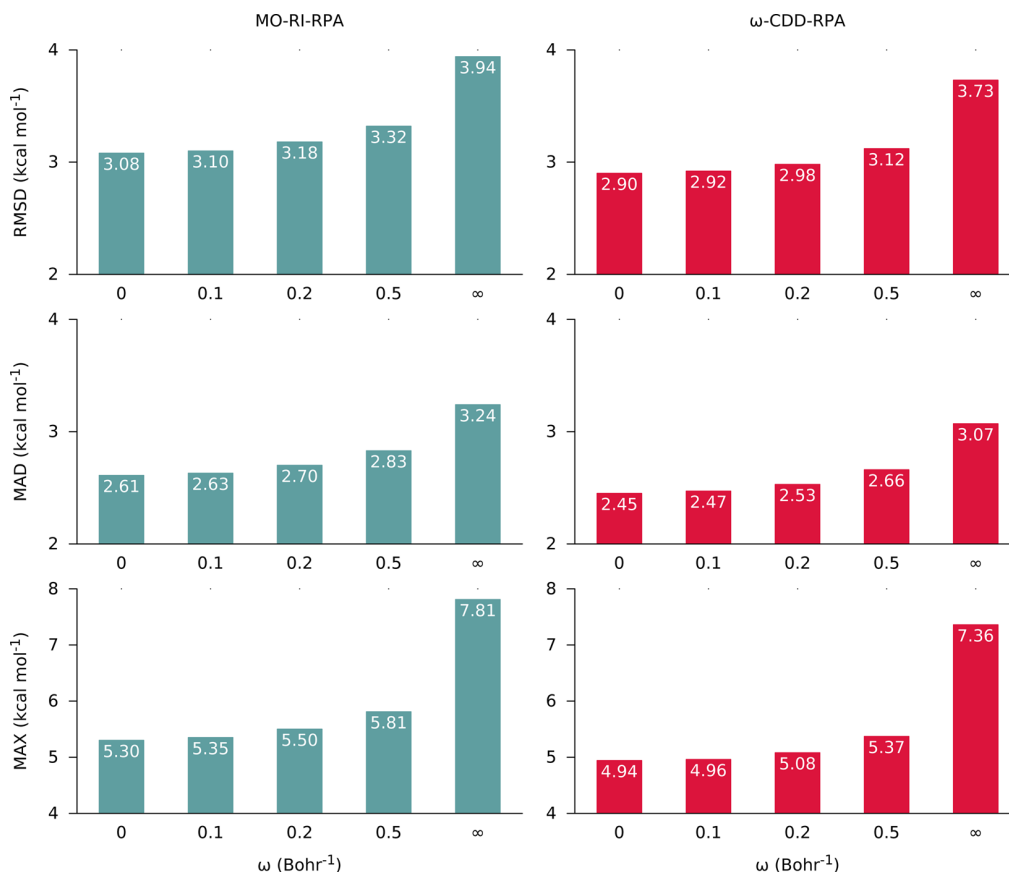


Figure 2. L7: Root mean square (RMSD), mean absolute (MAD), and maximum absolute (MAX) deviations in kcal mol⁻¹ from the QCISD(T)/CBS reference interaction energies⁵¹ for different attenuation parameters ω (def2-TZVP). Left column: Canonical MO-RI-RPA. Right column: ω -CDD-RPA.

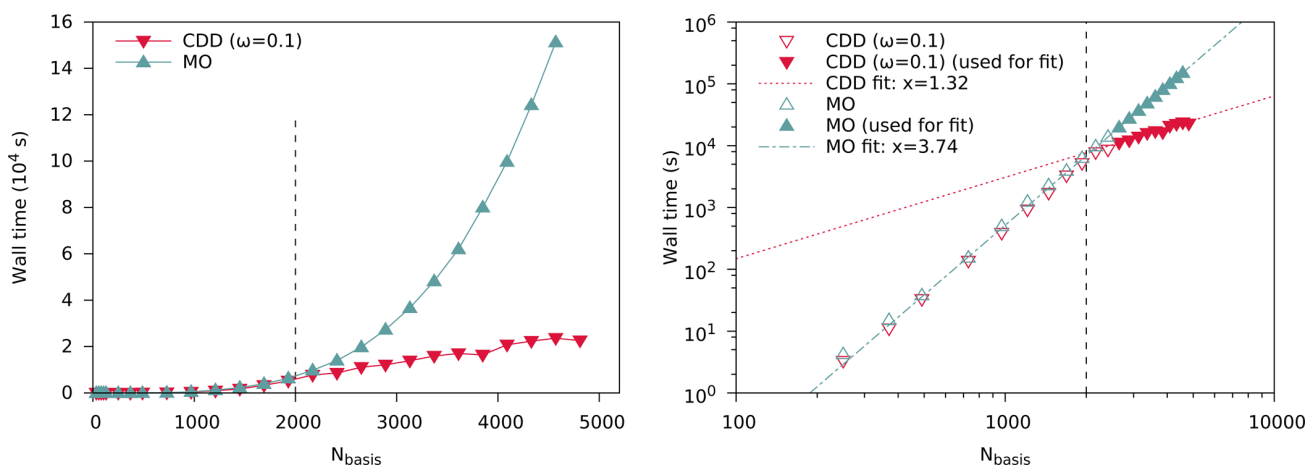


Figure 3. Plots of wall time against number of basis functions showing the computational complexity of the MO and ω -CDD formulations for linear n -alkanes (def2-SVP, erfc-attenuated Coulomb metric, $\omega = 0.1$). Left: Linear plot. Right: Log–log plot, with linear fits for MO and ω -CDD. The vertical dashed line indicates the point after which sparse algebra is used.

discussed in section 4.1, they are not as large as to provide usable matrix sparsity. Consequently, dense matrix algebra is used for all calculations, and performance is similar for the ω -CDD and MO variants of RI-RPA.

4.3. Scaling Behavior. Utilizing the rank deficiency of density matrices (cf. section 3.1) reduces the computational prefactor of AO-RPA, as well as its formal scaling from $\mathcal{O}(N_{\text{aux}}^2 N_{\text{basis}}^2)$

to $\mathcal{O}(N_{\text{aux}}^2 N_{\text{basis}} N_{\text{occ}})$ in the limit of densely populated matrices. In the limit of large molecules with sparse electronic structures, however, we must ensure that the Cholesky factorization does not destroy usable matrix sparsity. Similarly, the introduction of an erfc-attenuated Coulomb metric instead of the overlap metric has to preserve the asymptotic $\mathcal{O}(N)$ scaling of AO-RPA. In the following, we focus on these two aspects. Calculations in this

section used 16 threads on a dual-processor Intel Xeon E5–2667 machine. We switched the ω -CDD formulation from dense to sparse algebra at 2000 basis functions. Ideally, this would be automatically decided based on usable sparsity in the density matrix and three-center integrals (eq 27). For the purpose of this work, we switched to sparse algebra as soon as it was faster, which for both test sets in sections 4.3.1 and 4.3.2 happened to be at 2000 basis functions. Structure files for the test systems can be found online.⁵²

4.3.1. Alkanes. Our first test set are linear n -alkanes of increasing length. We calculated the RI-RPA correlation energy with canonical MO-RPA and ω -CDD-RPA ($\omega = 0.1$), which includes construction of $\mathbf{Q}(u)$ and evaluation of the matrix logarithm via eq 16. The data is plotted in Figure 3 in linear and log–log plots. From the linear fit in the log–log plots, MO-RPA scales as $O(N^{3.7})$, which is slightly better than the theoretical $O(N^4)$. Our own ω -CDD-RPA scales as $O(N^{1.3})$ for large systems.

Selected data points are given in Table 3. ω -CDD-RPA gives speedups over MO-RI-RPA of around 20–40% for systems with around 1000 basis functions. As discussed in section 4.1, whether or not a speedup can be attained for these system sizes depends critically on the number of u -frequency quadrature nodes used.

For large molecular sizes, however, the scaling behavior of ω -CDD will always give large speedups over MO-RPA. Table 3

Table 3. Wall Times and Computational Complexity of the ω -CDD and MO Formulations for Linear n -Alkanes (def2-SVP, erfc-Attenuated Coulomb Metric, $\omega = 0.1$)^a

	N_{basis}	ω -CDD		MO		total speedup
		time (s)	$O(N^x)$	time (s)	$O(N^x)$	
C ₂₀ H ₄₂	490	33		38		1.2×
C ₅₀ H ₁₀₂	1210	919	3.7	1244	3.9	1.4×
C ₁₀₀ H ₂₀₂	2410	8585	3.2	13 995	3.5	1.6×
C ₁₂₀ H ₂₄₂	2890	12100	1.9	27 359	3.7	2.3×
C ₁₅₀ H ₃₀₂	3610	17022	1.5	62 025	3.7	3.6×
C ₂₀₀ H ₄₀₂	4810	22593	1.0	*182 875	(3.7)	*8.1×

^aThe column headed $O(N^x)$ contains the scaling exponents relative to the row above. Values marked with an asterisk (*) are extrapolated conservatively.

shows the scaling exponents for ω -CDD and MO for progressively larger molecules. While ω -CDD-RPA reaches perfect $O(N)$ scaling for the largest system, MO-RPA scales as $O(N^{3.7})$. ω -CDD outperforms MO 8-fold for the largest system.

4.3.2. Glycine Chains. As a second test set for the scaling behavior, we used glycine chains of increasing length. The corresponding linear and log–log plots are given in Figure 4. Similarly to the results of section 4.3.1, linear fits in the log–log plots reveal $O(N^{3.6})$ scaling for MO, and $O(N^{1.4})$ scaling for ω -CDD. These timing data contain both the construction of $\mathbf{Q}(u)$ via eq 2 (MO) or eqs 11 and 33–35 (ω -CDD), as well as evaluation of the matrix logarithm (eq 16).

Selected data points are given in Table 4, where we separately resolved the construction of $\mathbf{Q}(u)$ and evaluation of the matrix logarithm (eq 16). The complexity of the time-determining steps in ω -CDD-RPA (eqs 33–35) reaches $O(N^{1.3})$ very quickly, whereas the time-determining step in MO-RPA scales as $O(N^4)$. Evaluation of the matrix logarithm is identical for both formulations, and predictably has $O(N^3)$ complexity with a small pre-factor. For the largest system, the time required for this step is less than 8% of the total time for ω -CDD-RPA, and will become dominant only for extremely large molecules. The total speedup (including matrix logarithm evaluation) of ω -CDD over MO steadily rises from 1.3× up to over 13× for the largest test system.

5. SUMMARY

Cholesky decomposition of densities (CDD) in atomic orbital RI-RPA¹⁶ calculations reduces the scaling with respect to basis set size by one order, removing the main drawback of the AO formulation over the canonical MO formulation. CDD can accelerate AO-RPA calculations by over 5× for double- ζ , over 10× for triple- ζ , and over 25× for quadruple- ζ basis sets, without any decrease in accuracy.

Depending on the number of necessary nodes for the frequency or Laplace quadrature, even for small molecular systems our method is competitive with the canonical MO-RI-RPA formulation of ref 6, due to the decoupling of the numerical integration in the frequency domain from the time-determining step. For sparse electronic systems, our ω -CDD-RPA method outperforms the canonical formulation over 10×.

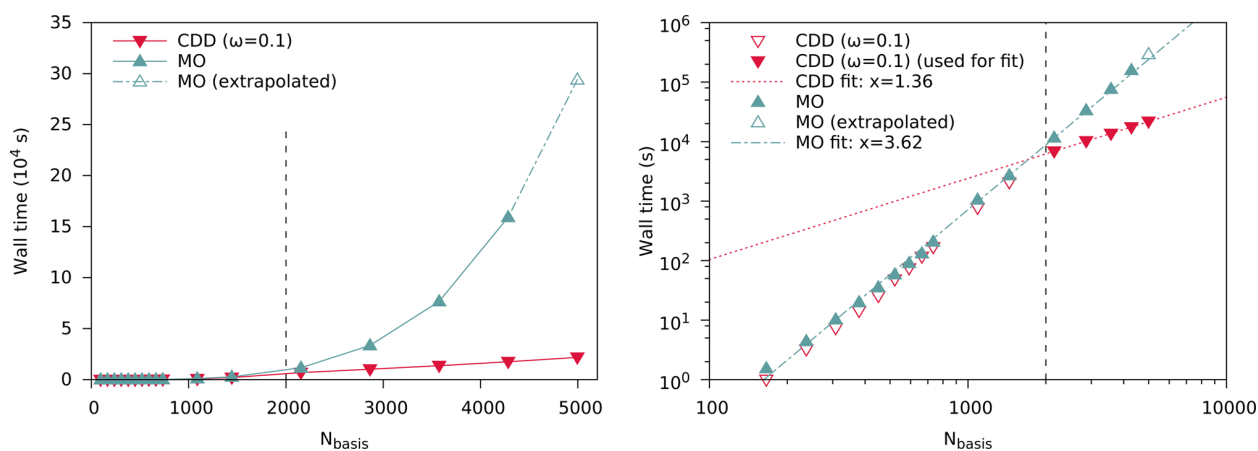


Figure 4. Plots of wall time against number of basis functions showing the computational complexity of the MO and ω -CDD formulations for glycine chains (def2-SVP, erfc-attenuated Coulomb metric, $\omega = 0.1$). Left: Linear plot. Right: Log–log plot, with linear fits for MO and ω -CDD. The vertical dashed line indicates the point after which sparse algebra is used.

Table 4. Wall Times and Computational Complexity of the ω -CDD and MO Formulations for Glycine Chains (def2-SVP, erfc-Attenuated Coulomb Metric, $\omega = 0.1$)^a

	N_{basis}	ω -CDD		MO		Tr ln (eq16)		total
		time (s)	$O(N^x)$	time (s)	$O(N^x)$	time (s)	$O(N^x)$	speedup
Gly ₂₀	1444	3690		2649		53 (3%)		1.3×
Gly ₃₀	2154	6719	3.0	11456	3.7	163 (2%)	2.8	1.7×
Gly ₄₀	2864	9850	1.3	33150	3.7	338 (3%)	2.6	3.3×
Gly ₅₀	3574	12970	1.2	76074	3.8	624 (5%)	2.8	5.6×
Gly ₆₀	4284	16402	1.3	158148	4.0	1063 (6%)	2.9	9.1×
Gly ₇₀	4994	20144	1.3	*292347	(4)	1667 (8%)	2.9	*13.5×

^aThe column headed $O(N^x)$ contains the scaling exponents relative to the row above. Values marked with an asterisk (*) are extrapolated. See text for detailed descriptions of the columns.

Furthermore, we introduced the use of the erfc-attenuated Coulomb metric for the resolution-of-the-identity in RPA calculations, which reproduces Coulomb-metric results to very high accuracy even in absolute energies while preserving the locality and performance benefits of the overlap metric. We demonstrated that the effective $O(N)$ scaling of AO-RPA in the overlap metric is fully retained, while improving accuracy at the same time.

Further research is required to obtain more efficient quadratures for the Laplace transform of eq 7, to increase accuracy and lower the number of necessary nodes. Similarly, the behavior of the transform for small-gap systems warrants further study.

APPENDIX A: RI-RPA EQUATIONS WITH CHOLESKY DECOMPOSITION OF OCCUPIED AND VIRTUAL SUBSPACES

When performing Cholesky factorizations also on all virtual pseudodensity matrices, eqs 19–21 simplify to

$$(\mathbf{F}_0)_{MN} = -\text{Tr}(\mathbf{U}_M^T \mathbf{U}_N) - \text{Tr}(\mathbf{V}_M^T \mathbf{V}_N) \quad (33)$$

$$(\mathbf{F}_{\text{INT}}^{(t_a)})_{MN} = \text{Tr}(\mathbf{W}_M^{(\alpha)T} \mathbf{W}_N^{(\alpha)}) \quad (34)$$

$$(\mathbf{F}_D^{(t_a)})_{MN} = -2\text{Tr}(\mathbf{X}_M^{(\alpha)T} \mathbf{X}_N^{(\alpha)}) - \text{Tr}(\mathbf{Y}_M^{(\alpha)T} \mathbf{Y}_N^{(\alpha)}) - \text{Tr}(\mathbf{Z}_M^{(\alpha)T} \mathbf{Z}_N^{(\alpha)}) \quad (35)$$

with

$$\mathbf{U}_M = \mathbf{L}^T \mathbf{B}_M \mathbf{L} \text{ and } \mathbf{P} = \mathbf{L} \mathbf{L}^T, \mathbf{P} \mathbf{P} = \mathbf{L} \mathbf{L}^T \quad (36)$$

$$\mathbf{V}_M = \mathbf{L}^T \mathbf{B}_M \mathbf{L}' \text{ and } -\mathbf{P} \mathbf{P} = \mathbf{L}' \mathbf{L}'^T, \mathbf{P}' = \mathbf{L} \mathbf{L}'^T \quad (37)$$

$$\mathbf{W}_M^{(\alpha)} = \mathbf{L}^{(\alpha)T} \mathbf{B}_M \mathbf{L}^{(\alpha)} \text{ and } \mathbf{P}^{(\alpha)} = \mathbf{L}^{(\alpha)} \mathbf{L}^{(\alpha)T}, \mathbf{P}^{(\alpha)} = \mathbf{L}^{(\alpha)} \mathbf{L}^{(\alpha)T} \quad (38)$$

$$\mathbf{X}_M^{(\alpha)} = \mathbf{L}^{(\alpha)T} \mathbf{B}_M \mathbf{L}^{(\alpha)} \text{ and } -\mathbf{P}^{(\alpha)} = \mathbf{L}^{(\alpha)} \mathbf{L}^{(\alpha)T}, \mathbf{P}^{(\alpha)} = \mathbf{L}^{(\alpha)} \mathbf{L}^{(\alpha)T} \quad (39)$$

$$\mathbf{Y}_M^{(\alpha)} = \mathbf{L}^{(\alpha)T} \mathbf{B}_M \mathbf{L}^{(\alpha)} \text{ and } \mathbf{P}^{(\alpha)} = \mathbf{L}^{(\alpha)} \mathbf{L}^{(\alpha)T} \quad (40)$$

$$\mathbf{Z}_M^{(\alpha)} = \mathbf{L}^{(\alpha)T} \mathbf{B}_M \mathbf{L}^{(\alpha)} \text{ and } \mathbf{P}^{(\alpha)} = \mathbf{L}^{(\alpha)} \mathbf{L}^{(\alpha)T} \quad (41)$$

AUTHOR INFORMATION

Corresponding Author

*E-mail: christian.ochsenfeld@uni-muenchen.de.

ORCID

Christian Ochsenfeld: 0000-0002-4189-6558

Notes

The authors declare no competing financial interest.

ACKNOWLEDGMENTS

The authors thank Dr. A. M. Burow and M. Beuerle (LMU Munich) for helpful discussions. Financial support was provided by the Deutsche Forschungsgemeinschaft (DFG) for the project Oc35/4-1, and the cluster of excellence EXC 114 "Center for Integrated Protein Science Munich" (CIPSM).

REFERENCES

- (1) Langreth, D. C. D.; Perdew, J. P. J. The Exchange-Correlation Energy of a Metallic Surface. *Solid State Commun.* **1975**, *17*, 1425.
- (2) Langreth, D. C.; Perdew, J. P. Exchange-correlation energy of a metallic surface: Wave-vector analysis. *Phys. Rev. B* **1977**, *15*, 2884.
- (3) Perdew, J. P. Jacob's ladder of density functional approximations for the exchange-correlation energy. *AIP Conf. Proc.* **2000**, 1–20.
- (4) Mezei, P. D.; Csonka, G. I.; Ruzsinszky, A.; Kállay, M. Construction and Application of a New Dual-Hybrid Random Phase Approximation. *J. Chem. Theory Comput.* **2015**, *11*, 4615–4626.
- (5) Furche, F. Molecular tests of the random phase approximation to the exchange-correlation energy functional. *Phys. Rev. B: Condens. Matter Mater. Phys.* **2001**, *64*, 195120.
- (6) Eshuis, H.; Yarkony, J.; Furche, F. Fast computation of molecular random phase approximation correlation energies using resolution of the identity and imaginary frequency integration. *J. Chem. Phys.* **2010**, *132*, 234114.
- (7) Eshuis, H.; Bates, J. E.; Furche, F. Electron correlation methods based on the random phase approximation. *Theor. Chem. Acc.* **2012**, *131*, 1–18.
- (8) Eshuis, H.; Furche, F. Basis set convergence of molecular correlation energy differences. *J. Chem. Phys.* **2012**, *136*, 084105.
- (9) Dunlap, B. I.; Rösch, N. On the gaussian-type orbitals approach to local density functional theory. *J. Chim. Phys. Physico-Chimie Biol.* **1989**, *86*, 671.
- (10) Shen, N.; van Aggelen, H.; Yang, Y.; Yang, W. Tensor hypercontracted ppRPA: Reducing the cost of the particle-particle random phase approximation from $O(r^6)$ to $O(r^4)$. *J. Chem. Phys.* **2014**, *141*, 024119.
- (11) Hohenstein, E. G.; Parrish, R. M.; Martínez, T. J. Tensor hypercontraction density fitting. I. Quartic scaling second- and third-order Møller-Plesset perturbation theory. *J. Chem. Phys.* **2012**, *137*, 044103.
- (12) Parrish, R. M.; Hohenstein, E. G.; Martínez, T. J.; Sherrill, C. D. Tensor hypercontraction. II. Least-squares renormalization. *J. Chem. Phys.* **2012**, *137*, 224106.
- (13) Hohenstein, E. G.; Parrish, R. M.; Sherrill, C. D.; Martínez, T. J. Communication: Tensor hypercontraction. III. Least-squares tensor hypercontraction for the determination of correlated wavefunctions. *J. Chem. Phys.* **2012**, *137*, 221101.
- (14) Kaltak, M.; Klimeš, J.; Kresse, G. Low Scaling Algorithms for the Random Phase Approximation: Imaginary Time and Laplace Transformations. *J. Chem. Theory Comput.* **2014**, *10*, 2498–2507.
- (15) Kállay, M. Linear-scaling implementation of the direct random-phase approximation. *J. Chem. Phys.* **2015**, *142*, 204105.

- (16) Schurkus, H. F.; Ochsenfeld, C. Communication: An effective linear-scaling atomic-orbital reformulation of the random-phase approximation using a contracted double-Laplace transformation. *J. Chem. Phys.* **2016**, *144*, 031101.
- (17) Wilhelm, J.; Seewald, P.; Del Ben, M.; Hutter, J. Large-Scale Cubic-Scaling Random Phase Approximation Correlation Energy Calculations Using a Gaussian Basis. *J. Chem. Theory Comput.* **2016**, *12*, 5851–5859.
- (18) Jiang, H.; Engel, E. Random-phase-approximation-based correlation energy functionals: Benchmark results for atoms. *J. Chem. Phys.* **2007**, *127*, 184108.
- (19) Eshuis, H.; Furche, F. A Parameter-Free Density Functional That Works for Noncovalent Interactions. *J. Phys. Chem. Lett.* **2011**, *2*, 983–989.
- (20) Paier, J.; Ren, X.; Rinke, P.; Scuseria, G. E.; Grüneis, A.; Kresse, G.; Scheffler, M. Assessment of correlation energies based on the random-phase approximation. *New J. Phys.* **2012**, *14*, 043002.
- (21) Ren, X.; Rinke, P.; Joas, C.; Scheffler, M. Random-phase approximation and its applications in computational chemistry and materials science. *J. Mater. Sci.* **2012**, *47*, 7447–7471.
- (22) Mussard, B.; Reinhardt, P.; Ángyán, J. G.; Toulouse, J. Spin-unrestricted random-phase approximation with range separation: Benchmark on atomization energies and reaction barrier heights. *J. Chem. Phys.* **2015**, *142*, 154123.
- (23) Rekkedal, J.; Coriani, S.; Iozzi, M. F.; Teale, A. M.; Helgaker, T.; Pedersen, T. B. Communication: Analytic gradients in the random-phase approximation. *J. Chem. Phys.* **2013**, *139*, 081101.
- (24) Burow, A. M.; Bates, J. E.; Furche, F.; Eshuis, H. Analytical First-Order Molecular Properties and Forces within the Adiabatic Connection Random Phase Approximation. *J. Chem. Theory Comput.* **2014**, *10*, 180–194.
- (25) Koch, H.; Sánchez De Merás, A.; Pedersen, T. B. Reduced scaling in electronic structure calculations using Cholesky decompositions. *J. Chem. Phys.* **2003**, *118*, 9481–9484.
- (26) Higham, N. J. Cholesky factorization. *Wiley Interdiscip. Rev. Comput. Stat.* **2009**, *1*, 251–254.
- (27) Harbrecht, H.; Peters, M.; Schneider, R. On the low-rank approximation by the pivoted Cholesky decomposition. *Appl. Numer. Math.* **2012**, *62*, 428–440.
- (28) Zienau, J.; Clin, L.; Doser, B.; Ochsenfeld, C. Cholesky-decomposed densities in Laplace-based second-order Møller-Plesset perturbation theory. *J. Chem. Phys.* **2009**, *130*, 204112.
- (29) Maurer, S. A.; Clin, L.; Ochsenfeld, C. Cholesky-decomposed density MP2 with density fitting: Accurate MP2 and double-hybrid DFT energies for large systems. *J. Chem. Phys.* **2014**, *140*, 224112.
- (30) Jung, Y.; Sodt, A.; Gill, P. M. W.; Head-Gordon, M. Auxiliary basis expansions for large-scale electronic structure calculations. *Proc. Natl. Acad. Sci. U. S. A.* **2005**, *102*, 6692–6697.
- (31) Jung, Y.; Shao, Y.; Head-Gordon, M. Fast evaluation of scaled opposite spin second-order Møller-Plesset correlation energies using auxiliary basis expansions and exploiting sparsity. *J. Comput. Chem.* **2007**, *28*, 1953–1964.
- (32) Reine, S.; Tellgren, E.; Krapp, A.; Kjærgaard, T.; Helgaker, T.; Jansik, B.; Host, S.; Salek, P. Variational and robust density fitting of four-center two-electron integrals in local metrics. *J. Chem. Phys.* **2008**, *129*, 104101.
- (33) Kussmann, J.; Luenser, A.; Beer, M.; Ochsenfeld, C. A reduced-scaling density matrix-based method for the computation of the vibrational Hessian matrix at the self-consistent field level. *J. Chem. Phys.* **2015**, *142*, 094101.
- (34) Ayala, P. Y.; Scuseria, G. E. Linear scaling second-order Møller-Plesset theory in the atomic orbital basis for large molecular systems. *J. Chem. Phys.* **1999**, *110*, 3660.
- (35) Luenser, A.; Kussmann, J.; Ochsenfeld, C. Computation of indirect nuclear spin-spin couplings with reduced complexity in pure and hybrid density functional approximations. *J. Chem. Phys.* **2016**, *145*, 124103.
- (36) Baerends, E.; Ellis, D.; Ros, P. Self-consistent molecular Hartree-Fock-Slater calculations I. The computational procedure. *Chem. Phys.* **1973**, *2*, 41–51.
- (37) Vahtras, O.; Almlöf, J.; Feyereisen, M. W. Integral approximations for LCAO-SCF calculations. *Chem. Phys. Lett.* **1993**, *213*, 514.
- (38) Adamson, R. D.; Dombroski, J. P.; Gill, P. M. W. Efficient calculation of short-range Coulomb energies. *J. Comput. Chem.* **1999**, *20*, 921–927.
- (39) Perdew, J. P.; Burke, K.; Ernzerhof, M. Generalized Gradient Approximation Made Simple. *Phys. Rev. Lett.* **1996**, *77*, 3865–3868.
- (40) Perdew, J. P.; Burke, K.; Ernzerhof, M. Generalized Gradient Approximation Made Simple [Phys. Rev. Lett. 77, 3865 (1996)]. *Phys. Rev. Lett.* **1997**, *78*, 1396–1396.
- (41) Weigend, F.; Furche, F.; Ahlrichs, R. Gaussian basis sets of quadruple zeta valence quality for atoms H-Kr. *J. Chem. Phys.* **2003**, *119*, 12753.
- (42) Weigend, F.; Ahlrichs, R. Balanced basis sets of split valence, triple zeta valence and quadruple zeta valence quality for H to Rn: Design and assessment of accuracy. *Phys. Chem. Chem. Phys.* **2005**, *7*, 3297.
- (43) Weigend, F.; Häser, M.; Patzelt, H.; Ahlrichs, R. RI-MP2: optimized auxiliary basis sets and demonstration of efficiency. *Chem. Phys. Lett.* **1998**, *294*, 143–152.
- (44) Hättig, C. Optimization of auxiliary basis sets for RI-MP2 and RI-CC2 calculations: Core-valence and quintuple- ζ basis sets for H to Ar and QZVPP basis sets for Li to Kr. *Phys. Chem. Chem. Phys.* **2005**, *7*, 59–66.
- (45) Takatsuka, A.; Ten-no, S.; Hackbusch, W. Minimax approximation for the decomposition of energy denominators in Laplace-transformed Møller-Plesset perturbation theories. *J. Chem. Phys.* **2008**, *129*, 044112.
- (46) Kussmann, J.; Ochsenfeld, C. Pre-selective screening for matrix elements in linear-scaling exact exchange calculations. *J. Chem. Phys.* **2013**, *138*, 134114.
- (47) Kussmann, J.; Ochsenfeld, C. Preselective Screening for Linear-Scaling Exact Exchange-Gradient Calculations for Graphics Processing Units and General Strong-Scaling Massively Parallel Calculations. *J. Chem. Theory Comput.* **2015**, *11*, 918–922.
- (48) TURBOMOLE, version 7.0; TURBOMOLE GmbH, 2015; <http://www.turbomole.com>. TURBOMOLE is a development of University of Karlsruhe and Forschungszentrum Karlsruhe GmbH, 1989–2007, and TURBOMOLE GmbH, since 2007.
- (49) Rezac, J.; Riley, K. E.; Hobza, P. S66: A Well-balanced Database of Benchmark Interaction Energies Relevant to Biomolecular Structures. *J. Chem. Theory Comput.* **2011**, *7*, 2427–2438.
- (50) Rezac, J.; Riley, K. E.; Hobza, P. Extensions of the S66 Data Set: More Accurate Interaction Energies and Angular-Displaced Non-equilibrium Geometries. *J. Chem. Theory Comput.* **2011**, *7*, 3466–3470.
- (51) Sedlak, R.; Janowski, T.; Pitoňák, M.; Řezáč, J.; Pulay, P.; Hobza, P. Accuracy of Quantum Chemical Methods for Large Noncovalent Complexes. *J. Chem. Theory Comput.* **2013**, *9*, 3364–3374.
- (52) Structures are available online at www.cup.lmu.de/pc/ochsenfeld/.

3.3 Kernel Projection

H. F. Schurkus, A. Luenser, and C. Ochsenfeld,
J. Chem. Phys. (Communication) **146**, 211106 (2017)

Almost error-free resolution-of-the-identity correlation methods by null space removal of the particle-hole interactions

Abstract from the publication: We present a method to improve upon the resolution-of-the-identity (RI) for correlation methods. While RI is known to allow for drastic speedups, it relies on a cancellation of errors. Our method eliminates the errors introduced by RI which are known to be problematic for absolute energies. In this way, independence of the error compensation assumption for relative energies is also achieved. The proposed method is based on the idea of starting with an oversized RI basis and projecting out all of its unphysical parts. The approach can be easily implemented into existing RI codes and results in an overhead of about 30%, while effectively removing the RI error. In passing, this process alleviates the problem that for many frequently employed basis sets no optimized RI basis sets have been constructed. In this paper, the theory is presented and results are discussed exemplarily for the random phase approximation and Møller–Plesset perturbation theory.

The following article is reproduced in agreement with its publisher (AIP Publishing LLC) and can be found online at

<http://aip.scitation.org/doi/pdf/10.1063/1.4985085>.



Communication: Almost error-free resolution-of-the-identity correlation methods by null space removal of the particle-hole interactions

Henry F. Schurkus, Arne Luenser, and Christian Ochsenfeld

*Chair of Theoretical Chemistry and Center for Integrated Protein Science Munich (CIPSM),
Department of Chemistry, University of Munich (LMU), Butenandtstr. 7, D-81377 Munich, Germany*

(Received 20 April 2017; accepted 24 May 2017; published online 7 June 2017)

We present a method to improve upon the resolution-of-the-identity (RI) for correlation methods. While RI is known to allow for drastic speedups, it relies on a cancellation of errors. Our method eliminates the errors introduced by RI which are known to be problematic for absolute energies. In this way, independence of the error compensation assumption for relative energies is also achieved. The proposed method is based on the idea of starting with an oversized RI basis and projecting out all of its unphysical parts. The approach can be easily implemented into existing RI codes and results in an overhead of about 30%, while effectively removing the RI error. In passing, this process alleviates the problem that for many frequently employed basis sets no optimized RI basis sets have been constructed. In this paper, the theory is presented and results are discussed exemplarily for the random phase approximation and Møller-Plesset perturbation theory. *Published by AIP Publishing.* [<http://dx.doi.org/10.1063/1.4985085>]

I. INTRODUCTION

The resolution-of-the-identity (RI) approximation^{1–6} is a common approach throughout the electronic structure theories of quantum chemistry in which an identity is resolved into a product of terms dependent on a preoptimized (auxiliary) basis. This allows to reformulate theories into a computationally more tractable form. For example, within explicitly correlated methods^{7–9} (F12) several three-electron integrals occur which are commonly split into products of two-electron integrals via RI. However, the by far most frequently encountered use of RI is the case of 4-center-2-electron repulsion integrals (ERIs) occurring in almost any correlation method, which are split into products of at most 3-center-2-electron integrals.^{10,11} The final formulations obtained in this case are identical to those that can be derived from another perspective, often called density-fitting¹² (DF). For this reason, in theories containing only this special type of RI the terms RI and DF are often used interchangeably.¹³ While we will focus on this major case of RI, i.e., DF, in the following, we expect the transfer to other types of RI to be straightforward. As an example, we sketch the application to F12 in the [supplementary material](#).

Preoptimized incomplete auxiliary bases have to balance accuracy against computational performance. Several attempts and discussions have therefore revolved around improving the RI approach.^{14–17} While a lot of effort has been put into advancing upon the approximation formula itself^{18–23} as well as the auxiliary basis sets,^{24–26} the null space structure of the physical models remains more or less opaque.

In this paper, we present an approach which explicitly recognizes the physical model of the correlation method. By starting with an oversized auxiliary basis, we eliminate the RI error and then project out any contribution spanned by the auxiliary basis which is not used by the physical model. While the theory extends to any precomputable null space structure

of the physical model, here we focus on the concrete examples of second order Møller-Plesset perturbation theory²⁷ (MP2; as a post-Hartree–Fock (HF) theory) and the direct random phase approximation²⁸ (RPA; as a post-Kohn–Sham (KS) theory) because the supports of their physical models are both encompassed by particle-hole space. This allows us to treat both of these theories simultaneously.

In formulating our theory, we employ the Cholesky decomposition (CD) and the singular value decomposition (SVD) which have been studied in related works by Aquilante, Lindh, and Pedersen^{21–23} and Kállay,²⁹ respectively.

II. THEORY

Consider a generic correlation method (Einstein's sum convention is used throughout)

$$E_C = Q_{\mu\nu\lambda\sigma}(\mu\nu|\lambda\sigma) \quad (1)$$

which contains a single set of ERIs

$$(\mu\nu|\lambda\sigma) \equiv (\mu\nu|\frac{1}{r_{12}}|\lambda\sigma) := \iint \chi_\mu(r_1)\chi_\nu(r_1)\frac{1}{|r_1-r_2|} \times \chi_\lambda(r_2)\chi_\sigma(r_2) dr_1 dr_2 \quad (2)$$

over basis functions $\{\chi\}$, where Q is given by the physical model $(\mu\nu|\frac{1}{r_{12}}|I)$ denotes a corresponding three-center integral. Note that if Q again depends on ERIs, the following considerations can be applied to each of them in turn. Even if the actual computation may be done in basis functions $\chi_\mu, \chi_\nu, \dots$, most physical models will not describe the interaction of all basis functions, but instead of a physically relevant subspace. Writing a theory like Eq. (1), however, hides this information in the physical model Q .

For the ERIs [Eq. (2)], the RI results in the following equality (see the [supplementary material](#) for details):

$$(\mu\nu|\lambda\sigma) = B_{\mu\nu,I} C_{I,J} B_{J,\lambda\sigma}^T, \quad (3)$$

where I and J are indices over an auxiliary basis set. The B and C matrices are computed in any chosen metric m_{12} as

$$B_{\mu\nu,I} = (\mu\nu|m_{12}|I), \quad (4)$$

$$C_{I,J} = (I|m_{12}|K)^{-1} (K|L)(L|m_{12}|J)^{-1}, \quad (5)$$

with the most common choice being the Coulomb metric $m_{12} = 1/r_{12}$. Note that $(K|L) = (K|\frac{1}{r_{12}}|L)$ is a Coulomb integral independent of the chosen metric. In typical approaches, a preoptimized auxiliary basis set is employed which is only 3-4 times larger in cardinality than the set $\{\chi\}$ because by the reasoning of DF one finds that Eq. (3) is the best approximation in a metric-specific sense also when the auxiliary basis is incomplete. While drastically improving performance, this introduces errors of several meVs in absolute energies. In contrast, our considerations start with a saturated auxiliary basis, such that Eq. (3) in fact effectively constitutes an identity.

By employing the RI, the correlation energy [Eq. (1)] becomes

$$E_C = \text{Tr}\{\tilde{Q}C\} \quad \text{with} \quad \tilde{Q}_{I,J} = B_{\mu\nu,I} Q_{\mu\nu\lambda\sigma} B_{\lambda\sigma,J}. \quad (6)$$

A. Example cases: RPA and MP2

As two exemplary cases we consider the RPA and MP2 methods. As post-KS/post-HF methods, they can be formulated in molecular orbitals as linear combinations of atomic orbitals. $c_{\mu i}$, $c_{\nu a}$, etc. denote the coefficient matrix elements, where i, j, k, \dots index the occupied orbitals and a, b, c, \dots the virtual orbitals. Within the RI-RPA^{11,30-33} in the time-determining step, one has to compute a quantity of the form

$$B_{I,ia}^T \frac{\varepsilon_a - \varepsilon_i}{(\varepsilon_a - \varepsilon_i)^2 + \omega^2} B_{ia,J}, \quad (7)$$

where ω is a variable to be integrated over in a later step of the algorithm and ε_i , etc. denote orbital energies. Therefore, we can associate

$$Q_{\mu\nu\lambda\sigma} \sim c_{\mu i} c_{\nu a} \frac{\varepsilon_a - \varepsilon_i}{(\varepsilon_a - \varepsilon_i)^2 + \omega^2} c_{\lambda i} c_{\sigma a}. \quad (8)$$

Within RI-MP2³⁴ on the other hand, the time-determining step is the recombination of the ERIs according to Eq. (3) in computing

$$t_{ij}^{ab} B_{ia,I} C_{I,J} B_{J,jb}^T \quad \text{with} \quad t_{ij}^{ab} = -\frac{(ia|jb) - (ib|ja)}{\varepsilon_a + \varepsilon_b - \varepsilon_i - \varepsilon_j}, \quad (9)$$

so we can associate

$$Q_{\mu\nu\lambda\sigma} \sim c_{\mu i} c_{\nu a} t_{ij}^{ab} c_{\lambda j} c_{\sigma b}. \quad (10)$$

Both of these methods share a commonality: Their physical models are built solely around particle-hole (ph) interactions as

$$Q_{\mu\nu\lambda\sigma} = c_{\mu i} c_{\nu a} \dots c_{\lambda i} c_{\sigma a}. \quad (11)$$

To treat both methods within the same derivation, we will only focus on this common property and restrict ourselves to treat the inner part as a black box.

B. Null space projection

We aim to project out all auxiliary basis functions and linear combinations in the null space of the physical model ($\text{Null}(\tilde{Q}) = \{x \mid \tilde{Q}x = 0\}$) because these will not contribute to the final energy, or equivalently project onto its complement, called support.

We begin with a thought experiment: If \tilde{Q} was known beforehand, one could construct a minimal-rank projector P onto the support of \tilde{Q} such that

$$\tilde{Q}P = \tilde{Q}. \quad (12)$$

To do so, one would first apply SVD to \tilde{Q}

$$\tilde{Q} = U\Sigma V^T, \quad (13)$$

where Σ is a diagonal matrix containing only $\text{rank}(\tilde{Q})$ non-zero singular values and the columns of the unitary matrices U and V are the corresponding left and right singular vectors. We now discard all singular vectors with a corresponding zero singular value. In numerical implementations, it is useful to further discard those corresponding to very small singular values. This step is justified by the Eckart-Young-Mirsky theorem.³⁵ Precisely which numerical values qualify as very small in this context will be further analyzed in Sec. III A.

As the left and right singular vectors form an orthogonal system each, recombining the remaining singular vectors according to

$$P^L = UU^T, \quad P^R = VV^T \quad (14)$$

defines a left and a right projector. The right projector fulfills Eq. (12) and the left projector can similarly be introduced to the left of \tilde{Q} at any point in the derivation.

Therefore one can redefine Eqs. (4) and (5) without changing the final correlation energy, Eq. (6),

$$B_{\mu\nu,I} \rightarrow B_{\mu\nu,J} V_{J,I}, \quad (15)$$

$$C \rightarrow V^T C V. \quad (16)$$

This reduces the effective size of the auxiliary basis in all the time determining steps to the width of the singular vector matrices, which *per constructionem* is exactly limited by the rank of the physical model.

For the case at hand, there is no need for additional steps in the construction. Nonetheless, we want to propose one that may prove useful in other cases. Once the projector matrix is known, it can be decomposed by pivoted CD as

$$P = LL^T, \quad (17)$$

where the number of columns in the Cholesky factor L again equals the rank of P . Therefore, Eqs. (15) and (16) can be carried out with L instead of V . This may prove useful, for example, when P is sparse because unlike the singular decomposition, pivoted CD on a sparse matrix can return sparse factors. Although not necessary, we use the Cholesky factors throughout, since their use does not deteriorate the results compared to the use of V .

C. Auxiliary matrix construction

Computing the exact physical model is almost always part of the time determining step. To exploit the previous

discussion, it is therefore necessary to find an auxiliary matrix H , such that

$$\text{Null}(H) \subseteq \text{Null}(\tilde{Q}), \quad (18)$$

and construct the projectors from H instead of \tilde{Q} . The central idea to finding H is to recognize that because in a k -linear map $N : W \rightarrow X$, e.g., a matrix or tensor product, the zero element in W is mapped to the zero element in X , in a succession of maps $M : V \rightarrow W, N : W \rightarrow X, \dots$ the null space of the first map is contained within the null space of the succession of all maps.

Returning to the generic example, Eq. (11), this means

$$\text{Null}(c_{\mu i} c_{\nu a} B_{\mu\nu, I}) \subseteq \text{Null}(\dots c_{\mu i} c_{\nu a} B_{\mu\nu, I}) \quad (19)$$

allowing the definition of H for this case as

$$H_{ia, I} = c_{\mu i} c_{\nu a} B_{\mu\nu, I}. \quad (20)$$

By the SVD decomposition of H , it becomes obvious that $H^T H$ in fact has the same span as H (although in numerical implementations a tighter threshold for the singular values is needed) so we may equally define

$$H_{I, J} = B_{I, \mu\nu}^T c_{\mu i} c_{\nu a} c_{\lambda i} c_{\sigma a} B_{\lambda\sigma, J}, \quad (21)$$

which is favorable as it allows for a cheaper SVD. Applying the discussion of Sec. II B to H instead of \tilde{Q} thus delivers the new projection. Because it does not make use of all the internal structure of \tilde{Q} , it may eliminate less than—however due to Eq. (18) never more than—the projector constructed directly from \tilde{Q} . Therefore no additional error is introduced.

While the argument extends naturally to any other operator with a non-trivial null space structure, e.g., $\tilde{Q}C$, by replacing \tilde{Q} with that operator in Eq. (18), we will only evaluate the straightforward example, which we have presented here, in Sec. III.

III. NUMERICAL EVALUATION

All calculations have been done in a development version of the program package FermiONS++^{36,37} employing the Coulomb metric. All RPA calculations have been based on self-consistent orbitals obtained with the Perdew-Burke-Ernzerhof (PBE) functional.

A. Accuracy

Two practical questions have yet to be addressed: The auxiliary basis to start the projection from and the numerical threshold to choose for the SVD.

In principle, any auxiliary basis large enough to fulfill Eq. (3) as an identity can be taken as the starting point. While a naïve overly large auxiliary basis can be used, it is advisable to make use of specialized auxiliary basis sets whenever available, to lessen the overhead of the projector construction.

To find a suitable choice for both the starting basis and the threshold, we evaluated all 198 monomers and dimers within the S66 test set of small to medium sized molecules.³⁸ In Fig. 1 we compare the deviation in energy from the RI-free result to the total number of auxiliary basis functions left

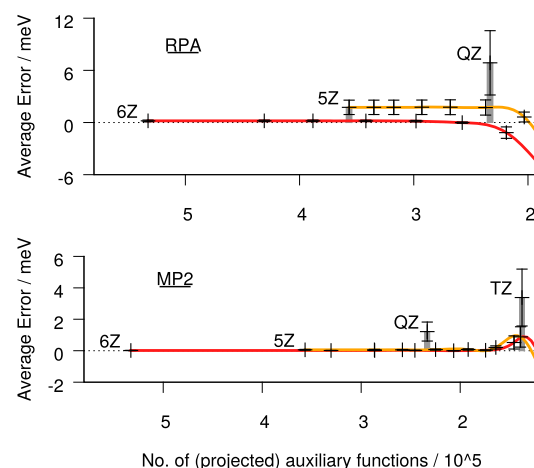


FIG. 1. Mean errors (left axis) and standard deviations (error bars) against the number of auxiliary functions using ph-projection. Solid lines: Projection from cc-pV6Z-RI (red) and cc-pV5Z-RI (orange). Larger thresholds result in fewer auxiliary basis functions. Gray bars labelled XZ = 6Z, 5Z, QZ, TZ represent the corresponding unprojected cc-pVXZ-RI bases. Mean error and standard deviation nearly vanish for cc-pV6Z-RI. Null space removal grants sub-meV accuracy with an auxiliary basis set size only slightly larger than the canonical RI basis.

after the projection along the continuous range of thresholds. The variation over the different molecules is expressed by the empirical standard deviation of the energy differences (at threshold values 0 and $10^{-10}, 10^{-9}, \dots, 10^{-5}$, respectively). The unprojected RI results with the canonical discrete set of preoptimized auxiliary basis sets (cc-pVXZ-RI) are also given for comparison.

RPA/cc-pVQZ results are effectively converged with an auxiliary basis two cardinality numbers larger than the AO basis, cc-pV6Z-RI (Fig. 1, top). Kállay’s very different reasoning²⁹ had focused on reducing the size of the typical auxiliary basis (here cc-pVQZ-RI). In contrast, our understanding as presented above, has led us to consider saturated auxiliary basis sets. We find that even when aiming for the same auxiliary size after reduction, projections based on larger basis sets lead to significantly better results. SVD thresholds tighter than 10^{-6} hardly change the results, so we recommend the combination cc-pV6Z-RI $\rightarrow 10^{-6}$ and use it for the following analysis.

For MP2 (Fig. 1, bottom), where the typical basis set size is triple- ζ , here cc-pVTZ, already the pentuple- ζ auxiliary basis can be considered converged. Because projecting from a smaller basis means that less auxiliary functions are left after

TABLE I. Comparison of accuracy gain and computational overhead of cc-pV6Z-RI $\rightarrow 10^{-6}$ ph-projection against canonical cc-pVQZ-RI for molecules in Fig. 2 (geometries and more detailed results are given in the supplementary material). All calculations were carried out at the RPA@PBE/cc-pVQZ level with 12 concurrent evaluation threads on an Intel E5-2620@2.0GHz architecture.

Molecule	A	B	C
Canonical RI error (meV)	30.2	40.9	56.5
ph-projection error (meV)	0.7	0.6	0.8
Total walltime overhead	+27%	+35%	+14%

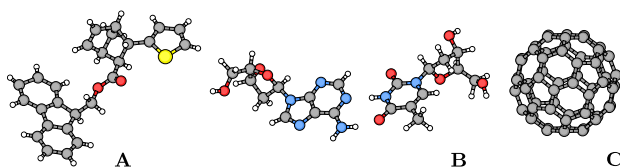


FIG. 2. Selection of molecules employed for testing (see Table I; $C_{26}H_{22}O_2S$,³⁹ adenosine-thymine base pair, and C_{60}).

projection with the same threshold, we recommend tightening the threshold to 10^{-7} in this case.

B. Overhead

Our recommended choices for the projector construction (see Sec. III A) in eliminating the RI error result in slightly more auxiliary functions entering the energy evaluation than canonical RI (e.g., cc-pVQZ-RI for cc-pVQZ). Additional compute time overhead is caused by the construction of the projector itself. While the most expensive step scales formally as $\mathcal{O}(N^4)$ [Eq. (21); asymptotic limit with a local metric: $\mathcal{O}(N)$] the same holds true for the RI correlation methods [MP2: $\mathcal{O}(N^5)$, RPA: $\mathcal{O}(N^4 \log(N))$], so the overhead is approximately given by a constant fraction of the total runtime. In Table I we compare the overall overhead of our method to the gains in accuracy for some larger molecules (Fig. 2). Timings comprise the complete correlation energy calculation after the generation of the Kohn–Sham orbitals. This includes projector construction, integral evaluation and transformation, and evaluation of the Hamiltonian expectation value as part of the full RPA energy. Our recommended choices eliminate the RI error to an insignificant residue of less than one meV in absolute energy also for these larger molecules, causing a total overhead of only about 30% compared to the canonical RI approach, which shows two orders of magnitude larger errors.

C. Potential energy surfaces

As the projection is essentially error-free, so are potential energy surfaces evaluated with it. We computed the dissociation curve of the C_{60} dimer in Fig. 3. The equilibrium distance can be deduced from experiment to be 9.93 Å,⁴⁰ in good agreement with our results. Obtaining a good experimental estimate for the binding energy is more intricate.^{41,42}

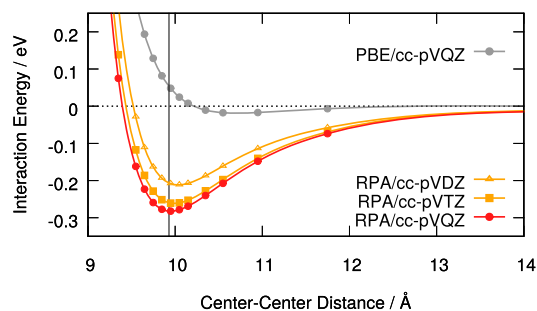


FIG. 3. cc-pV6Z-RI $\rightarrow 10^{-6}$ ph-projected potential energy dissociation curve of the C_{60} dimer. Geometries were taken from Ref. 43. The experimental equilibrium distance^{40,44} is given as a black line for reference. All calculations have been counter-poise corrected.⁴⁵

IV. CONCLUSION

We have introduced the concept of null space projection of the physical model. The theory was presented in a general manner and is not limited to the discussed applications at the MP2 and RPA levels. For these specifically we have shown that the RI error can be eliminated to a residue of less than one meV while overall runtime increases by only about 30%, within a few lines of code. Other correlation methods may similarly benefit from our presented null space projection idea.

SUPPLEMENTARY MATERIAL

See [supplementary material](#) for further results and discussions as indicated in the text.

ACKNOWLEDGMENTS

We acknowledge funding by DFG: Oc35/4-1, SFB749, and EXC114.

- ¹S. F. Boys and I. Shavitt, “A fundamental calculation of the energy surface for the system of three hydrogen atoms,” Technical Report, University of Wisconsin, 1959.
- ²J. L. Whitten, *J. Chem. Phys.* **58**, 4496 (1973).
- ³E. Baerends, D. Ellis, and P. Ros, *Chem. Phys.* **2**, 41 (1973).
- ⁴B. I. Dunlap, J. W. D. Connolly, and J. R. Sabin, *J. Chem. Phys.* **71**, 4993 (1979).
- ⁵C. Van Alsenoy, *J. Comput. Chem.* **9**, 620 (1988).
- ⁶O. Vahtras, J. Almlöf, and M. W. Feyereisen, *Chem. Phys. Lett.* **213**, 514 (1993).
- ⁷W. Kutzelnigg, *Theor. Chim. Acta* **68**, 445 (1985).
- ⁸C. Hättig, W. Klopper, A. Köhn, and D. P. Tew, *Chem. Rev.* **112**, 4 (2012).
- ⁹L. Kong, F. A. Bischoff, and E. F. Valeev, *Chem. Rev.* **112**, 75 (2012).
- ¹⁰M. Feyereisen, G. Fitzgerald, and A. Komornicki, *Chem. Phys. Lett.* **208**, 359 (1993).
- ¹¹H. Eshuis, J. Yarkony, and F. Furche, *J. Chem. Phys.* **132**, 234114 (2010).
- ¹²H.-J. Werner, F. R. Manby, and P. J. Knowles, *J. Chem. Phys.* **118**, 8149 (2003).
- ¹³In Ref. 12 the term DF was introduced as a synonym to RI, highlighting the difference in perspective. Some authors have adapted this nomenclature [cf. J. G. Hill, *Int. J. Quantum Chem.* **113**, 21 (2013)], others have not [cf. T. Kjærgaard, *J. Chem. Phys.* **146**, 044103 (2017)].
- ¹⁴I. Duchemin, J. Li, and X. Blase, *J. Chem. Theory Comput.* **13**, 1199 (2017).
- ¹⁵F. Weigend, M. Kattannek, and R. Ahlrichs, *J. Chem. Phys.* **130**, 164106 (2009).
- ¹⁶L. Grajciar, *J. Comput. Chem.* **36**, 1521 (2015).
- ¹⁷S. Manzer, P. R. Horn, N. Mardirossian, and M. Head-Gordon, *J. Chem. Phys.* **143**, 024113 (2015).
- ¹⁸E. G. Hohenstein, R. M. Parrish, and T. J. Martínez, *J. Chem. Phys.* **137**, 044103 (2012).
- ¹⁹R. M. Parrish, E. G. Hohenstein, T. J. Martínez, and C. D. Sherrill, *J. Chem. Phys.* **137**, 224106 (2012).
- ²⁰E. G. Hohenstein, R. M. Parrish, C. D. Sherrill, and T. J. Martínez, *J. Chem. Phys.* **137**, 221101 (2012).
- ²¹F. Aquilante, T. B. Pedersen, A. Sánchez de Merás, and H. Koch, *J. Chem. Phys.* **125**, 174101 (2006).
- ²²T. B. Pedersen, F. Aquilante, and R. Lindh, *Theor. Chem. Acc.* **124**, 1 (2009).
- ²³F. Aquilante, L. Boman, J. Boström, H. Koch, R. Lindh, A. Sánchez de Merás, and T. B. Pedersen, *Linear-Scaling Techniques in Computational Chemistry and Physics* (Springer, Dordrecht, The Netherlands, 2011), Vol. 13, pp. 301–343.
- ²⁴F. Weigend, A. Köhn, and C. Hättig, *J. Chem. Phys.* **116**, 3175 (2002).
- ²⁵C. Hättig, *Phys. Chem. Chem. Phys.* **7**, 59 (2005).
- ²⁶G. L. Stoychev, A. A. Auer, and F. Neese, *J. Chem. Theory Comput.* **13**, 554 (2017).
- ²⁷C. Möller and M. S. Plesset, *Phys. Rev.* **46**, 618 (1934).
- ²⁸D. Bohm and D. Pines, *Phys. Rev.* **92**, 609 (1953).
- ²⁹M. Kállay, *J. Chem. Phys.* **141**, 244113 (2014).

211106-5 Schurkus, Luenser, and Ochsenfeld

J. Chem. Phys. **146**, 211106 (2017)

- ³⁰F. Furche, *J. Chem. Phys.* **129**, 114105 (2008).
- ³¹H. Eshuis and F. Furche, *J. Chem. Phys.* **136**, 084105 (2012).
- ³²H. F. Schurkus and C. Ochsenfeld, *J. Chem. Phys.* **144**, 031101 (2016).
- ³³A. Luenser, H. F. Schurkus, and C. Ochsenfeld, *J. Chem. Theory Comput.* **13**, 1647 (2017).
- ³⁴F. Weigend, M. Häser, H. Patzelt, and R. Ahlrichs, *Chem. Phys. Lett.* **294**, 143 (1998).
- ³⁵C. Eckart and G. Young, *Psychometrika* **1**, 211 (1936).
- ³⁶J. Kussmann, M. Beer, and C. Ochsenfeld, *Wiley Interdiscip. Rev.: Comput. Mol. Sci.* **3**, 614 (2013).
- ³⁷J. Kussmann, A. Luenser, M. Beer, and C. Ochsenfeld, *J. Chem. Phys.* **142**, 094101 (2015).
- ³⁸J. Řezáč, K. E. Riley, and P. Hobza, *J. Chem. Theory Comput.* **7**, 2427 (2011).
- ³⁹T. Gatzemeier, M. van Gemmeren, Y. Xie, D. Hofler, M. Leutzsch, and B. List, *Science* **351**, 949 (2016).
- ⁴⁰P. A. Heiney, J. E. Fischer, A. R. McGhie, W. J. Romanow, A. M. Denenstein, J. P. McCauley, Jr., A. B. Smith, and D. E. Cox, *Phys. Rev. Lett.* **66**, 2911 (1991).
- ⁴¹J. Abrefah, D. R. Olander, M. Balooch, and W. J. Siekhaus, *Appl. Phys. Lett.* **60**, 1313 (1992).
- ⁴²F. Tournus, J.-C. Charlier, and P. Mélinon, *J. Chem. Phys.* **122**, 094315 (2005).
- ⁴³D. I. Sharapa, J. T. Margraf, A. Hesselmann, and T. Clark, *J. Chem. Theory Comput.* **13**, 274 (2017).
- ⁴⁴Y.-y. Ohnishi, K. Ishimura, and S. Ten-no, *J. Chem. Theory Comput.* **10**, 4857 (2014).
- ⁴⁵S. Boys and F. Bernardi, *Mol. Phys.* **19**, 553 (1970).

SUPPLEMENTARY MATERIAL

**Almost Error-Free Resolution-of-the-Identity Correlation Methods
By Null Space Removal Of The Particle-Hole Interactions**

Henry F. Schurkus, Arne Luenser, and Christian Ochsenfeld

*Chair of Theoretical Chemistry and Center for Integrated
Protein Science Munich (CIPSM), Department of Chemistry,
University of Munich (LMU), Butenandtstr. 7, D-81377 Munich,
Germany*

I. GEOMETRIES

A. $C_{26}H_{22}O_2S$

Element	x/Bohr	y/Bohr	z/Bohr
C	2.30641074	10.10228689	5.48436316
H	2.28581272	11.98539897	5.63780892
C	-0.36792968	9.06841773	5.35888534
C	-2.28354505	9.20485595	7.15166852
H	-2.03939243	10.10247586	8.68744894
C	-4.57710565	7.99467534	6.64711164
H	-5.89367784	8.04569795	7.86560705
C	-5.11528075	6.52700065	4.02723314
H	-6.51955513	5.88101667	4.07065904
C	-3.06135632	6.63067103	2.53393376
H	-3.32931949	5.79125468	0.96924053
C	-0.76892956	7.81704109	3.05700995
C	1.55845713	7.95933746	1.54881953
C	2.16109080	6.93718460	-0.80370052
H	0.92747758	6.05184791	-1.76368139
C	4.61301044	7.24275332	-1.71700516
H	5.05766300	6.54771205	-3.31174503
C	6.42242321	8.55649092	-0.32276522
H	8.08689398	8.73034572	-0.96924053
C	5.81430934	9.62002878	2.01218038
H	7.04017468	10.53824671	2.94853967
C	3.37353908	9.30879089	2.94230358
C	3.94159075	8.93141258	7.55191251
H	4.05421843	7.08099276	7.30605914
H	5.67031221	9.64100474	7.47518963
C	4.16609021	8.67611058	11.98332027

C	2.87597419	9.24321739	14.45961739
H	3.42796319	10.95625413	15.03503899
C	-0.07917952	9.19786397	14.38100478
H	-0.90971416	10.64917363	13.50077035
C	-0.81069251	6.57908150	13.46278686
H	-1.54636289	6.17619189	11.87636178
C	-0.22922378	4.94333457	15.30130140
H	-0.45977037	3.16377948	15.24801113
C	0.86814018	6.44812348	17.49262782
H	0.79595264	5.61437632	19.18771215
C	3.55646457	7.28735085	16.57459887
H	4.41515612	5.80467174	15.77770136
C	-0.62984572	8.93991635	17.23071178
H	-2.45191965	8.74073922	17.60695625
H	0.09391939	10.33755779	18.24303806
C	5.23850979	8.32821200	18.61739281
O	2.81418014	9.48113391	9.98285620
O	6.22211224	7.68343745	11.77601732
S	8.33066865	8.89116142	18.08014367
C	8.82861148	9.85529968	21.15340527
H	10.42013882	10.40350923	21.78136126
C	6.70304754	9.74588454	22.57750287
H	6.61933267	10.20130854	24.31227146
C	4.60753024	8.85903607	21.13167342
H	2.95685447	8.64927647	21.80328208

B. DNA (AT-base pair)

Element	x/Bohr	y/Bohr	z/Bohr
---------	--------	--------	--------

H	-50.07585257	-13.74775756	7.89017349
O	-48.92330861	-12.77341477	6.89031940
H	-48.44426304	-15.75974896	4.43953358
H	-44.47621612	-12.74658066	5.94829092
C	-48.15059960	-13.72167934	4.49792612
H	-51.43437669	-11.83818931	3.00617632
H	-49.22812144	-13.14285622	0.61718455
C	-45.34586809	-13.14134444	4.12319343
H	-42.25333128	-14.26648738	1.76519317
H	-43.08348797	-16.49844290	4.12394932
C	-49.49079337	-12.20857563	2.43415622
O	-45.33793124	-10.73288850	2.79036960
H	-48.37264242	-8.80480093	4.35033851
C	-44.10394008	-15.15106818	2.75219713
C	-47.86241637	-9.84037085	2.64429377
H	-48.53270222	-10.54901815	-2.66470281
O	-45.40917391	-16.45441228	0.96583902
N	-48.05819199	-8.13111357	0.41498386
C	-48.38416975	-8.76284901	-2.06603757
C	-47.94197383	-5.54540131	0.46562852
N	-48.48375831	-6.83343864	-3.57441696
H	-48.32558824	0.74946538	-4.94503532
H	-48.60999202	-2.23970340	-6.24800149
N	-47.63168081	-4.05629713	2.51144602
H	-47.38412668	-0.43463701	3.28528887
C	-48.20370090	-4.76891285	-1.98099990
N	-48.38057927	-1.12797752	-4.73716545
C	-47.60768128	-1.65785673	1.86213612
C	-48.14644220	-2.15485470	-2.43207752
N	-47.83898376	-0.62682216	-0.42216482

H	-44.91066416	10.68961377	-6.04882435
H	-46.52997047	8.12374364	-7.49994504
H	-48.23507036	10.85609864	-6.53108246
O	-47.05455845	4.26643467	-5.21602205
H	-47.76056013	2.90658775	-0.81995217
C	-46.66225130	9.60642275	-6.07622538
C	-47.24542079	5.71528769	-3.40112908
N	-47.64075149	4.78421963	-0.99739745
O	-48.23431447	5.19277842	3.23388832
C	-47.09027427	8.43649331	-3.53019737
H	-47.20989393	11.73141978	-1.56903960
C	-47.88736075	6.19093176	1.18693698
C	-47.32346647	9.84981948	-1.43505802
H	-50.98764543	17.48355713	0.16742973
N	-47.71426184	8.76341593	0.88212415
H	-47.50506915	9.22054068	4.85546230
O	-50.38312204	17.04589656	1.81678270
H	-53.55748399	14.81979919	2.41110156
H	-52.79195593	16.91871799	4.90969744
C	-47.97069767	10.34814026	3.19571585
H	-44.41102057	12.32063639	3.76131088
H	-46.55378102	13.75569441	1.38932665
C	-51.73446519	15.64787717	3.49391463
O	-50.49858431	11.23328797	3.32308339
H	-51.44552607	13.07161355	6.56226294
C	-46.33891916	12.72333702	3.15886619
C	-50.52787506	13.56521001	4.78535347
H	-47.44100744	16.15999295	5.32694897
C	-47.73467088	14.12211230	5.26591082
O	-47.02526769	13.04383457	7.62239930

H -47.88811664 13.90422688 8.96637252
H -44.33354180 -17.71674934 0.23035761

C. C60

Element	x/Bohr	y/Bohr	z/Bohr
C	-1.36154741	-4.88927519	4.34643598
C	1.36154741	4.88927519	-4.34643598
C	-1.36154741	-4.88927519	-4.34643598
C	1.36154741	-4.88927519	-4.34643598
C	-1.36154741	4.88927519	-4.34643598
C	1.36154741	-4.88927519	4.34643598
C	-1.36154741	4.88927519	4.34643598
C	1.36154741	4.88927519	4.34643598
C	-2.68624518	-5.70798339	2.20303021
C	2.68624518	5.70798339	-2.20303021
C	-2.68624518	-5.70798339	-2.20303021
C	2.68624518	-5.70798339	-2.20303021
C	-2.68624518	5.70798339	-2.20303021
C	2.68624518	-5.70798339	2.20303021
C	-2.68624518	5.70798339	2.20303021
C	2.68624518	5.70798339	2.20303021
C	-2.20303021	-2.68624518	5.70798339
C	2.20303021	2.68624518	-5.70798339
C	-2.20303021	-2.68624518	-5.70798339
C	2.20303021	-2.68624518	-5.70798339
C	-2.20303021	2.68624518	-5.70798339
C	2.20303021	-2.68624518	5.70798339
C	-2.20303021	2.68624518	5.70798339

C 2.20303021 2.68624518 5.70798339
C -4.88927519 -4.34643598 1.36154741
C 4.88927519 4.34643598 -1.36154741
C -4.88927519 -4.34643598 -1.36154741
C 4.88927519 -4.34643598 -1.36154741
C -4.88927519 4.34643598 -1.36154741
C 4.88927519 -4.34643598 1.36154741
C -4.88927519 4.34643598 1.36154741
C 4.88927519 4.34643598 1.36154741
C -1.32469777 -6.54946600 0.00000000
C 1.32469777 -6.54946600 0.00000000
C -1.32469777 6.54946600 0.00000000
C 1.32469777 6.54946600 0.00000000
C -6.54946600 0.00000000 1.32469777
C 6.54946600 0.00000000 -1.32469777
C -6.54946600 0.00000000 -1.32469777
C 6.54946600 0.00000000 1.32469777
C 0.00000000 -1.32469777 6.54946600
C 0.00000000 1.32469777 -6.54946600
C 0.00000000 -1.32469777 -6.54946600
C 0.00000000 1.32469777 6.54946600
C -4.34643598 -1.36154741 4.88927519
C 4.34643598 1.36154741 -4.88927519
C -4.34643598 -1.36154741 -4.88927519
C 4.34643598 -1.36154741 -4.88927519
C -4.34643598 1.36154741 -4.88927519
C 4.34643598 -1.36154741 4.88927519
C -4.34643598 1.36154741 4.88927519
C 4.34643598 1.36154741 4.88927519
C -5.70798339 -2.20303021 2.68624518

C	5.70798339	2.20303021	-2.68624518
C	-5.70798339	-2.20303021	-2.68624518
C	5.70798339	-2.20303021	-2.68624518
C	-5.70798339	2.20303021	-2.68624518
C	5.70798339	-2.20303021	2.68624518
C	-5.70798339	2.20303021	2.68624518
C	5.70798339	2.20303021	2.68624518

II. EXTENDED TABLES

Here, we present more detailed results for the three example molecules of the main text. All calculations are RPA energy evaluations and have been carried out in a cc-pVQZ atomic orbital basis and based on PBE orbitals.

N_{atoms} : Number of atoms in the molecule.

N_{aux} : Number of (projected) pure auxiliary functions

6Z-RI: Evaluation with cc-pV6Z-RI auxiliary basis.

QZ-RI: Evaluation with cc-pVQZ-RI auxiliary basis.

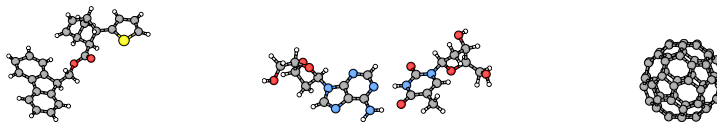
proj: Evaluation with cc-pV6Z-RI auxiliary basis projected to threshold 10^{-6} .

Speedup vs 6Z-RI: comparing “proj” with 6Z-RI

Overhead vs QZ-RI: comparing “proj” with QZ-RI

E_{total} : Absolute correlated energy.

E_C^{RPA} : RPA correlation energy.

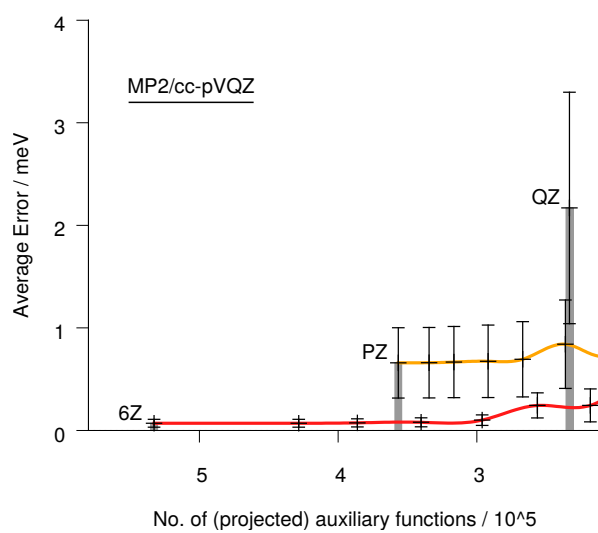
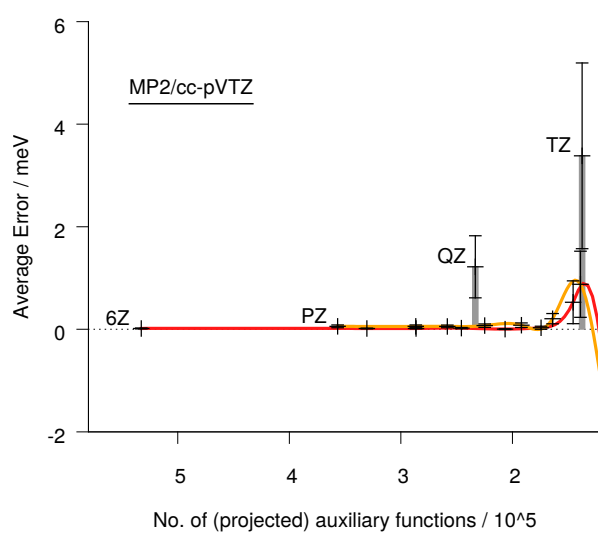


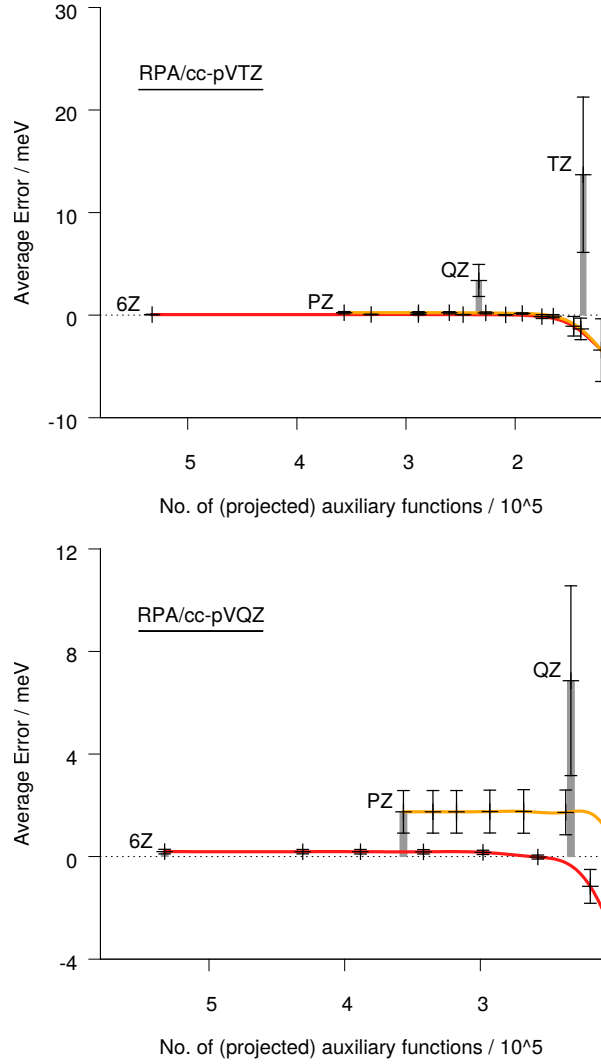
N_{atoms}	51	62	60
Speedup vs 6Z-RI	2.5x	2.8x	1.9x
Naux-Reduction	-50.0%	-49.3%	-47.7%
Error of proj.	2.6e-5 hartree	2.4e-5 hartree	2.8e-5 hartree
Error of QZ-RI	1.1e-3 hartree	1.5e-3 hartree	2.1e-3 hartree
Overhead vs QZ-RI	+27.2%	+35.4%	+14.4%
cc-pV6Z-RI:			
walltime[s]	27890	56531	172617
N_{aux}	11346	13685	16980
E_{total} [hartree]	-1552.5715171846	-1764.3369534545	-2272.0007428025
E_C^{RPA} [hartree]	-8.09901141777614	-10.90586404074700	-14.45599212934066
cc-pVQZ-RI:			
walltime[s]	8611	14874	80667
N_{aux}	5064	6105	7920
E_{total} [hartree]	-1552.5704047828	-1764.3354520156	-2272.0007428025
E_C^{RPA} [hartree]	-8.09789901599577	-10.90436260185441	-14.45391667695902
cc-pV6Z-RI\rightarrow1e-6:			
walltime[s]	10954	20141	92273
N_{aux}	5650	6935	8873
E_{total} [hartree]	-1552.5715434597	-1764.3369772871	-2272.0007428025
E_C^{RPA} [hartree]	-8.09903769282070	-10.90588787332585	-14.45601973832719

III. EXTENSION ON S66 ACCURACY

In the following we present more results as in fig. 1 of the main text (see caption of fig. 1 for details). While in fig. 1 we show only the typical combinations of atomic orbital

basis sets and correlation methods, here we present all combinations of RPA/MP2 with cc-pVTZ/cc-pVQZ.





IV. DENSITY FITTING AS A SPECIAL CASE OF RESOLUTION-OF-THE-IDENTITY

In the literature both terms, “density fitting” (DF) and “resolution-of-the-identity” (RI), are used to denote the factorization of the ERIs as

$$(\mu\nu|\lambda\sigma) = (\mu\nu|m_{12}|I)(I|m_{12}|J)^{-1}(J|K)(K|m_{12}|L)^{-1}(L|m_{12}|\lambda\sigma) . \quad (1)$$

However, they differ in perspective: While RI considers an exact identity to be introduced, DF considers how to minimize the error of fitting a product of functions by a linear combination over single functions in some metric. We now show that both perspectives yield

eq. 1 – RI as an exact identity over a complete set, DF as an optimal approximation over an incomplete set.

In DF one is interested in fitting the “density” $|\mu\nu\rangle$ with an in general incomplete auxiliary function set

$$|\mu\nu\rangle \approx |\tilde{\mu}\tilde{\nu}\rangle = \alpha_I^{\mu\nu}|I\rangle \quad (2)$$

where the coefficients α are to be determined such as to minimize the error within a metric m_{12}

$$0 \stackrel{!}{=} \frac{\partial}{\partial \alpha_K^{\mu\nu}} (\mu\nu - \tilde{\mu}\tilde{\nu}|m_{12}|\lambda\sigma - \tilde{\lambda}\tilde{\sigma}) \quad (3)$$

$$= -(K|m_{12}|\lambda\sigma) + (K|m_{12}|J)\alpha_J^{\lambda\sigma} \quad (4)$$

So by solving for α

$$\alpha_J^{\lambda\sigma} = (J|m|K)^{-1}(K|m|\lambda\sigma) \quad (5)$$

one obtains eq. 1 as

$$(\mu\nu|\lambda\sigma) \approx \alpha_I^{\mu\nu}(I|J)\alpha_J^{\lambda\sigma} \quad (6)$$

We are now going to show eq. 1 again, but not from a DF perspective but by insertion and resolution of an identity. Consider the ERI $(\mu\nu|\lambda\sigma)$ as a chain of operations. One can insert two identities into it, obtaining

$$(\mu\nu|\mathbf{I}|\frac{1}{r}|\mathbf{I}|\lambda\sigma) . \quad (7)$$

Again, we will omit the $\frac{1}{r_{12}}$ operator and replace it with a vertical bar whenever an integral contains no other operators. A three center overlap integral is therefore denoted by $(\mu\nu\lambda)$.

Let us first only consider the identity to the right of $\frac{1}{r}$. Given a complete and orthogonal set $\{|\tilde{R}\rangle\}$ one can “resolve” this identity as

$$\mathbf{I} = |\tilde{R}\rangle\langle\tilde{R}| \quad (8)$$

so that

$$(\mu\nu|\lambda\sigma) = (\mu\nu|\tilde{R}\rangle\langle\tilde{R}|\lambda\sigma) \quad (9)$$

Given a complete, however non-orthogonal set $\{|I\rangle\}$ one can similarly “resolve” the identity. To find the explicit form we first note that

$$|I\rangle = |\tilde{R}\rangle\langle\tilde{R}|I\rangle \quad (10)$$

and so by completeness of the new set $\{|I\rangle\}$

$$|\tilde{R}\rangle = |I\rangle(I\tilde{R})^{-1} \quad (11)$$

where we have introduced the notational shorthand of $(I\tilde{R})^{-1}$ meaning the (I, \tilde{R}) -th element of the inverse of the matrix $(\tilde{R}I)$ for easier readability.

If $\{|J\rangle\}$ is a complete set of functions $J(x)$ and $m_{12} = m(x_1, x_2)$ is a two-point function (which we call metric), in many cases

$$m_J(x) = \int J(x')m(x', x) dx' \quad (12)$$

forms again a complete set $\{|m_J\rangle\}$. Specifically this is the case for the choices $m(x_1, x_2) = \delta(x_1 - x_2)$ (overlap metric), $m(x_1, x_2) = \frac{1}{|x_1 - x_2|}$ (Coulomb metric), and $m(x_1, x_2) = \frac{\text{erfc}(w|x_1 - x_2|)}{|x_1 - x_2|}$ (attenuated Coulomb metric). With $\{|m_J\rangle\}$ being a complete set one can write in analogy to eq. 10

$$(m_J| = (J|m_{12}|\tilde{R})(\tilde{R}| \quad (13)$$

as

$$(\tilde{R}| = (\tilde{R}|m_{12}|J)^{-1}(m_J| \quad (14)$$

Expanding $|\tilde{R}\rangle$ in eq. 8 according to eqs. 11 and 14 respectively one obtains

$$\mathbf{I} = |I\rangle(I\tilde{R})^{-1}(\tilde{R}|m_{12}|J)^{-1}(m_J| \quad (15)$$

where for the inner matrix product the elements can be found as

$$(I\tilde{R})^{-1}(\tilde{R}|m_{12}|J)^{-1} = ((I|m_{12}|\tilde{R})(\tilde{R}J))^{-1} = (I|m_{12}|J)^{-1} \quad (16)$$

due to eq. 8. So concluding one finds

$$\mathbf{I} = |I\rangle(I|m_{12}|J)^{-1}(J|m_{12}| \quad (17)$$

or by exchanging $|I\rangle$ with $\langle I|$, etc. throughout the argument

$$\mathbf{I} = \langle m|I\rangle(I\langle m|J)^{-1}(J| \quad (18)$$

Inserted into eq. 7 this yields the final formulation, eq. 1, which we take as the starting point in the main text (eq. 3 and following).

V. OUTLOOK: KERNEL PROJECTION FOR EXPLICITLY CORRELATED METHODS

While the main text is focused solely on RI in the context of ERIs, for which it is equivalent to DF, in the following we briefly outline some related ideas for use in another type of RI, as it applies to explicitly correlated (F12) methods (c.f. [W. Klopper, C.C.M. Samson: J. Chem. Phys. 116 (2002), 6397] and references therein). There, integrals of the form

$$\langle xy|F_{12}o_1g_{12}|ij\rangle \quad (19)$$

occur where F_{12} and g_{12} are operators acting on both electrons, while o_1 acts on the first electron only, projecting it onto the occupied space, while the second electron is effectively acted on by an identity operation

$$o_1 = |k\rangle \langle k| \otimes \mathbf{I} \quad (20)$$

Writing eq. 19 in explicit integral form makes it obvious that this is in fact a three-electron integral

$$\langle xy|F_{12}o_1g_{12}|ij\rangle = \quad (21)$$

$$= \int \langle x(r)y(r')|F_{12}(r,r')|k(r)\rangle \langle k(r'')|g_{12}(r'',r')|i(r'')j(r')\rangle dr' \quad (22)$$

$$= \iiint x(r)y(r')k(r'')F_{12}g_{32}k(r)j(r')i(r'')drdr'dr'' \quad (23)$$

$$= \langle xyk|F_{12}g_{32}|kji\rangle \quad (24)$$

However, within the RI the identity in eq. 20 is resolved according to eq. 8. For this outlook we disregard, that commonly the complementary auxiliary basis set (CABS, [E.F. Valeev: Chem. Phys. Lett. 395 (2004), 190]) approach is used, by which certain contributions are already projected out of the otherwise formally complete auxiliary set. Within RI eq. 20 then becomes

$$o_1 = |kI\rangle \langle kI| \quad (25)$$

and therefore

$$\langle xy|F_{12}o_1g_{12}|ij\rangle = \langle xy|F_{12}|kI\rangle \langle kI|g_{12}|ij\rangle \quad (26)$$

which is a sum of products of two-electron integrals.

With $\langle xy|F_{12}|kI\rangle$ being linear in each index (specifically I) one could consider it as a linear operator $F_{xyk,I}$ and build an auxiliary matrix as

$$H_{IJ} = F_{I,xyk}^\dagger F_{xyk,J} \quad (27)$$

This would suggest that the projector P^R constructed from H (following the scheme of the main text) would not change the result when introduced as

$$\langle xy|F_{12}|kI\rangle \langle kI|g_{12}|ij\rangle = \langle xy|F_{12}|kI\rangle P_{IJ}^R \langle kJ|g_{12}|ij\rangle \quad (28)$$

How well this approach would perform in terms of auxiliary reduction compared to overhead costs caused by the projector construction remains to be seen and will have to be studied in future work.

Chapter 4

Conclusion

The random phase approximation is a highly accurate electronic structure theory. In this work it has been extended for molecular systems from the few atom scale to hundreds or even a thousand atoms. To this end, the theory has been reformulated by the newly developed double-Laplace transform and the change of RI metric. The effective evaluation time of the reformulated theory scales only linearly with system size in contrast to the original formulation that scaled with the fourth power. The double-Laplace transform extends the idea of Laplace transform in the context of MP2 theory beyond the separable denominator form and the local RI metric allows to exploit the locality of the physical interactions by eliminating the long-ranged Coulomb interaction from the time-determining step.

Furthermore, the Cholesky decomposition has been applied to the pseudo densities of the resultant reformulation to reduce the scaling with basis set size. This allows to compute correlation energies with this new theory even when converging results with basis set size. By also employing the attenuated Coulomb metric RI, it furthermore allows for identical results as the original formulation while reducing the computational overhead. This makes the new formulation more efficient than the original one already for moderately sized molecules and further extends the maximal size of systems accessible by the theory.

The RI is a mathematical tool that is used not only in the context of RPA but also within other theories. It is typically evaluated with preoptimized auxiliary basis sets to reduce computational cost. The newly proposed nullspace projection scheme allows to effectively eliminate the errors that would otherwise arise by this procedure while still obtaining almost the same reduction in computational cost. This not only makes RI-error free absolute energies available for significantly reduced cost but also makes the error cancellation assumption, on which many RI calculations had previously relied, unnecessary.

Overall, the presented new methods open a door for highly accurate quantum chemistry of large molecular systems. In this way, new possibilities for reliable benchmarks of large and complex molecules arise, allowing for new links between experiment and theory.

Bibliography

- ¹ N. Schuch and F. Verstraete, *Nat. Phys.* **5**, 732 (2009).
- ² J. Watrous, “Quantum Computational Complexity” in R. A. Meyers, *Encyclopedia of Complexity and Systems Science*, 7174 (2009).
- ³ E. Schrödinger, *Phys. Rev.* **28** 1049 (1926).
- ⁴ P. A. M. Dirac, *Principles of Quantum Mechanics*, 255 (Oxford University Press, 1958).
- ⁵ D. Bohm and D. Pines, *Phys. Rev.* **92**, 609 (1953).
- ⁶ A. D. Becke, *J. Chem. Phys.* **98**, 5648 (1993).
- ⁷ D. R. Hartree, *Proc. Cambridge Phil. Soc.* **24**, 89 (1928).
- ⁸ D. R. Hartree, *Proc. Cambridge Phil. Soc.* **24**, 111 (1928).
- ⁹ J. C. Slater, *Phys. Rev.* **35**, 210 (1930).
- ¹⁰ V. Fock, *Z. Physik* **61**, 126 (1930).
- ¹¹ C. Møller and M. S. Plesset, *Phys. Rev.* **46**, 618 (1934).
- ¹² F. Coester, *Nuc. Phys.* **7**, 421 (1958).
- ¹³ F. Coester and H. Kümmel, *Nuc. Phys.* **17**, 477 (1960).
- ¹⁴ S. F. Boys and I. Shavitt, *Tech. Rep.*: “A fundamental calculation of the energy surface for the system of three hydrogen atoms” (U. Wisconsin, 1959)
- ¹⁵ J. L. Whitten, *J. Chem. Phys.* **58**, 4496 (1973).
- ¹⁶ E. Baerends, D. Ellis, and P. Ros, *Chem. Phys.* **2**, 41 (1973).
- ¹⁷ B. I. Dunlap, J. W. D. Connolly, and J. R. Sabin, *J. Chem. Phys.* **71**, 4993 (1979).
- ¹⁸ C. Van Alsenoy, *J. Comput. Chem.* **9**, 620 (1988).
- ¹⁹ H. Eshuis, J. Yarkony, and F. Furche, *J. Chem. Phys.* **132**, 234114 (2010).
- ²⁰ M. Häser, *Theor. Chimica Acta* **87**, 147 (1993).
- ²¹ H. F. Schurkus, and C. Ochsenfeld, *J. Chem. Phys.* **144**, 031101 (2016).
- ²² H.-J. Werner, F. R. Manby, and P. J. Knowles, *J. Chem. Phys.* **118**, 8149 (2003).

- ²³ H. Koch, A. Sánchez de Merás, and T. B. Pedersen, *J. Chem. Phys.* **118**, 9481 (2003).
- ²⁴ J. Zienau, L. Clin, B. Doser, and C. Ochsenfeld, *J. Chem. Phys.* **130**, 204112 (2009).
- ²⁵ S. A. Maurer, L. Clin, and C. Ochsenfeld, *J. Chem. Phys.* **140**, 224112 (2014).
- ²⁶ A. Luenser, H. F. Schurkus, and C. Ochsenfeld, *J. Chem. Theory Comput.* **13**, 1647 (2017).
- ²⁷ F. Weigend, M. Häser, H. Patzelt, and R. Ahlrichs, *Chem. Phys. Lett.* **294**, 143 (1998).
- ²⁸ T. H. Dunning, Jr., *J. Chem. Phys.* **90**, 1007 (1989).
- ²⁹ R. A. Kendall, T. H. Dunning, Jr., and R. J. Harrison, *J. Chem. Phys.* **96**, 6796 (1992).
- ³⁰ D. E. Woon and T. H. Dunning, Jr., *J. Chem. Phys.* **98**, 1358 (1993).
- ³¹ K. A. Peterson, D. E. Woon and T. H. Dunning, Jr., *J. Chem. Phys.* **100**, 7410 (1994).
- ³² A. K. Wilson, T. van Mourik, and T. H. Dunning, Jr., *J. Mol. Struct* **388**, 339 (1996).
- ³³ O. Vahtras, J. Almlöf, and M. Feyereisen, *Chem. Phys. Lett.* **213**, 514 (1993).
- ³⁴ J. Wilhelm, P. Seewald, M. Del Ben, and J. Hutter, *J. Chem. Theory Comput.* **12**, 5851 (2016).
- ³⁵ K. J. H. Giesbertz, *Phys. Chem. Chem. Phys.* **18**, 21024 (2016).
- ³⁶ M. Grundei, A. M. Burow, *J. Chem. Theory Comput.* **13**, 1159 (2017).
- ³⁷ D. Kosov, *J. Chem. Phys.* **146**, 054103 (2017).
- ³⁸ G. P. Chen, V. K. Voora, M. M. Agee, S. G. Balasubramani, and F. Furche, *Ann. Rev. Phys. Chem.* **68**, 421 (2017).
- ³⁹ A. Heßelmann, *J. Chem. Phys.* **146**, 174110 (2017).
- ⁴⁰ C. D. Sherill, and H. F. Schaefer III., *Adv. Quant. Chem.* **34**, 143 (1999).
- ⁴¹ W. Kohn and L. J. Sham, *Phys. Rev.* **140**, A1133 (1965).
- ⁴² J. P. Perdew and K. Schmidt, *AIP Conf. Proc.* **577**, 1 (2001).
- ⁴³ Y. Zhao and D. G. Truhlar, *Theor. Chem. Acc.* **120**, 215 (2007).
- ⁴⁴ M. G. Medvedev, I. S. Bushmarinov, J. Sun, J. P. Perdew, and K. A. Lyssenko, *Science* **355**, 49 (2017).
- ⁴⁵ O. Gunnarson and B. I. Lundqvist, *Phys. Rev. B* **13**, 4274 (1976).

- ⁴⁶ H. F. Schurkus, *Wissenschaftliche Arbeit im Rahmen der Promotionseignungsprüfung: "The Description of Electron Correlation with the Random Phase Approximation"* (LMU Munich, 2013).
- ⁴⁷ P. Bachmann, *Analytische Zahlentheorie* (Teubner, 1894).
- ⁴⁸ E. Landau, *Handbuch der Lehre von der Verteilung der Primzahlen* (Teubner, 1909).
- ⁴⁹ W. Kohn, *Phys. Rev. Lett.* **76**, 3168 (1996).
- ⁵⁰ E. Prodan and W. Kohn, *Proc. Nat. Acad. Sci.* **102**, 11635 (2005).
- ⁵¹ A. Einstein, *Ann. Phys.* **49** (1916).
- ⁵² P.-O. Löwdin, *Arkiv Mat. Astr. Fysik* **35A**, No. 9 (1947).
- ⁵³ P.-O. Löwdin, *Adv. Phys.* **5**, 1 (1956).
- ⁵⁴ P.-O. Löwdin, *Adv. Quantum Chem.* **5**, 185 (1970).
- ⁵⁵ R. P. Feynman, *Phys. Rev.* **76**, 749 (1949).
- ⁵⁶ R. P. Feynman, *Phys. Rev.* **76**, 769 (1949).
- ⁵⁷ F. J. Dyson, *Phys. Rev.* **75**, 486 (1949).
- ⁵⁸ F. J. Dyson, *Phys. Rev.* **75**, 1736 (1949).
- ⁵⁹ A. L. Fetter and J. D. Walecka, *Quantum Theory of Many-Particle Systems*, (McGraw-Hill Book Company, 1971).
- ⁶⁰ J. C. Slater, *Phys. Rev.* **34**, 1293 (1929).
- ⁶¹ P. A. M. Dirac, *Proc. Roy. Soc. A* **113**, 621 (1927).
- ⁶² P. Jordan and O. Klein, *Z. Physik* **45**, 751 (1927).
- ⁶³ P. Jordan and E. P. Wigner, *Z. Physik* **47**, 631 (1928).
- ⁶⁴ V. Fock, *Z. Physik* **75**, 622 (1932).
- ⁶⁵ M. Gell-Mann and F. Low, *Phys. Rev.*, **84**, 350 (1951).
- ⁶⁶ G. C. Wick, *Phys. Rev.* **80**, 268 (1950).
- ⁶⁷ V. M. Galitskii and A. B. Migdal, *Sov. Phys.-JETP* **7**, 96 (1958).
- ⁶⁸ A. Klein and R. Prange, *Phys. Rev.* **112**, 994 (1958).
- ⁶⁹ P. C. Martin and J. Schwinger, *Phys. Rev.* **115**, 1342 (1959).
- ⁷⁰ H. Lehmann, *Nuovo Cimento* **11**, 342 (1954).
- ⁷¹ H. F. Schurkus, A. Luenser, and C. Ochsenfeld, *J. Chem. Phys* **146**, 211106 (2017).
- ⁷² R. Car and M. Parrinello, *Phys. Rev. Lett.* **55**, 2471 (1985).

⁷³ G. Kresse and J. Furthmüller, *Comput. Mat. Sci.* **6**, 15 (1996).

⁷⁴ K. Raghavachari, G. W. Trucks, J. A. Pople, and M. Head-Gordon, *Chem. Phys. Lett.* **157**, 479 (1989).

Curriculum Vitae

July 2017

Personal Details

Name	Henry Franz Schurkus
Date of birth	September 28, 1990
Place of birth	Landshut, Germany
Citizenship	German

Education

March 2015	Master of Science in “Chemistry” LMU Munich (grade: <i>excellent</i>)
September 2012	Additional Bachelor of Science in “Physics” LMU Munich (grade: <i>good</i>)
August 2012	Bachelor of Science in “Chemistry and Biochemistry” LMU Munich (grade: <i>very good</i>)
June 2009	Abitur (High School Diploma) Gymnasium München/Moosach (grade: <i>very good</i>)

Awards

December 2015	Prize of the Dr. Klaus Römer Foundation (LMU Munich)
Since March 2011	Fellow of the Bavarian EliteAcademy
February 2010 – July 2014	Scholarship of the German National Academic Foundation
November 2008	Honors of the Bavarian Academy of Fine Arts
September 2006 – July 2007	Bavarian Ambassador Scholarship of the Bavarian Ministry of Culture and Education